TRANSNUCLEAR
AN AREVA COMPANY

Non-Proprietary

NUHOMS®-MP197
MULTI-PURPOSE
CASK

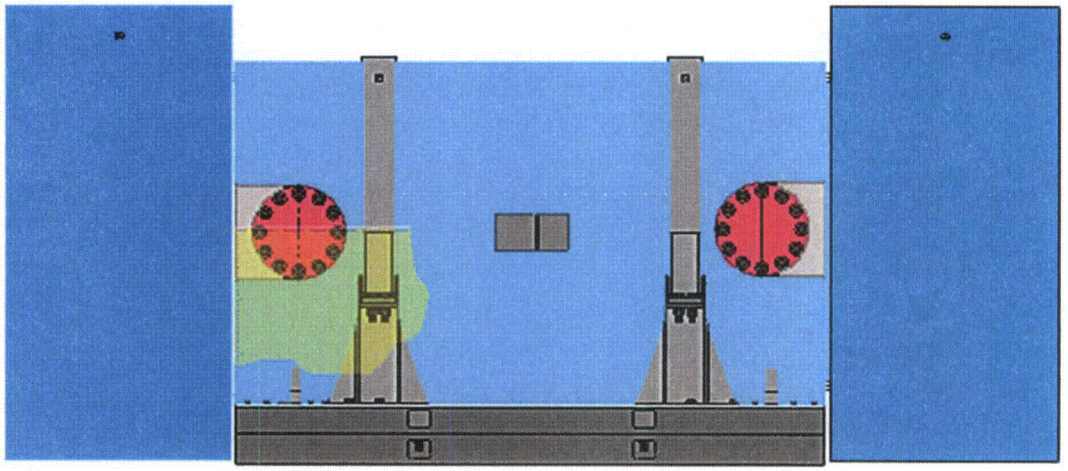

TRANSPORT
PACKAGING

SAFETY ANALYSIS REPORT
NUH09.0101
Volume 2 of 4

Figure 2.10.9-21

Acceleration Time History, with 1,000 Hz. Low-Pass Filter, 90° End Drop,
Accelerometer 11 (Bottom / Impact End)

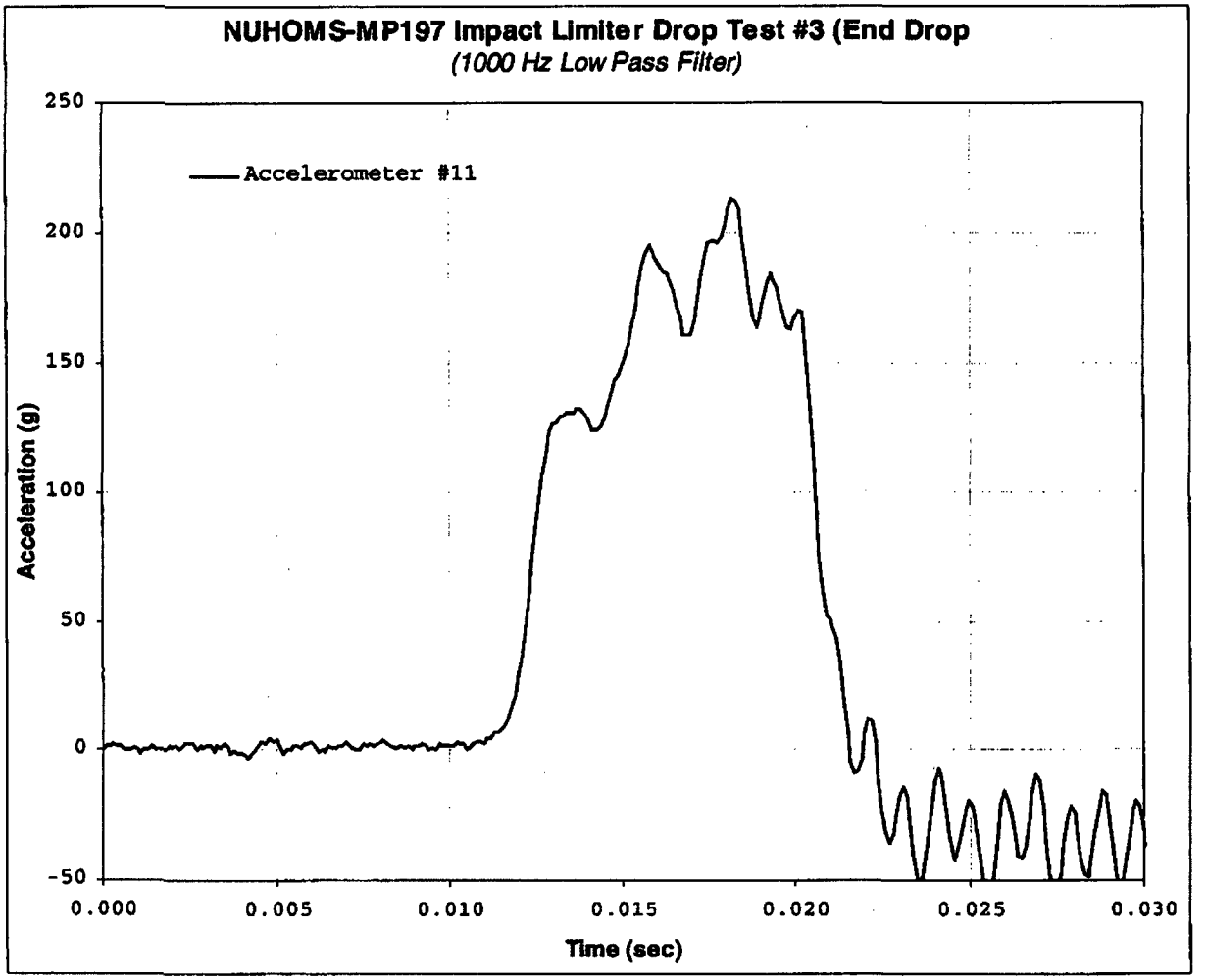

Figure 2.10.9-22

NUHOMS®-MP197 Cask Dummy and Impact Limiters After 90° End Drop

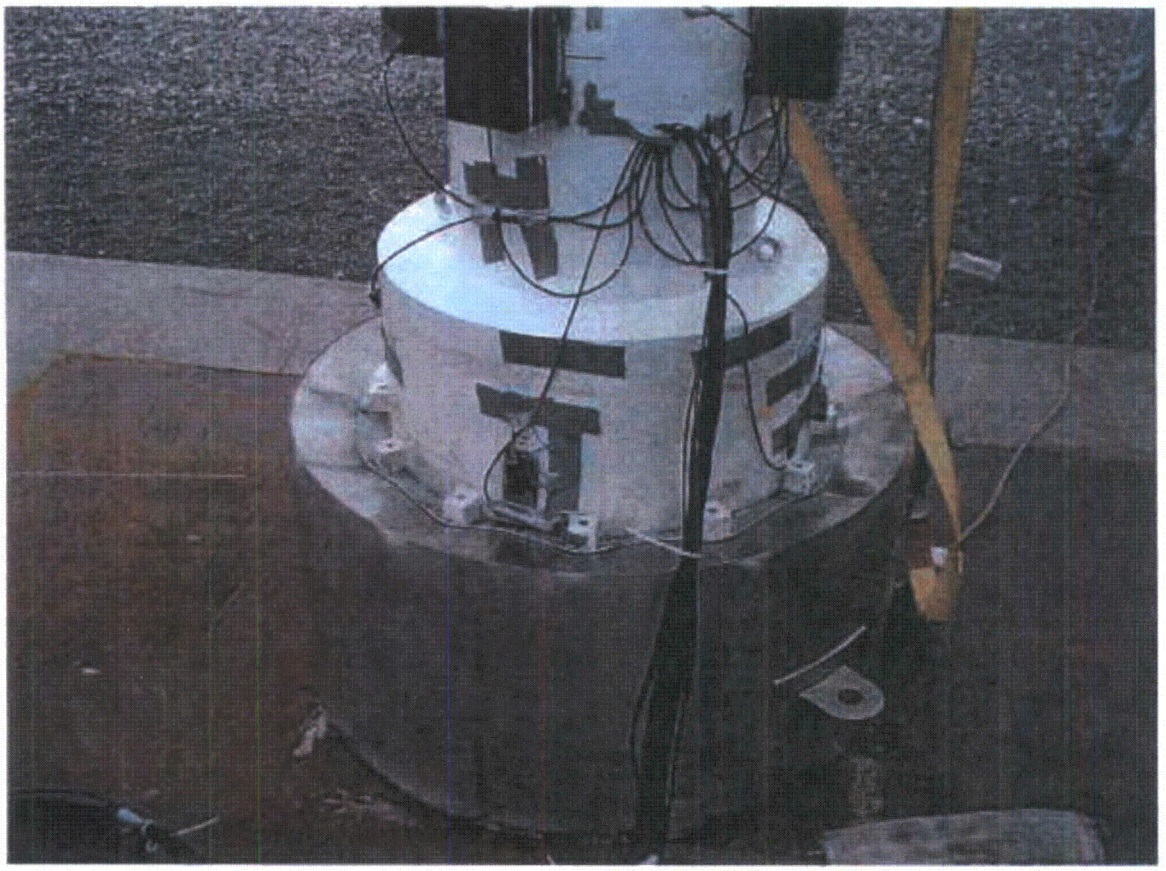

Figure 2.10.9-23

NUHOMS®-MP197 Cask Dummy and Impact Limiters After 90° End Drop

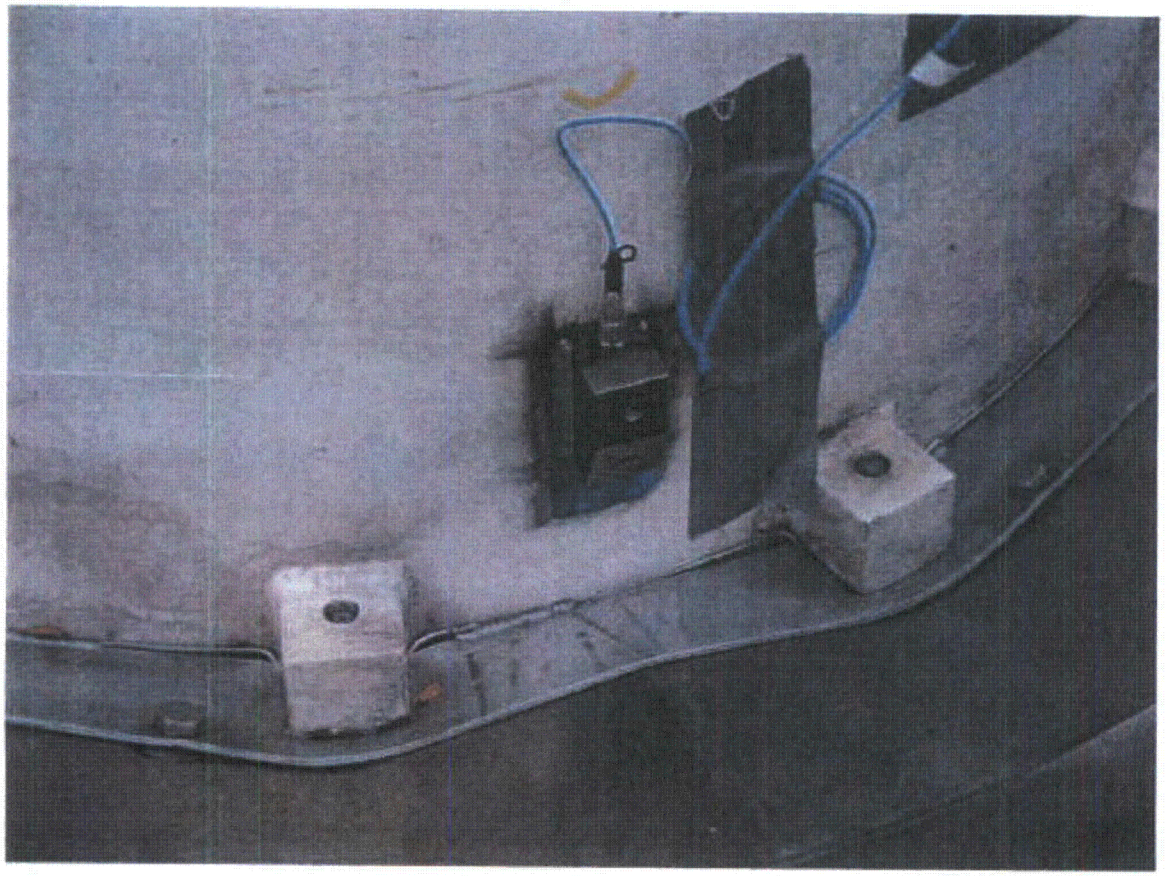

Figure 2.10.9-24

NUHOMS®-MP197 Cask Dummy and Impact Limiters After Puncture Drop

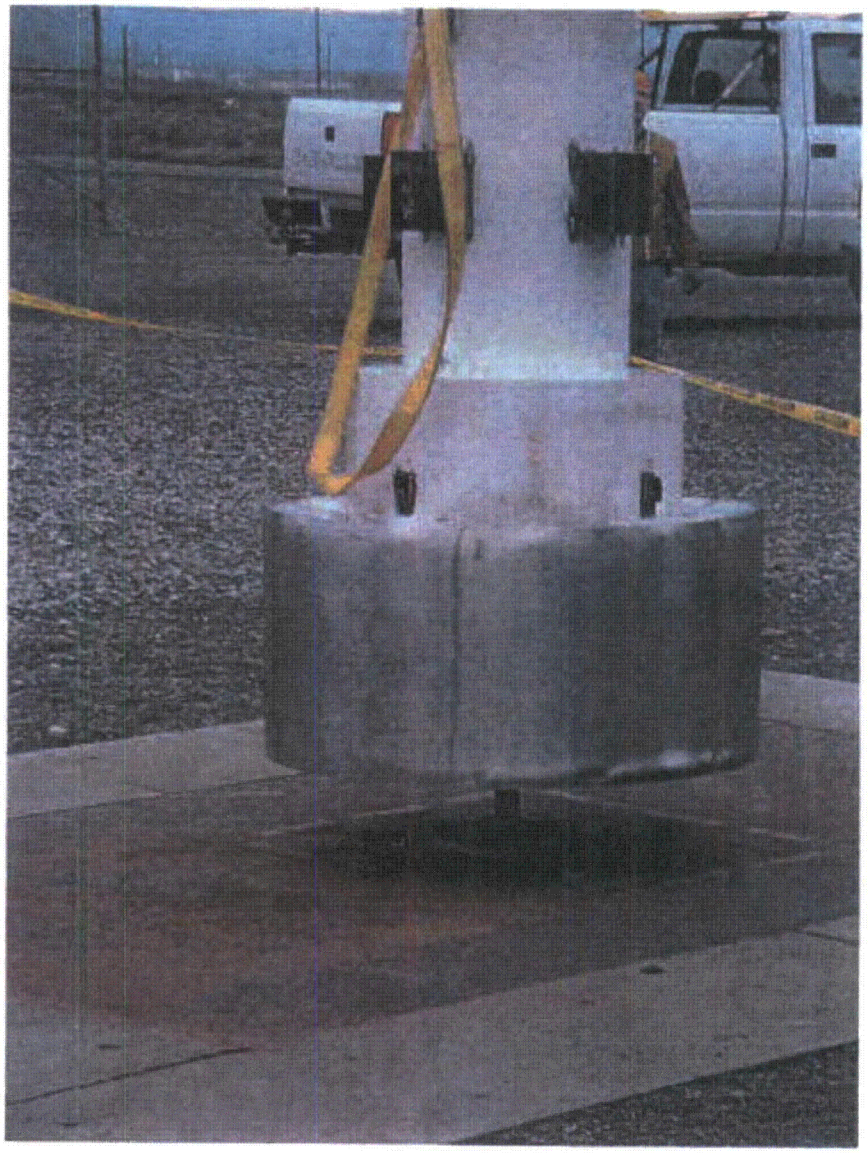

APPENDIX 2.10.10

TABLE OF CONTENTS

LIST OF TABLES

LIST OF FIGURES

LIST OF FIGURES
(continued)

This page intentionally blank

APPENDIX 2.10.10

NUHOMS®-MP197 PACKAGE FINITE ELEMENT ANALYSIS DETAILS

2.10.10.1 Introduction

This appendix provides additional detail information of the NUHOMS®-MP197 Transport Cask structural analysis. The primary focus of this appendix is the following.

- A detailed description of each component of the transport cask finite element model, including method of construction, mesh density, element types and evaluation of ANSYS warnings.
- An evaluation of the bearing load on the top surface of the flange where it contacts the bottom surface of the lid.
- An evaluation of the maximum stresses in each major component of the transport cask as well as the overall stress distribution.

2.10.10.2 3D Finite Element Model Description

The 3D finite element model of the NUHOMS®-MP197 Transport Cask is shown below in Figure 2.10.10-1. This model is symmetric about a diametrical plane. The details of the components are described below.

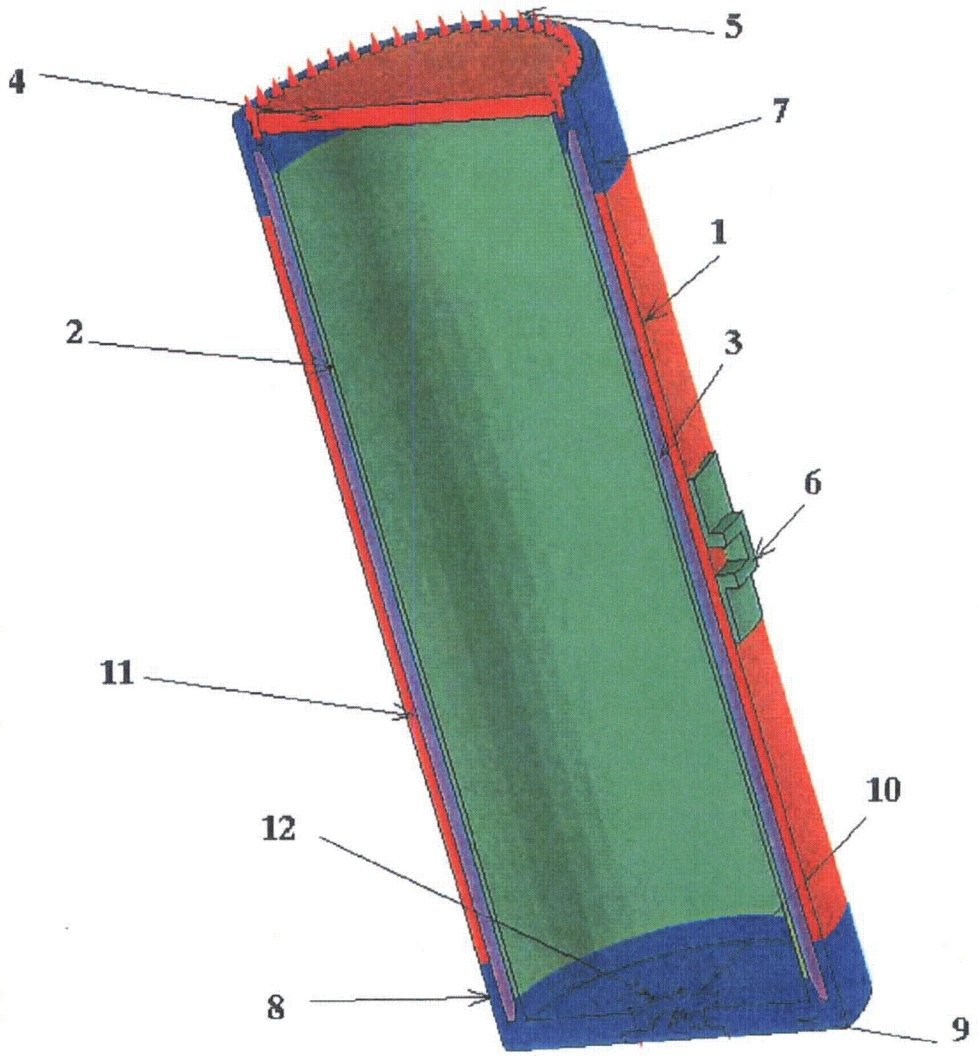

Figure 2.10.10-1
3D FEA model of NUHOMS®-MP197 Transport Cask Showing the Components.

1.Cask outer shell
2.Cask inner shell
3.Lead shield
4.Lid
5.Lid bolts
6.Shear key bearing block / Pad
7. Top flange region
8. Bottom flange region
9. Bottom
10. Ram cover plate
11. Lead /cask shell interface
12. Ram cover bolts

The model consists of a total of 39,044 elements and 40,494 nodes. The assembly consists of the following elements from the ANSYS element library: SOLID45, CONTACT52, LINK8, TARGET170 and CONTACT173. A maximum aspect ratio of about 6.11 was observed in the model. An element error/warning check for the entire model invoked ANSYS warning messages (due to element aspect ratio and distortion (Jacobean errors)), that are summarized later. Sweeping and copying about the axis of the cask generated most of the elements. A brief description of the individual components is included. Circumferential shifts of some nodes have been made to accommodate the shear key bearing block and the trunnions. In regions where stress variations were significant, a finer mesh was generated relative to regions where only displacements and load transfer was of interest.

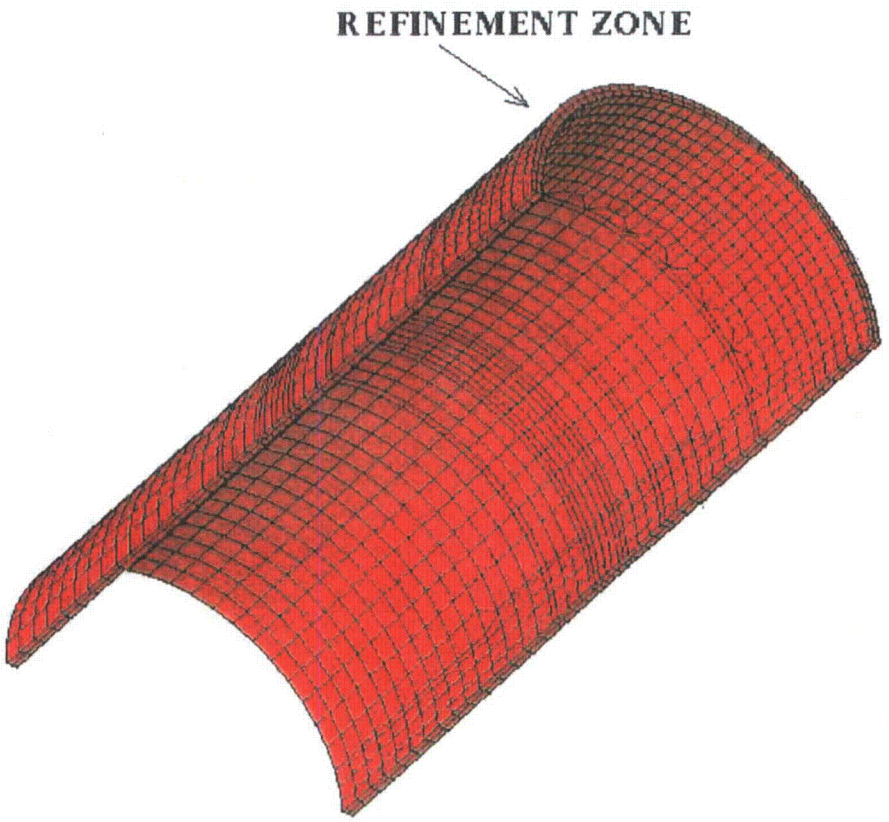

Figure 2.10.10-2: Cask Outer Shell (2,884 elements and 4,581 nodes)

The cask outer shell (Figure 2.10.10-2) is made of ANSYS SOLID45 elements. The maximum aspect ratio is 6.11. The elements were constructed using a combination of sweeping and copying about the cask centerline. The mesh is refined towards the lid to accommodate the details of the lid and the bolt assembly.

The lead shield is shown in Figure 2.10.10-3. This component is modeled with SOLID45 elements. There are, for the most part, two elements through the thickness with four elements through the thickness at the refinement zone to accommodate the details towards the top flange region. This part of the cask is isolated from the outer shell, inner shell, top and bottom flanges by surface-to-surface contact elements TARGET170 and CONTACT173. These elements provide contact and friction and allow relative movement between the lead shield and the shell. The elements are generated in a manner similar to the shell.

Figure 2.10.10-3: Lead Shield (4432 elements and 6588 nodes)

The FE mesh of the inner shell is shown in figure 2.10.10-4. Construction of the inner shell is similar to the outer shell with the necessary refinement towards the lid to accommodate the bolt assembly. The idealization is done using the SOLID45 element from the ANSYS element library. The maximum aspect ratio is about 6.0. The inner shell is separated from the lead lining by surface TARGET170 and CONTACT173. The ends of the shell connect to the top and bottom flanges. Symmetric boundary conditions are applied to the longitudinal edges for identical loading about the plane of symmetry.

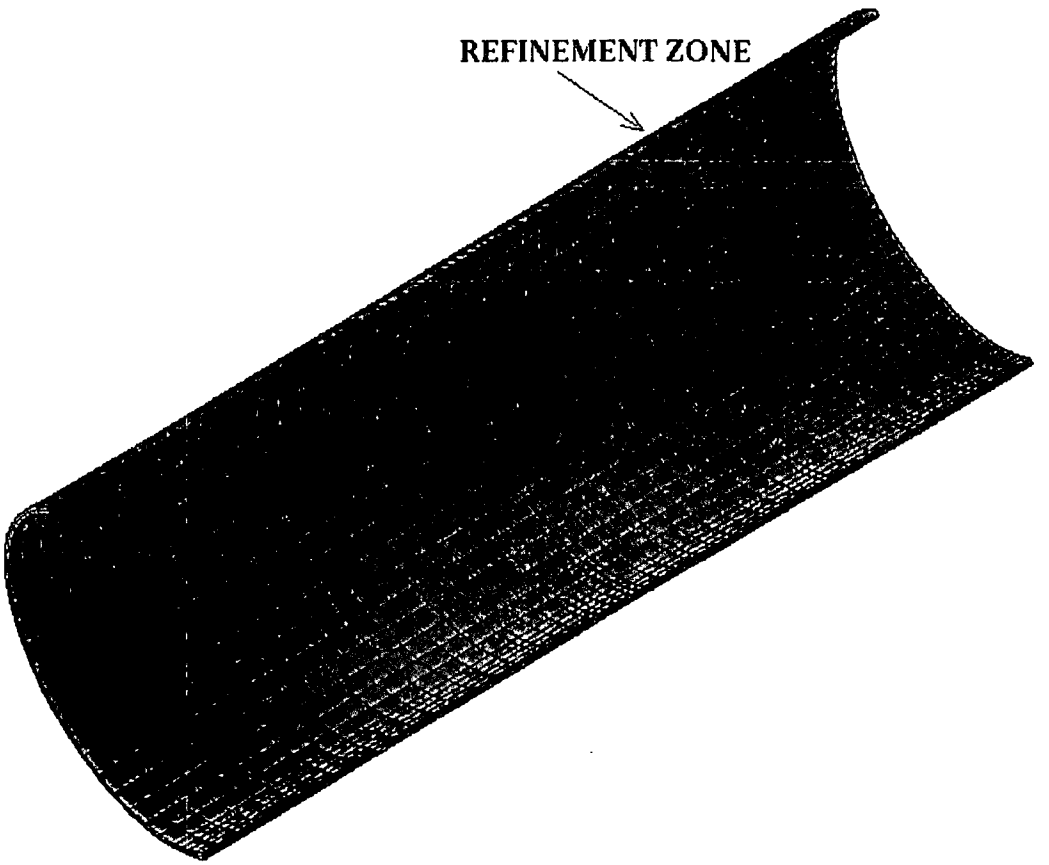

Figure 2.10.10-4: Cask Inner Shell (3276 elements and 5184 nodes)

Figures 2.10.10-5 and 2.10.10-6 show the details of the surface contact elements used. TARGET 170 and CONTACT173 are used together to establish contact and provide a friction surface to enable both surfaces to slide relative to each other. Figure 2.10.10-5 shows CONTACT173 with and without the gridlines. It can be seen that the surface configuration of the grid lines conforms to that of the lead liner. These contact elements envelop the lead liner completely. Construction of the TARGET170 contact is similar to CONTACT173 but conforms to the inner and outer shell along with the top and bottom flange assemblies. Figure 2.10.10-6 shows the grid differences between the two sets of contact elements at the end of the lead liner near the top flange.

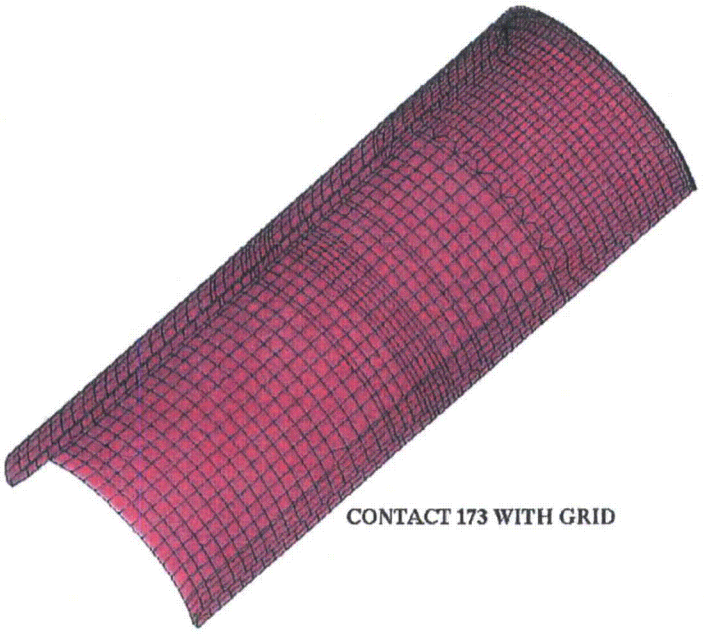

Figure 2.10.10-5: CONTACT173 Elements at Lead Shield / Shell Interface)

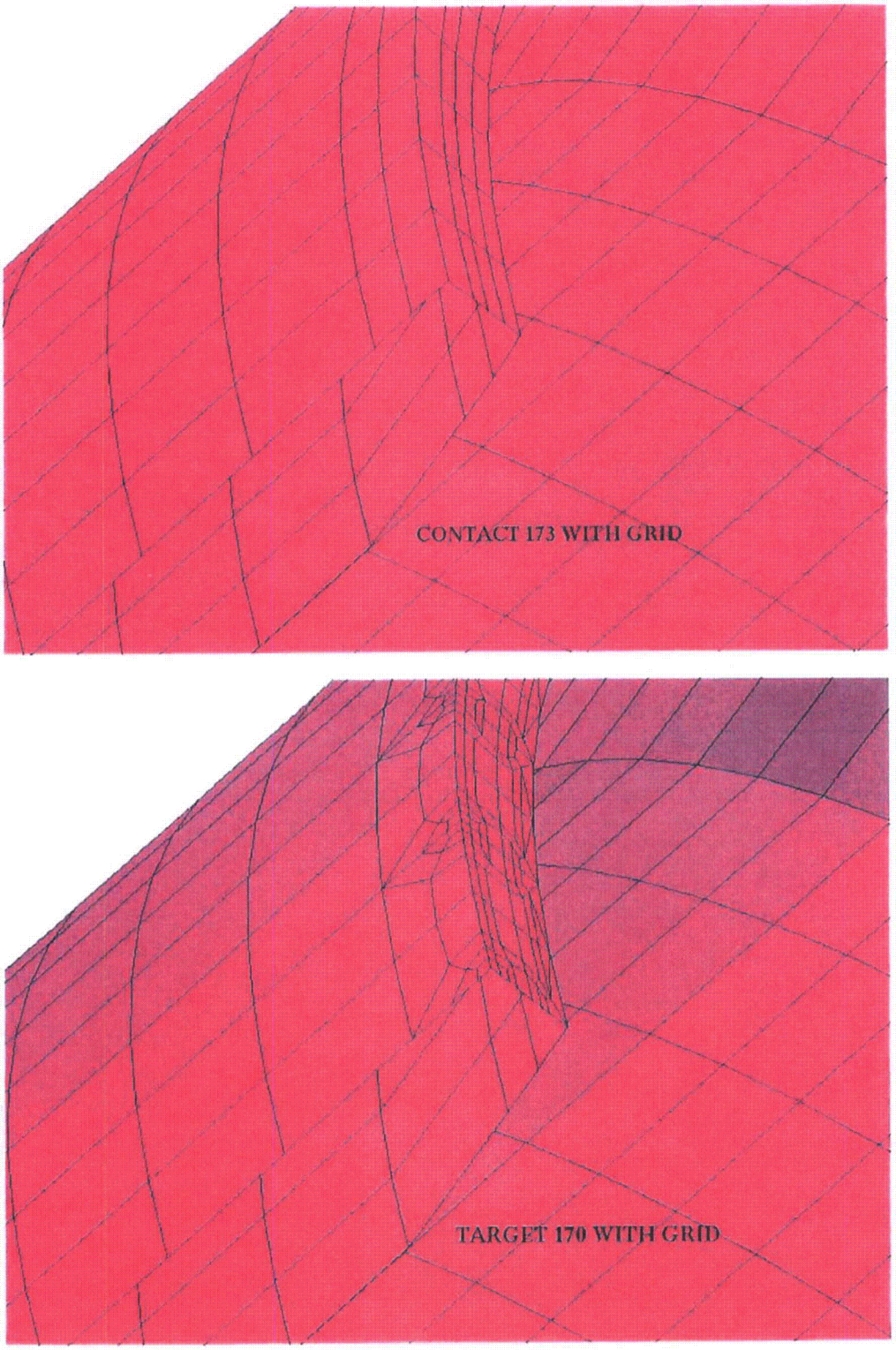

Figure 2.10.10-6: CONTACT173 and TARGET170 Detail (Lead / Shell Interface) Near the Top Flange.

Figure 2.10.10-7 shows the finite element idealization of the lid. Forty-eight bolts (twenty-four in the half model) connect the lid to the top shell flange. The lid is modeled with SOLID45 elements. The lid is connected to the top flange shell assembly (Figure 2.10.10-8) through ANSYS LINK8 clusters and CONTACT52 elements. The mesh has sufficient density to calculate the bending and extensional stresses accurately. The detail in Figure 2.10.10-7 shows the modeling details at the bolt recess.

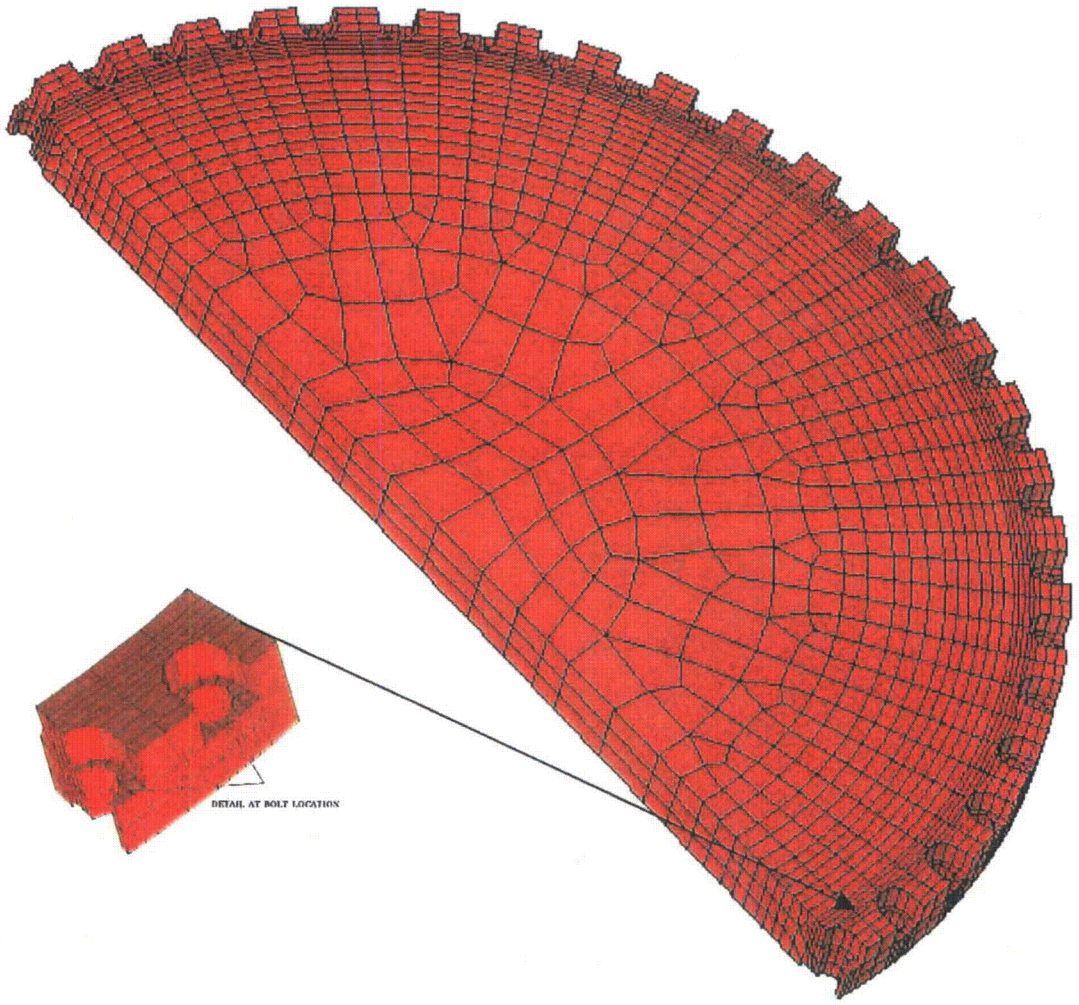

Figure 2.10.10-7: Cask Lid with Bolt Head Recess Detail (3828 Elements and 6124 Nodes)

The top flange and detail are shown in Figure 2.10.10-8. Figure 2.10.10-9 shows a segment of the assembly with details of modeling.

Figure 2.10.10-8: Shell Top Flange

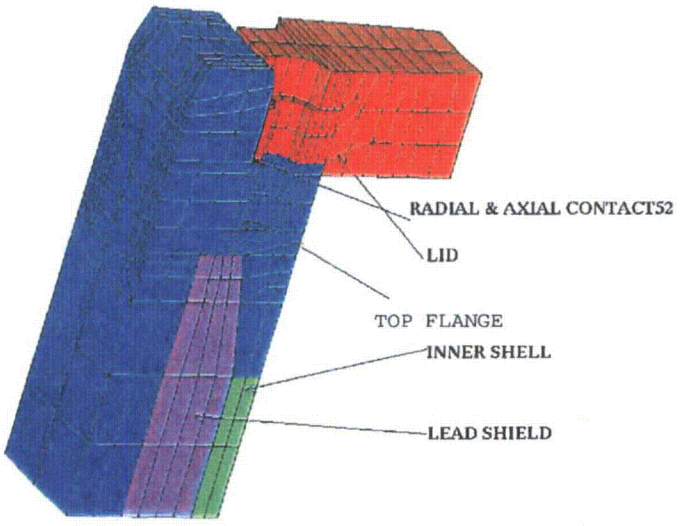

Figure 2.10.10-9: Segment at Top Flange Assembly Showing Modeling Details-Lead Shield, Inner Shell, Lid and Top Flange and Location of CONTACT52 Elements.

The details of the bolted joints between the top flange and the lid are shown in Figure 2.10.10-10. There are 48 bolted joints (24 in the half model) modeled with LINK8 elements. These are in addition to the CONTACT52 elements used in the radial and axial directions. A representative bolted joint consists of a shank representing the bolt (in area and material) and two sets of spider formations (LINK8 clusters) to transfer the loads. One set (green) connects to the counter bore and the other set (brown) to the bolt threads in the cask top flange.

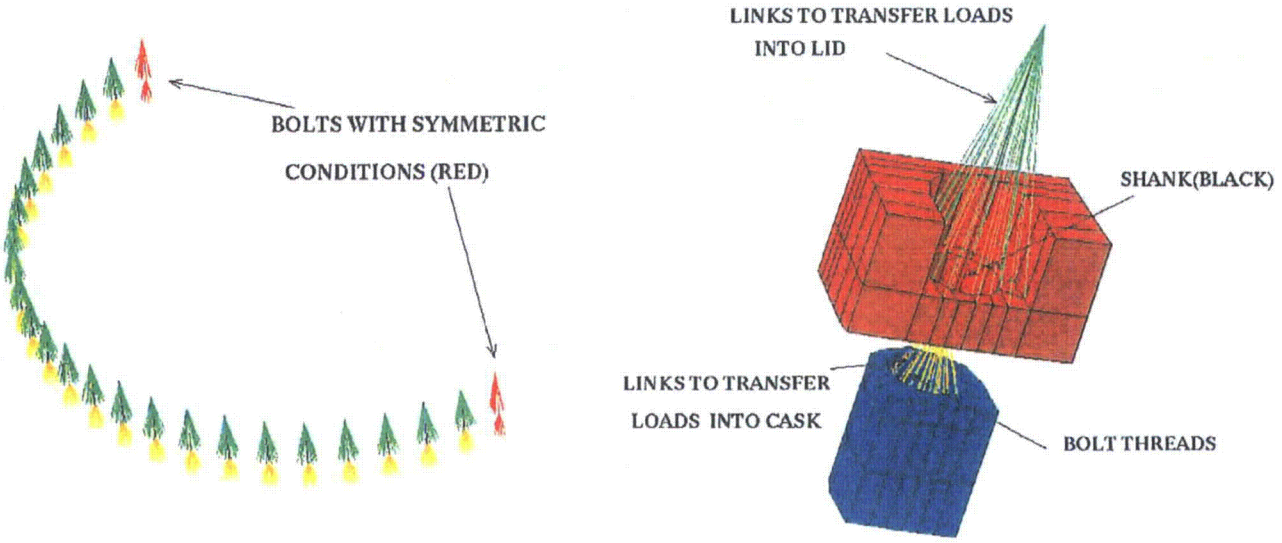

Figure 2.10.10-10: Details of Bolt Assembly LINK8 Elements

The bottom cover and flange assembly is shown in Figure 2.10.10-11. This component is constructed out of SOLID45 elements and connects to the ram cover plate (Figure 2.10.10-12) through bolts represented by LINK8 elements. The ram cover plate is also connected at the side to the bottom plate by CONTACT52 elements. The bottom flange is connected to the inner and outer shell directly and to the lead shield through CONTACT173 and TARGET170 elements. Details of this assembly are shown below in Figure 2.10.10-13. There are 12 bolts (six in the half model) connecting the bottom plate to the ram cover plate. Details of the spider formation of the LINK8 elements are shown in Figure 2.10.10-13. A representation of the bolted joint joining the bottom plate to the ram cover plate is shown in Figure 2.10.10-14

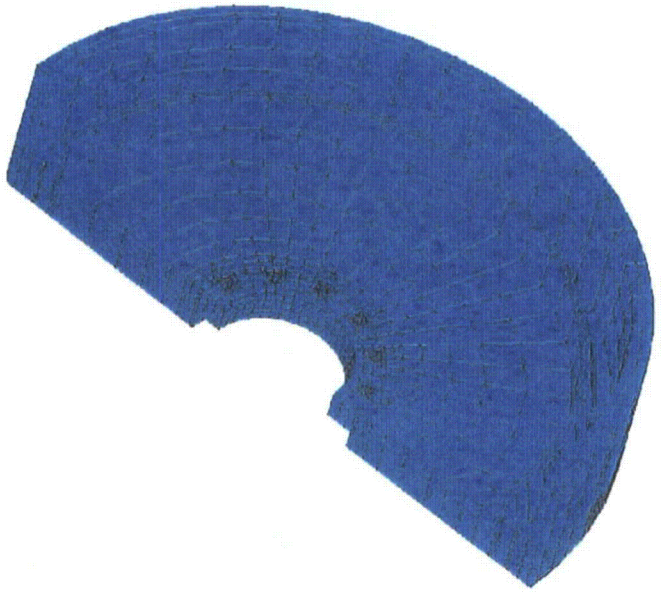

Figure 2.10.10-11: Cask Bottom Cover and Flange (3437 Elements and 4399 Nodes)

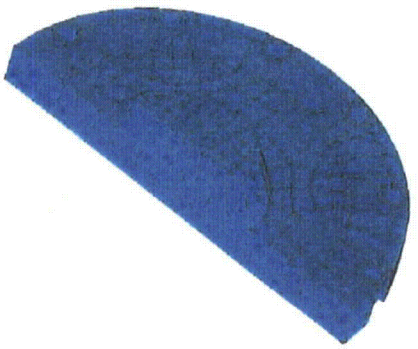

Figure 2.10.10-12: Cask Bottom Ram Cover Plate

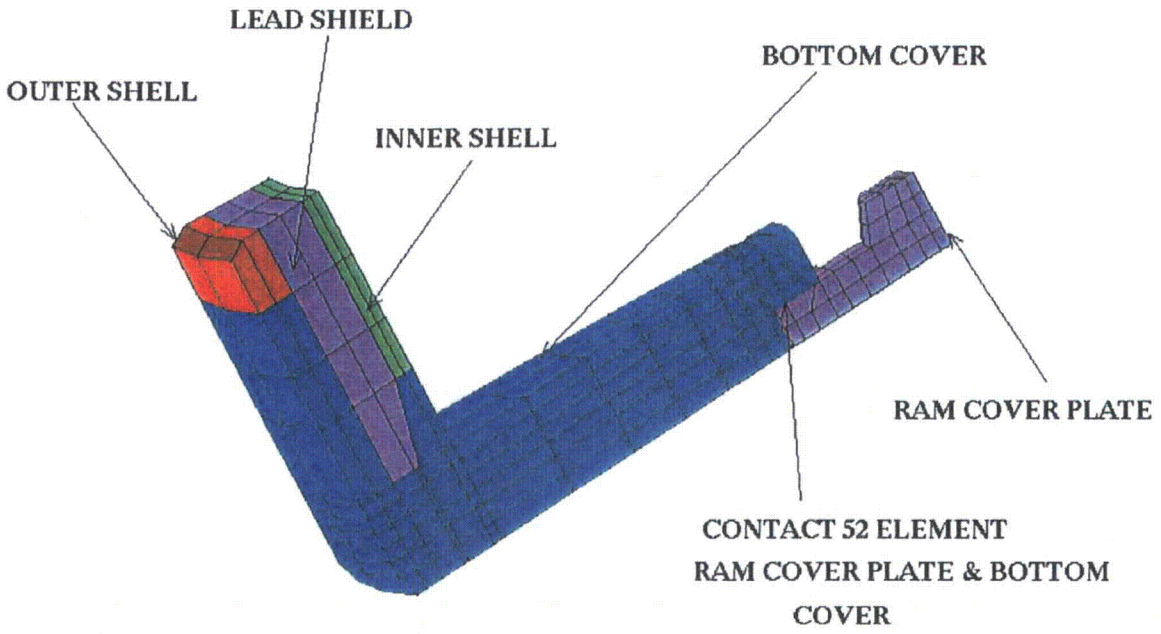

Figure 2.10.10-13. Segment of Cask at the Bottom Showing Assembly of Bottom Flange / Cover, Cam Cover Plate, Lead Shield, Inner and Outer Shell. Also included is the location of a typical CONTACT 52 element.

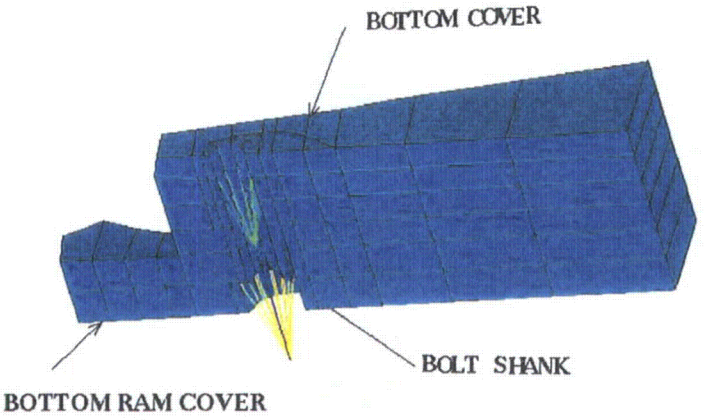

Figure 2.10.10-14. Cask Bottom and Ram Cover Bolted Joints

Fig 2.10.10-15 shows the details of the shear key bearing block and pad. This is attached to the outer shell with 48 coupled sets each in the x y and z directions around the edge. The aspect ratio of these elements is within acceptable limits.

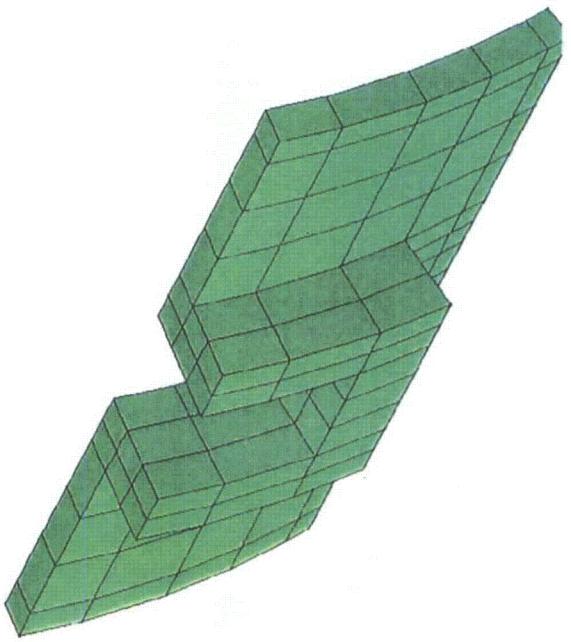

Figure 2.10.10-15: Shear Key Bearing Block and Pad (99 Elements and 240 Nodes)

2.10.10.3 Review of 3D FEM warning elements

Figure 2.10.10-16 shows a view of all warning elements output by the ANSYS program. The warning elements are divided into five groups: A, B, C, D and E. Detailed descriptions of the groupings are given below. The locations of these individual groups are shown with respect to the entire model. A total of 387 elements, out of 39,044, are indicated as warning elements (less than 1%).

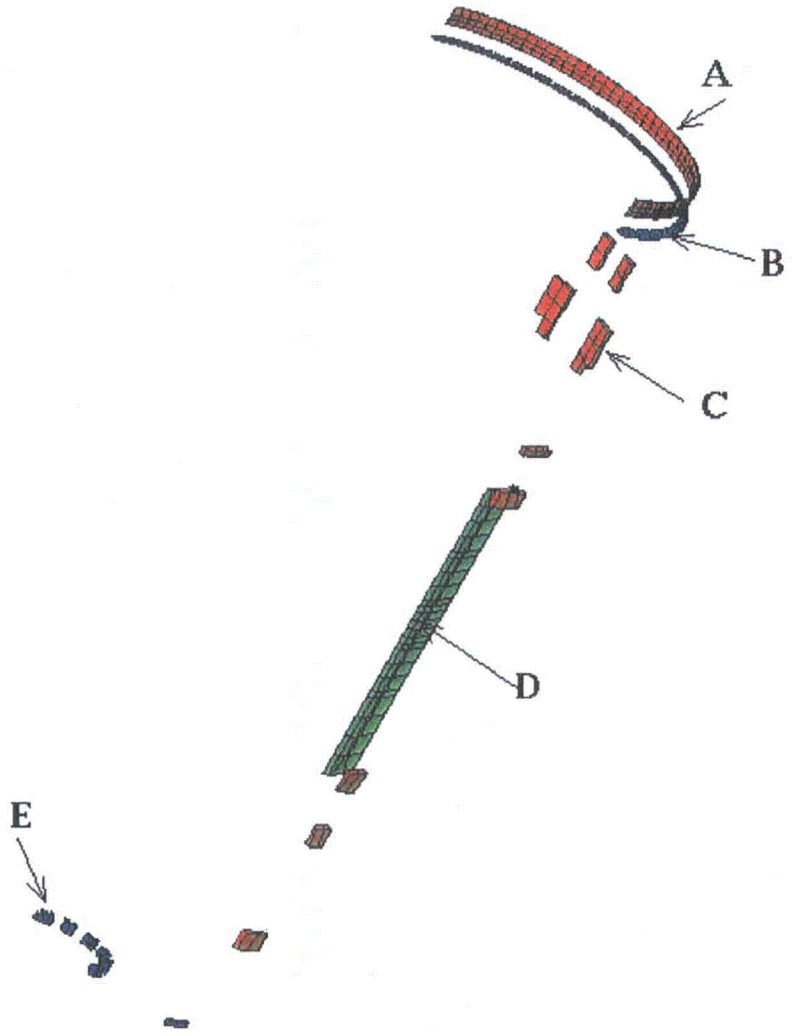

Figure 2.10.10-16: Warning Elements from the 3D FEM

Figure 2.10.10-17 shows the elements of group A and their relative position in the lid. There are 144 elements in this set. The ANSYS warning messages (2 per element) is indicated as:

1. "Brick element has a pair of opposite edges that are 71.25 degrees away from being parallel. This exceeds the warning limit of 70 degrees."
2. "Brick element 14040 has an angle between adjacent edges of 167.3 degrees, which exceeds the warning limit of 155 degrees."

The interior angles differ from the set warning limits of 70 and 155 degrees. This distortion was due to modeling of the bolt holes. Since the warning elements are in a localized region and these warning factors are also close to the set limits, therefore they are deemed acceptable.

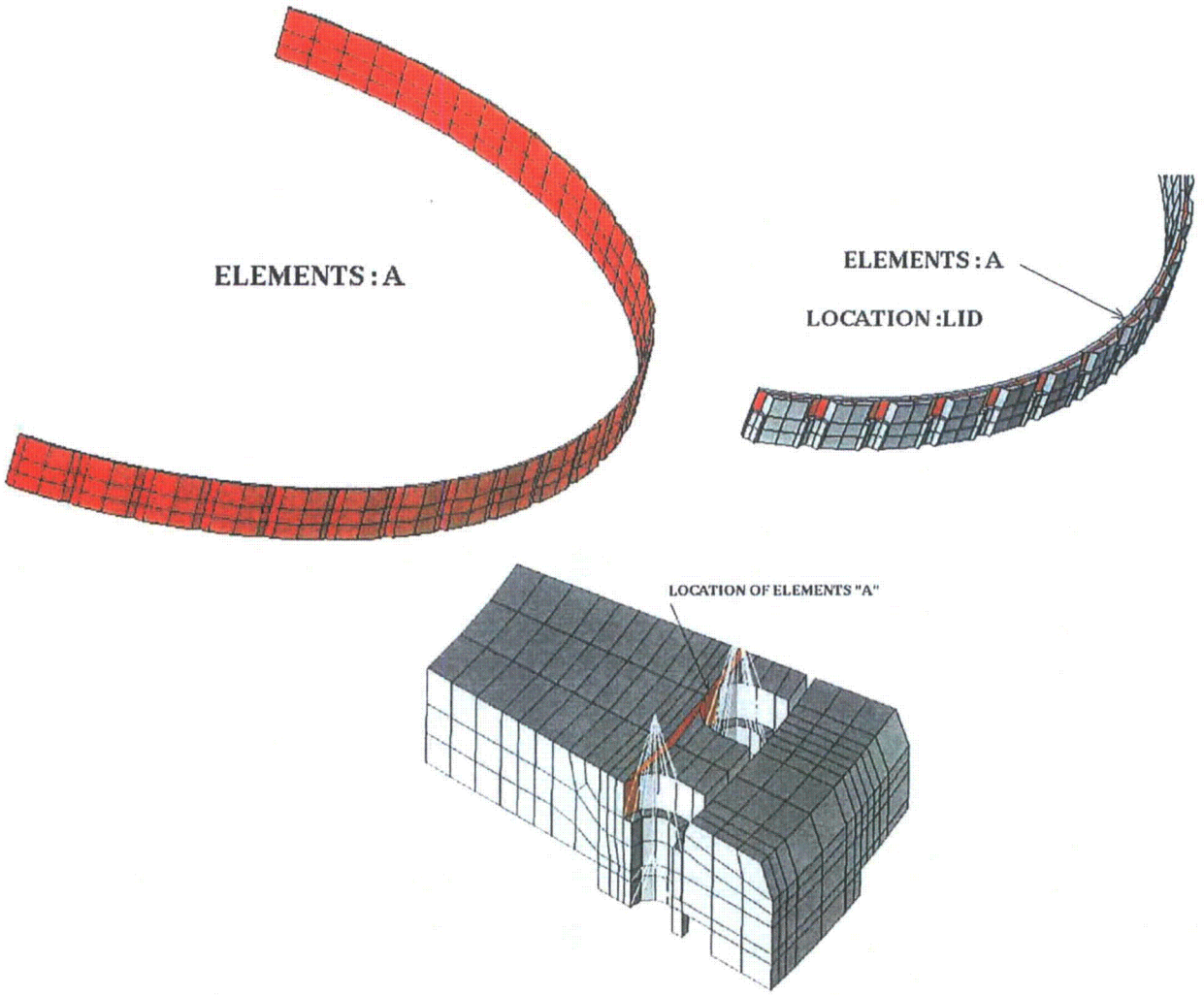

Figure 2.10.10-17: Warning Elements A from the 3D FEM in the Lid near the Bolt Holes

Figure 2.10.10-18 shows the details of the warning elements of group B. There are 96 elements and the ANSYS warning message is given as:

1. "Brick element has a pair of opposite edges that are 77.11 degrees away from being parallel. This exceeds the warning limit of 70 degrees."
2. "Wedge element has an aspect ratio of 24.38, which exceeds the warning limit of 20.

Since these warning factors are close to the set limits, therefore they are deemed acceptable.

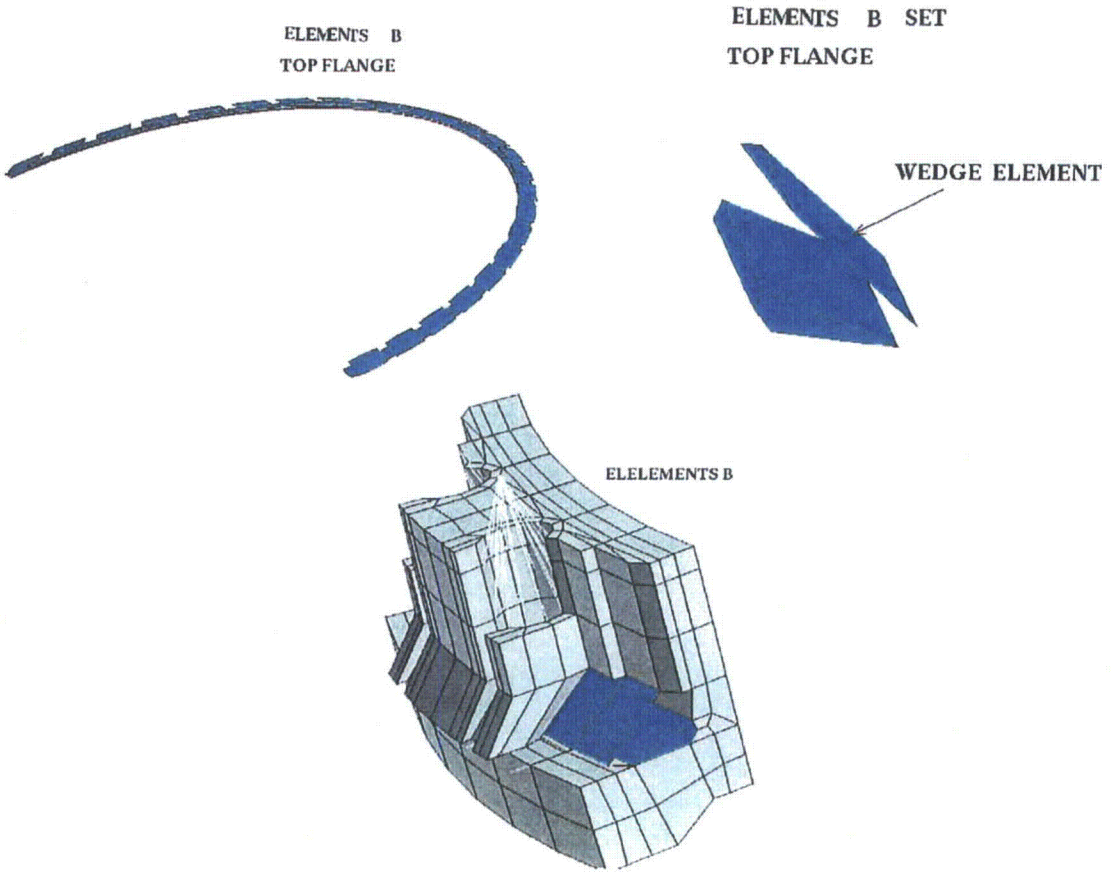

Figure 2.10.10-18: Warning Group B from the 3D FEM in Top Flange near the Bolt Holes

Details of group C elements are given in Figure 2.10.10-19. There are a total of 26 elements in this group. These elements are located in the outer shell (see figure). Distortions of these elements are due to the changes (circumferential shifts) made in the outer shell nodes to accommodate the shear key and the trunnions. The typical ANSYS warning messages given are as follows:

1. "Brick element has a face with a warping factor of 0.2036, which exceeds the warning limit of 0.2."
2. "Brick element has a pair of opposite edges that are 76.28 degrees away from being parallel. This exceeds the warning limit of 70 degrees."
3. "Brick element 8138 has an angle between adjacent edges of 159.9degrees, which exceeds the warning limit of 155 degrees."

These warning factors are very close to the limits set and deemed acceptable based on Engineering judgment.

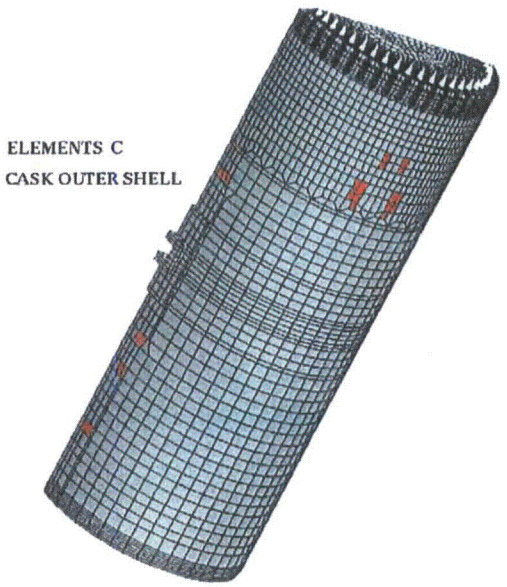

Figure 2.10.10-19: Location of Warning Group C Elements in the Cask Outer Shell

There are 69 elements in group D of the warning element category. Sample ANSYS warning messages are indicated below:

1. "Brick element has an angle between adjacent edges of 170.7 degrees, which exceeds the warning limit of 155 degrees."
2. "Brick element has a pair of opposite edges that are 132.6 degrees away from being parallel. This exceeds the warning limit of 70 degrees."
3. "Brick element has an angle between adjacent edges of 162.3 degrees, which exceeds the warning limit of 155 degrees."
4. "Brick element has a pair of opposite edges that are 84.47 degrees away from being parallel. This exceeds the warning limit of 70 degrees.

The above warnings are generated in the shear key bearing block area. Since the stress generated in this region is calculated separately in SAR Section 2.5.2, therefore these warning are deemed acceptable.

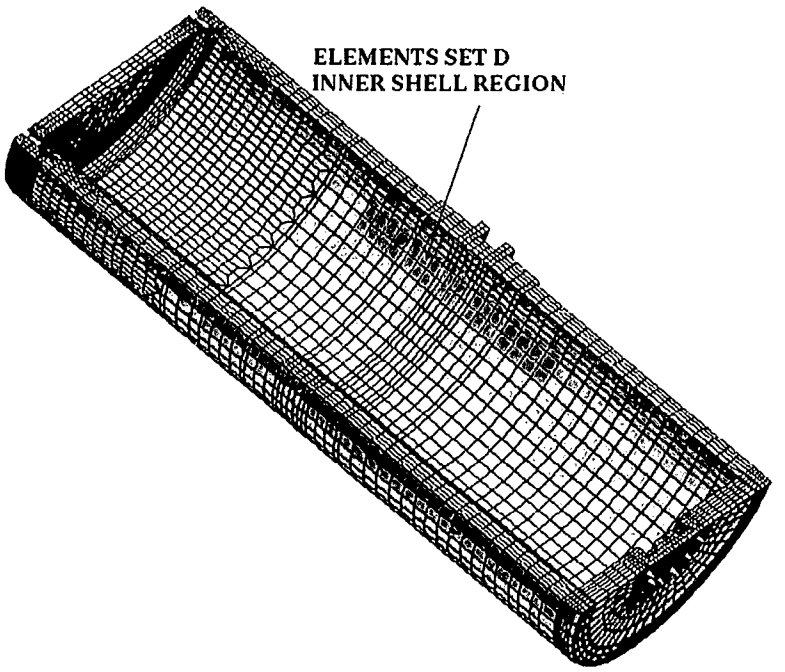

Figure 2.10.10-20: Warning Group D Elements in the Inner Shell Region

The set comprising warning group E elements is shown in Figure 2.10.10-21. There are 52 elements in this category. Three of these elements are in the bottom cover/flange region. Two of these had a warping factor of 0.4002, which was close to the error limit of 0.4. The details of the other elements in the ram cover plate are also shown. Distortions in this set of elements were due to modeling around the bolt holes. The ANSYS warning message was as follows:

1. "Brick element has a face with a warping factor of 0.2154, which exceeds the warning limit of 0.2."

These elements are deemed acceptable based on warning factors are very close to the default limits set, engineering judgment deems acceptable.

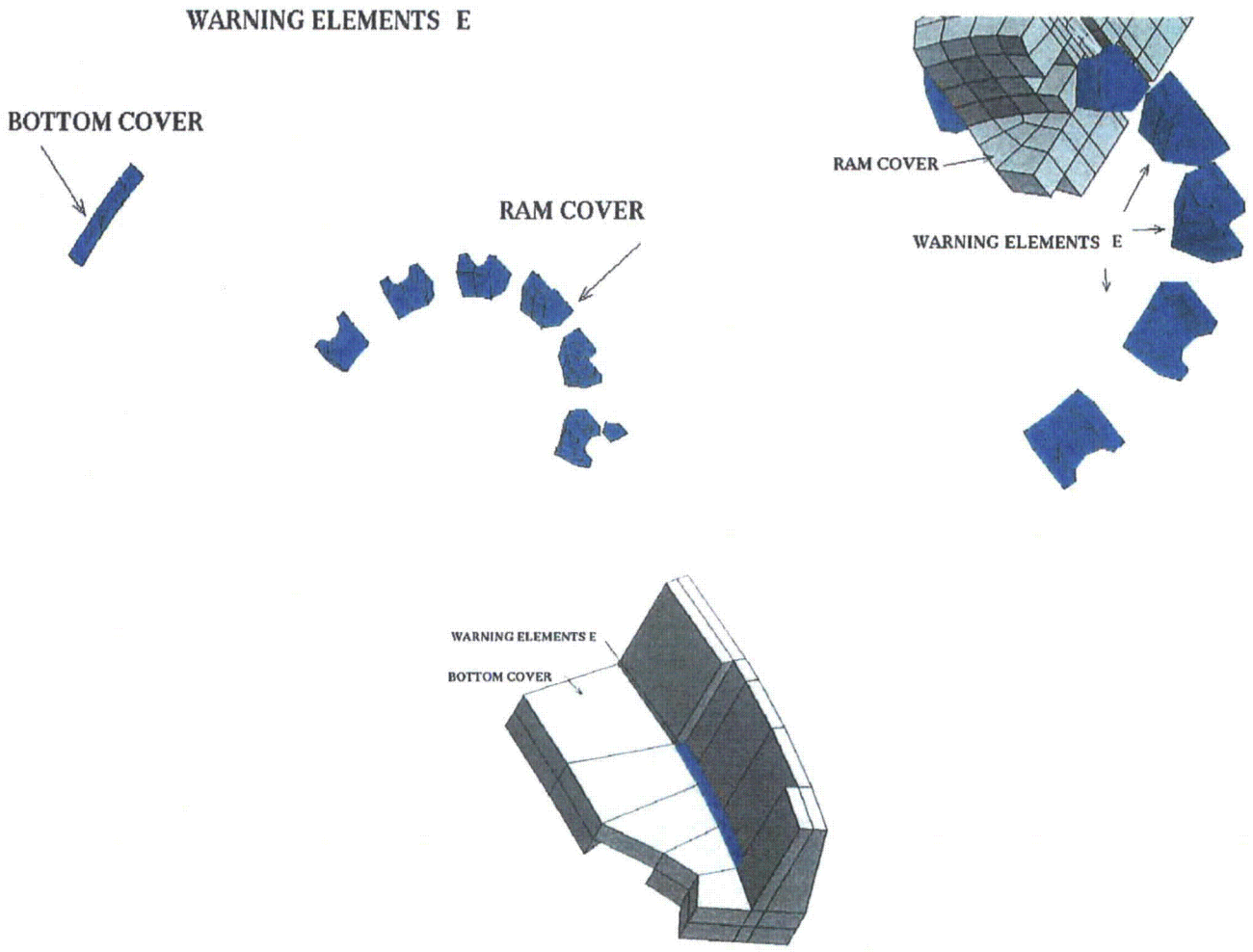

Figure 2.10.10-21: Warning Group E Elements in Bottom Plate / Flange and Ram Cover

2.10.10.4 Axisymmetric (2D) Finite Element Model Description

For all axisymmetric loading cases the 2D model used is shown in Figure 2.10.10-22. There are a total of 801 elements and 907 nodes in the model. The model is used to simulate the inner shell, outer shell, lead shield, lid, ram cover plate, bottom cover and top and bottom flanges as shown in Figure 2.10.10-22. The 3-D model of the NUHOMS®-MP197, described in Section 2.10.10.2, forms the basis for the 2D axisymmetric model construction.

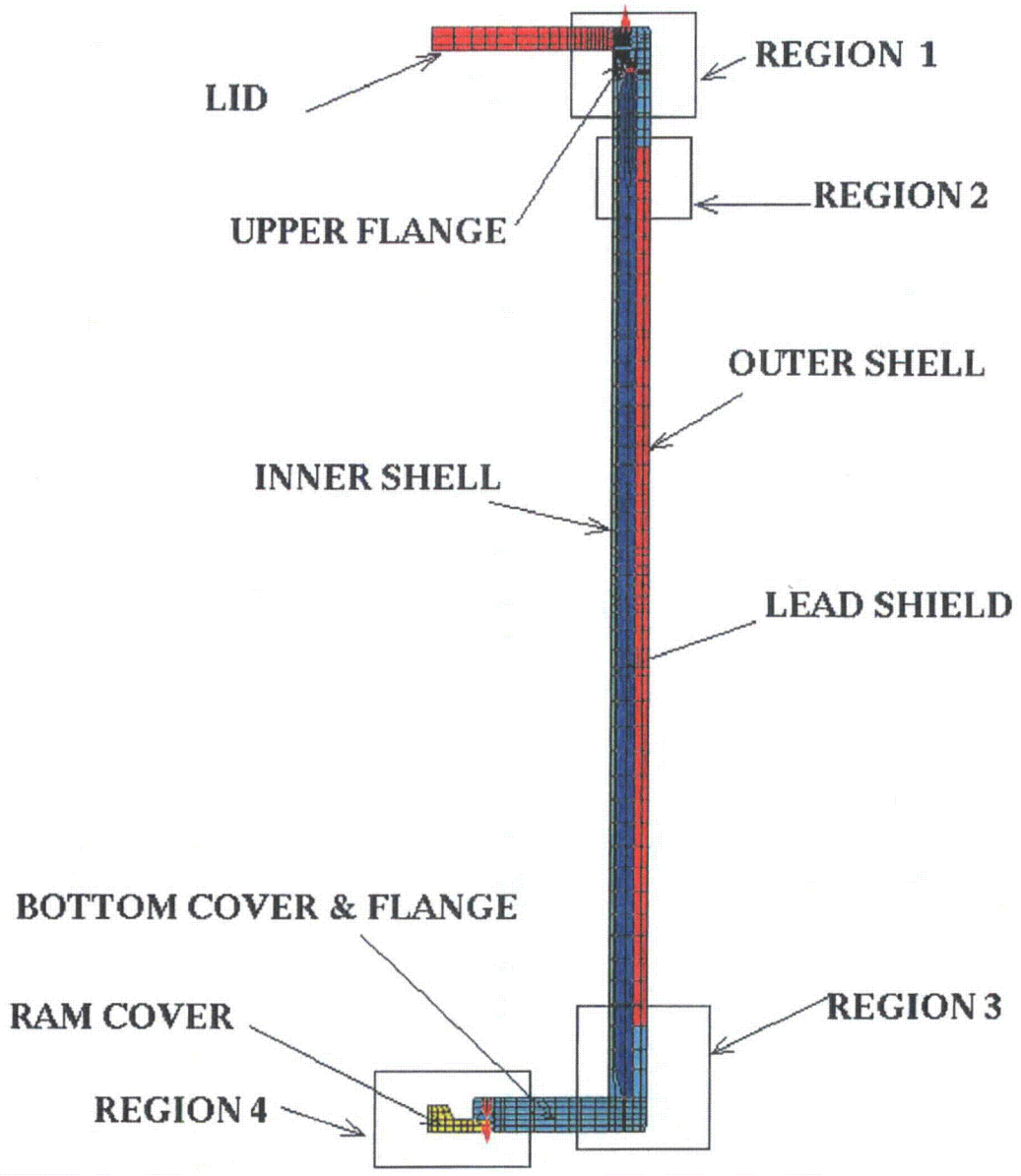

Figure 2.10.10-22: Axisymmetric Finite Element Model of the NUHOMS®-MP197 Transport Cask

The "surface effect" feature of ANSYS was used to create the PLANE42 axisymmetric elements through the thickness preserving the mesh density of the 3D model. The lid, upper flange, inner shell, outer shell, bottom flange, bottom cover and ram cover were modeled with PLANE42 elements. The surface elements TARGET170 and CONTACT173 in the 3D model were replaced with CONTACT12 elements. These CONTACT12 elements connect on a point-to-point basis. The four regions shown in Figure 2.10.10-22 are described below.

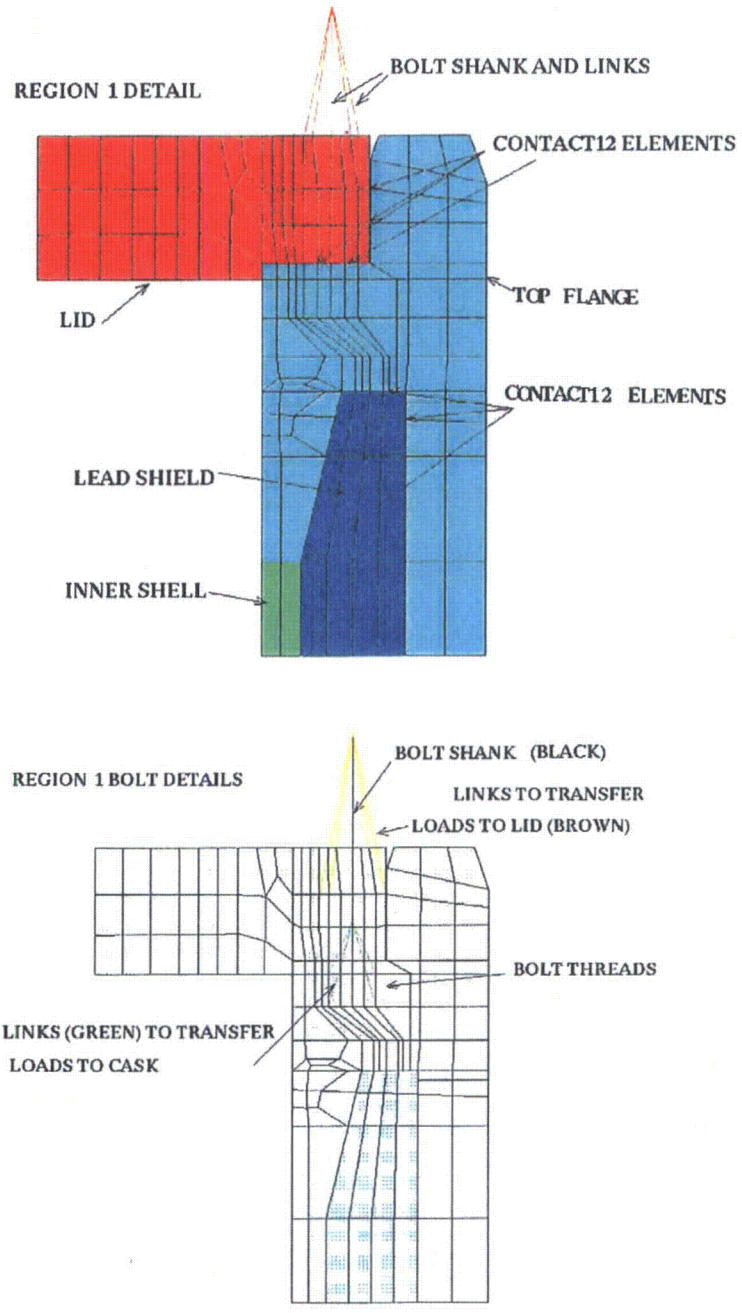

Figure 2.10.10-23a & b: Region 1 Showing Modeling Detail and Bolt Idealization

Figure 2.10.10-23a and b show the details of the cask in the area indicated as region 1. The color scheme distinguishes the various components of the cask in this region. The locations near the lead shield where the CONTACT173 and TARGET 170 elements were replaced by CONTACT12 elements are shown. The other set of CONTACT12 elements connecting the lid to the top flange is also indicated. Figure 2.10.10-23b shows a transparent mesh giving details of a single bolt connection. Two sets of LINK1 elements (brown and green) connect the bolt shank to the lid and top flange.

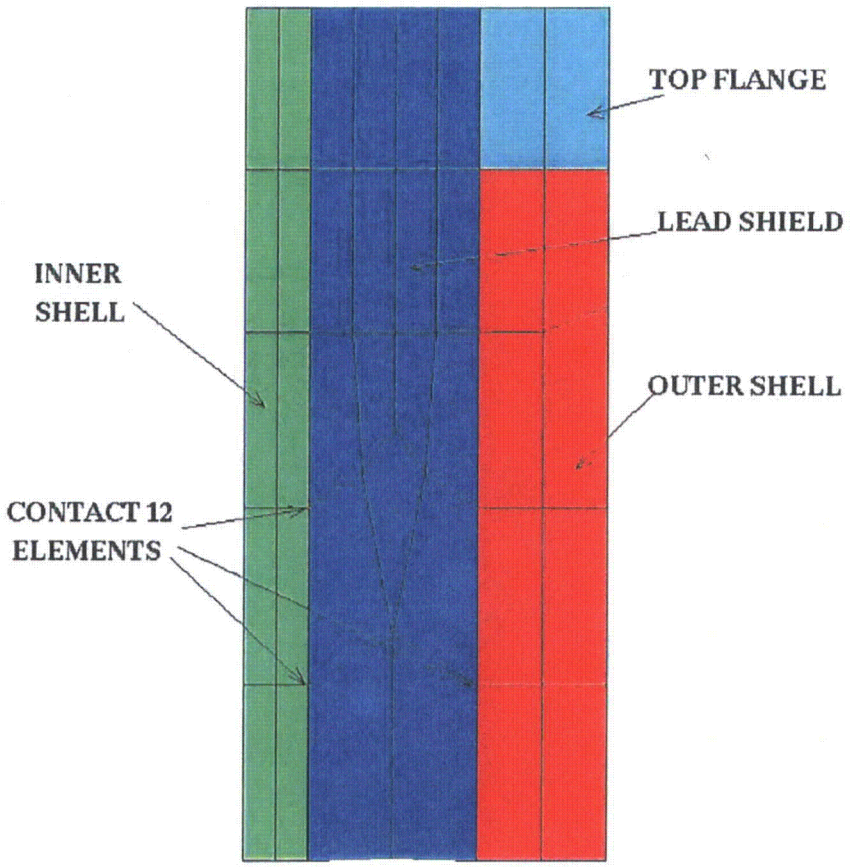

Figure 2.10.10-24: Details of Region 2

Figure 2.10.10-24 shows the details of the assembly in region 2. The transition 2 to 4 elements in the lead shield can be seen. This is done to accommodate the detailed mesh near the top flange. The lead shield is isolated from the inner shell, outer shell and the flanges using CONTACT12 elements. Some locations of the CONTACT12 elements are also shown. This region is very similar to the 3D mesh.

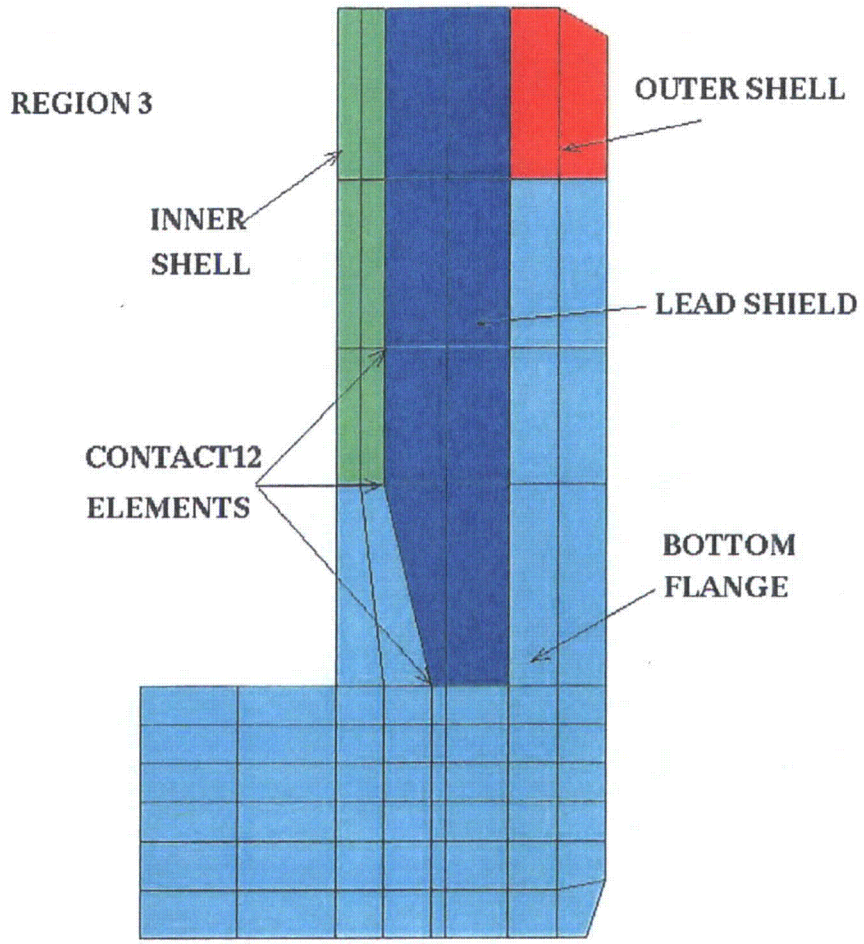

Figure 2.10.10-25: Region 3 Showing Finite Element Idealization near the Bottom Flange

A detailed view of the finite element idealization near the bottom flange is shown in Figure 2.10.10-25. Also shown are some of the CONTACT12 elements that separate the lead shield and the rest of the structure. The taper in the lead shield near the bottom has been retained from its 3D counterpart. All four noded elements are axisymmetric PLANE42 from the ANSYS finite element library.

CONTACT12 elements and bolted joint connecting the ram cover to the bottom flange are shown in figures 2.10.10-26a and b. This is the area marked Region 4 in Figure 2.10.10-22. The axial and radial contact locations (CONTACT12) are indicated in Figure 2.10.10-26a. The transparent mesh of figure 2.10.10-26b shows the details of the LINK1 assembly used in the bolted joint idealization, which is similar to the lid/ top flange connection.

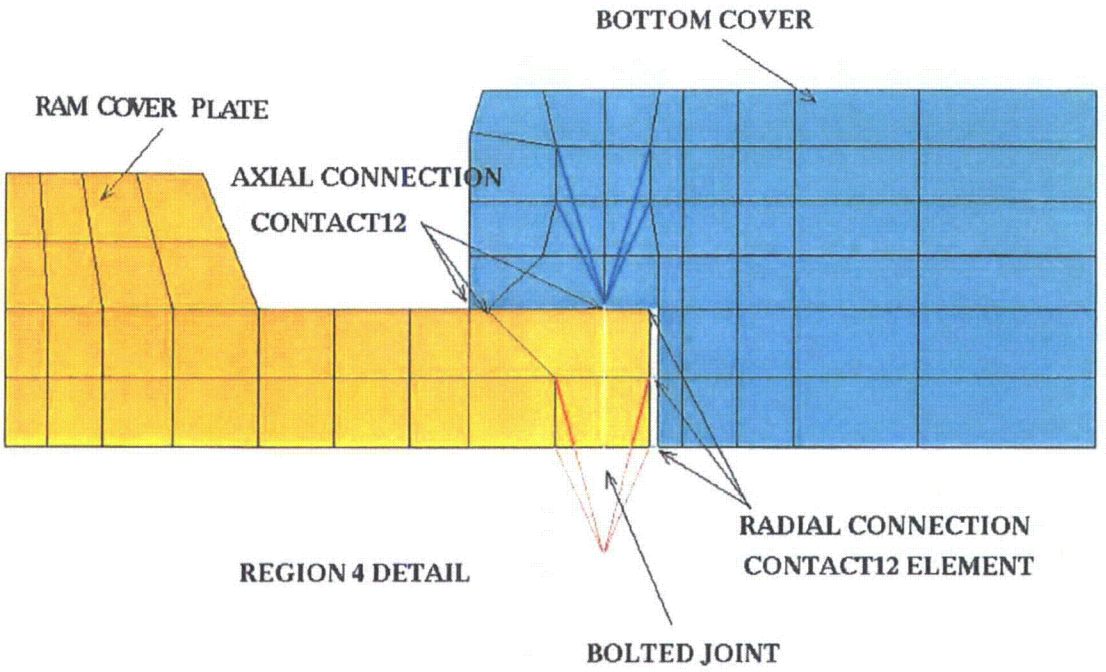

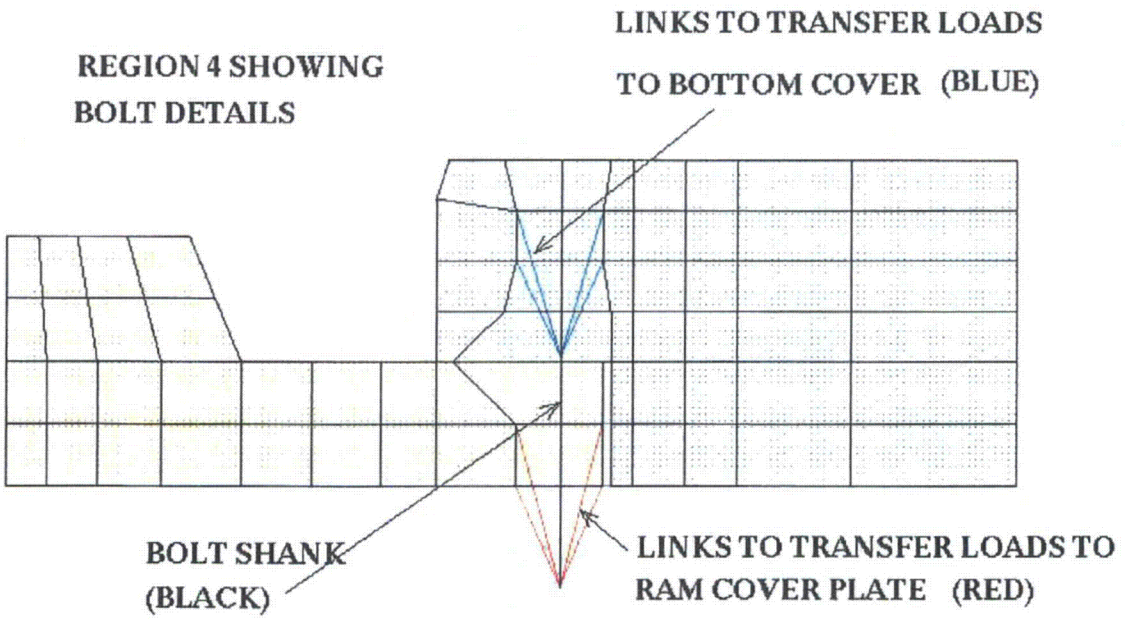

Figure 2.10.10-26a & b: Region 4 Showing Ram Cover, Bottom Flange Detail

2.10.10.5 Review of 2D FEM Warning Elements

An elements check command yielded two sets of warnings.

1. All CONTACT12 elements not coincident gave the warning:

    i. "Nodes I and J of element (CONTAC12) are not coincident".

2. The three PLANE42 warning elements (Region 1) are shown in Figure 2.10.10-27. The warning messages as follows:

    i. "Quadrilateral element has a pair of opposite edges that are 95.83 degrees away from being parallel. This exceeds the warning limit of 70 degrees."
    ii. "Quadrilateral element has an angle between adjacent edges of 162 degrees, which exceeds the warning limit of 155 degrees."
    iii. "Quadrilateral element has a pair of opposite edges that are 95.7 degrees away from being parallel. This exceeds the warning limit of 70 degrees."
    iv. "Quadrilateral element has an angle between adjacent edges of 161.7 degrees, which exceeds the warning limit of 155 degrees. "

Since the 3 warning elements are in a localized region and stress results are not critical at this region, therefore the elements warning are deemed acceptable based on Engineering judgment.

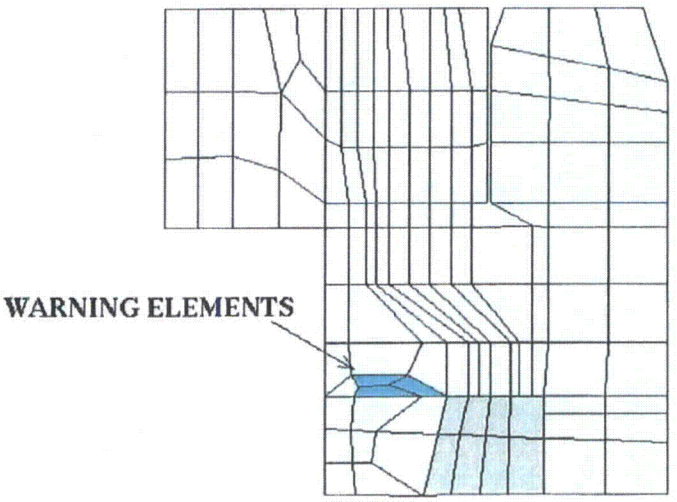

Figure 2.10.10-27: Warning Elements (Region 1) in Top Flange Area

2.10.10.6 Maximum Component Stress Evaluation

2.10.10.6.1 Approach

This section evaluates the maximum stresses that occur in each major component of the NUHOMS®-MP197 Transport Cask during all normal and hypothetical accident conditions of transport.

This analysis employs the same finite element model, loading conditions and results described in SAR Appendix 2.10.1. No new finite element analysis runs are made for this section. This analysis provides a more detailed evaluation of the stress analysis results generated in SAR Appendix 2.10.1. In particular, the maximum stress and the overall stress distribution in each major component of the transport cask are extracted from the ANSYS results for each normal and hypothetical accident condition load combination. The overall stress distributions are plotted, and the maximum component stresses and are tabulated and compared to allowable values.

The NUHOMS®-MP197 Transport Cask is separated into the following three major components, for stress reporting purposes.

HUOMS®-MP197 Transport Cask Components

Component	Material
Lid	SA-693 Type 630 H1100
Body Containment (Bottom Plate, Ram Port Cover, Flange, and Inner Shell)	SA-240 Type XM-19
Outer Shell	SA-240 Type 316

An element plot of each major component listed above is provided in Figures 2.10.10-28, 2.10.10-29, and 2.10.10-30 of this Appendix.

For each load combination the maximum stress in each of these components is extracted from the result files and compared to the allowable values for each material.

The load combinations evaluated (runs 13 through 42) are described in SAR Appendix 2.10.1 and listed in Tables 2.10.10-2 and 2.10.10-3 of this Appendix. These load combinations are generated through the combination of the twelve individual loads also described in SAR Appendix 2.10.1 and listed in Table 2.10.10-1 of this Appendix.

2.10.10.6.2 Stress Reporting Methodology for 3-Dimensional Model

Within the 3-dimensional finite element model there are a few locations where boundary conditions or contact elements generate spurious local high stresses. When reporting the component maximum stresses, the elements at the following locations are unselected so that the unrealistic stresses are not reported. Stresses at these unselected locations are evaluated separately.

Point Displacement Boundary conditions

For several loading conditions, a displacement boundary condition was placed on a single node of the large 3D model. This boundary condition is used to react any unbalanced global forces in the model. Because of the complicated three-dimensional nature of the finite element model, it is difficult to balance global forces and accelerations perfectly. Consequently, small residual unbalanced forces act as a point load at the support location. This type of loading generates extremely high and localized stresses that are fictitious. In order to eliminate this incorrect stress, elements attached to the supported node are unselected.

Contact Elements

Node-to-node contact elements are used at the intersection between the top surface of the transport cask flange and the bottom surface of the lid. Due to the their nonlinear and node-to-node nature, these elements can sometimes generate unrealistic bearing stresses. This is because they do not evenly distribute the reaction forces generated between the flange and the lid evenly. Also, since link elements are used to model the closure lid bolts, the modeled bolts are only capable of generating tensile forces and not bending moments. Consequently the moments in the lid generated during load cases such as the end drop or corner drop on the lid, must be reacted by concentrated forces couple in the lid bolts and flange. Therefore, additional unrealistic bearing forces are generated in the flange. For these reasons, elements attached to the contact elements are unselected, so that no spurious stresses are reported. The bearing stresses on the top surface of the flange and shear stress in flange thread are evaluated by hand calculation separately in Section 2.10.10.7 of this Appendix.

Bearing Block

Under certain loading conditions, such as rail car shock and vibration, the transport cask model is supported in the longitudinal direction at the shear key. Axial displacement boundary conditions are placed on a few nodes on the inner surface of the bearing block. This boundary condition is relatively localized, and results in unreasonably high local stresses. Consequently, the bearing block elements are unselected. A separate hand calculation, in SAR Section 2.5.2, evaluates the stresses in the bearing block and in the outer shell.

2.10.10.6.3 Results

For each load combination listed in Tables 2.10.10-2 and 2.10.10-3 of this Appendix, the maximum stress intensity for each component is extracted from the result files. These stress intensities are listed in Tables 2.10.10-4 and 2.10.10-5 of this Appendix for normal and hypothetical accident condition load combinations respectively. A stress intensity plot is also provided for each load case in order to give an overall description of the stress distribution throughout the transport cask (see Figures 2.10.10-31 through 2.10.10-60 of this Appendix)

The maximum component nodal stress intensities are compared to the allowable membrane stress intensity given in SAR Appendix 2.10.1. If the maximum nodal stress intensity exceeds the membrane allowable, the nodal stresses are linearized through the thickness of the component. Both linearized membrane and membrane plus bending stress intensities are then reported and compared to allowable membrane and membrane plus bending stress intensities respectively (see Table 2.10.10-4 and 2.10.10-5 of this Appendix). For all load combinations, the maximum stresses in the NUHOMS-61B transport Cask are less than their corresponding allowable stresses.

2.10.10.7 Evaluation of Bearing Stresses in Flange

2.10.10.7.1 Approach

The stress analysis of the NUHOMS®-MP197 Transport Cask for normal and accident conditions is described in SAR Appendix 2.10.1. The cask lid bolt and bolt head are represented with ANSYS LINK1 elements in 2D model and LINK8 in 3D model. The Link elements are uniaxial tension-compression elements with no bending capabilities. Also the thread connections between the bolt and flange were modeled by link elements. Since these links were modeled at a few nodes only, this resulted in high local stresses. The purpose of this evaluation is to calculate the flange thread shear stresses and lid / flange bearing stress based on the actual bolt engagement length and bearing area. The stress evaluation is conducted both for normal and accident conditions.

Link elements are adequate to transfer axial tension or compression loads. However, since they are connected between a few nodes of the model to simulate flange-thread connection, it resulted in high local flange stresses at the connection nodes. In reality, the bolt thread connection is continuous at the thread contact. Further, since link elements were not capable of taking any bending load, entire bending had to be resisted by the perforated lid and the flange. In order to obtain realistic results, the flange thread shear stress and lid / flange bearing stress are calculated here by using the actual thread geometry and the bearing areas. The bolt forces and the lid-flange contact forces, for the stress calculations are, however, taken from the ANSYS result files in Reference 3.

This calculation is based on the results of the ANSYS runs described in SAR Appendix 2.10.1. Therefore, assumptions used in that Appendix are also applicable to this evaluation. All material properties are taken from ASME B&PV Code Section II, Part D [2] at 300°F. The bolt hole areas are subtracted to obtain the net bearing area for the uniformly distributed loads.

2.10.10.7.2 Loading Conditions

All load combinations for the Normal and the Accident Conditions are listed in Tables 2.10.10-2 and 2.10.10-3 of this Appendix. A screening of all load combinations indicated that for the maximum flange thread shear stress and lid-flange bearing stress, it will suffice to analyze the following load combinations. The stress results from these selected load combinations will envelop the stress results from all load combinations.

Normal Conditions

A. Preload + Internal pressure (50 psi) + Thermal hot + Rail car Shock (Run 19)
B. Preload + Ext. pressure (25 psi) + Thermal cold + 1 ft. Drop on Lid end (Run 22)

Accident Conditions

C. Preload + Ext. pressure (25 psi) + Thermal cold + 30 ft. Drop on Lid end (Run 30)
D. Preload + Ext. pressure (25 psi) + Thermal cold + 30 ft. Drop on C.G.-Over-Corner (Run 36)

2.10.10.7.3 Normal Condition Stresses

In order to calculate the shear stresses the flange threads and flange bearing stresses, the maximum bolt force and contact forces for each load case are obtained using the ANSYS postprocessor with the appropriate result file.

A. Preload + Internal Pressure (50 psi) + Thermal Hot + Rail Car Shock

Maximum Shear Stress in Flange Threads

From the ANSYS results file, the maximum lid bolt force = 128,200 lb.

The cask flange (SA-240, Gr. XM-19, S_u = 100.0 ksi. at room temperature) threads have helicoil inserts (1185-24CN-2250) of Type 304, stainless steel wire (ultimate strength at room temperature is 200 to 250 ksi, [3]). The lid bolts are constructed from SA-540 Gr. B24 (S_u = 165 at room temperature). The flange material is, therefore, weaker than the helicoil and bolt materials.

A_n = shear area of internal threads = $3.1416\, nL\, D_{s\,min}\, [1/(2n) + .57735(D_{s\,min} - E_{n\,max})]$[4]

For the tapped hole for Helicoil insert connection:

$E_{n\,max}$ = maximum pitch diameter of internal threads = 1.6177 in. [3]
$D_{s\,min}$ = minimum major diameter of external threads = 1.702 in. [3]
L = engagement length = 2.25 in.
n = threads/inch = 6

Therefore,

$A_n = 3.1416(6)(2.25)(1.702)[1/(2\times6) + .57735\,(1.702 - 1.6177)] = 9.528$ in.^{2}
Max. Shear Stress = 128,200/9.528 = 13,455 psi.

For SA-240, Gr. XM-19, S_m = 31.4 ksi. at 300°F. Therefore, the allowable shear stress = $0.6S_m$ = 0.6 (31.4) = 18.84 ksi. > 13.46 ksi ... o.k.

Bearing Stress between Flange and Lid

From the ANSYS results file for run 19, the total contact force on the 180° model = 2,797,309 lbs. This total force is computed by summing all normal forces in the contact elements between the flange and the lid. Therefore, the contact force for full lid and flange = 2 × 2,797,309 = 5,594,618 lbs.

From SAR Appendix 2.10.2, the lid-bolt preload (maximum torque) = 120,800 lbs. Therefore, the total bolt force = 48 × 120,800 = 5,798,400 lbs. Thus, there is only a small loss of preload contact force due to pressure, thermal and rail car shock loads, and the contact forces are quite uniformly distributed over the entire flange-lid bearing area.

The bearing area is computed between the lid shoulder diameter (72.31 in.) and the flange diameter (68.42 in.). 48-lid bolt half-hole areas are subtracted to get the net bearing area.

$$\text{Net Bearing Area} = \pi/4\,(72.31^2 - 68.42^2) - \pi/4 \times \tfrac{1}{2}\,(1.69^2) \times 48$$
$$= 429.959 - 53.836 = 376.123 \text{ in.}^2$$

Bearing Stress = 5,594,618 / 376.123 = 14,874 psi

The flange is constructed from SA-240, Gr. XM-19, which has a larger yield strength than that of the lid (SA-705, Type 630).

Allowable Bearing Stress = S_y, Flange = 43.3 ksi. > 14.87 ksi ... o.k.

B. Preload + External Pressure (25 psi) + Thermal Cold + 1 Foot Lid Drop

Maximum Shear Stress in Flange Threads

From the ANSYS results file (Run 22), the lid bolt force in 48 bolts = 5,920,600 lb. Therefore, the force in one bolt = 5,920,600/48 = 123,346 lb.

Thread Shear Area = 9.528 in.^{2}
Shear Stress = 123,346/9.528 = 12,946 psi.

Allowable Shear Stress = $0.6S_m$ = 0.6 (31.4) = 18.84 ksi. > 12.95 ksi ... o.k.

Bearing Stress between Flange and Lid

From the ANSYS results file for run 22, the total contact force = 5,994,840 lbs.

Net Bearing Area = 376.123 in.^{2}
Bearing Stress = 5,994,840 / 376.123 = 15,939 psi

Allowable Bearing Stress = S_y, Flange = 43.3 ksi. > 15.94 ksi ... o.k.

2.10.10.7.4 Accident Condition Stresses

C. Preload + External Pressure (25 psi) + Thermal Cold + 30 Foot Lid Drop

Maximum Shear Stress in Flange Threads

From the ANSYS results file, the lid bolt force in 48 bolts = 5,950,400 lb. Therefore, the force in one bolt = 5,950,400/48 = 123,967 lb.

Thread Shear Area = 9.528 $in.^2$
Shear Stress = 123,967/9.528 = 13,011 psi

Allowable Shear Stress = 0.42 S_u = 0.42 (94.2) = 39.56 ksi. > 13.01 ksi ... o.k.

Bearing Stress between Flange and Lid

From the ANSYS results file for run 30, the total contact force = 6,006,630 lbs.

Net Bearing Area = 376.123 in
Bearing Stress = 6,006,630 / 376.123 = 15,970 psi.

Allowable Bearing Stress = S_u, Flange = 94.2 ksi. > 15.97 ksi... o.k.

D. Preload + External Pressure (25 psi) + Thermal Cold + 30 ft. CG Over Corner Drop

Maximum Shear Stress in Flange Threads

From the ANSYS results file (Run 19), the maximum lid bolt force = 174,790 lb.

Thread Shear Area = 9.528 in^2
Max. Shear Stress = 174,790/9.528 = 18,345 psi.

Allowable Shear Stress = 0.42S_u = 0.42 (94.2) = 39.56 ksi. > 18.35 ksi... o.k.

Bearing Stress between Flange and Lid

From the ANSYS results file for run 19, the total contact force on the 180° model = 8,563,485 lbs. Therefore, the contact force for full lid and flange = $2 \times 8{,}563{,}485 = 17.127 \times 10^6$ lb.

Due to the nature of the CG over corner drop event, this contact force is comprised of the following two components.

- A uniform distributed force due to the bolt preload and the 25 psi external pressure load.
- A non-uniform contact force due to the corner dorp impact acceleration forces.

The uniform distributed force acts on the entire net bearing area while the non-uniform force is assumed to be distributed only on half of the net bearing area.

Uniform Distributed Load Bearing Stress:

Total Bolt Preload Force = $120{,}840 \times 48 = 5.800 \times 10^6$ lb. (Appendix 2.10.2)
25 psi. Pressure Force (on 74.68" diameter Lid) = $\pi/4\ (74.68^2) \times 25 = 0.109 \times 10^6$ lb.
Total Uniform Bearing Load = $5.800 \times 10^6 + 0.109 \times 10^6 = 5.909 \times 10^6$ lb.
Bearing Stress = 5.909×10^6 / 376.123 = 15,710 psi.

Non- Uniform Load Bearing Stress:

The non-uniform contact load is the difference between the total contact force from the ANSYS results file and the uniformly distributed force computed above.

Non-Uniform Bearing Force = $17.127 \times 10^6 - 5.909 \times 10^6 = 11.218 \times 10^6$ lb.
Bearing Area = 50% (376.123) = 188.06 in^2
Bearing Stress = 11.218×10^6 / 188.06 = 59,651 psi.

Total Bearing Stress = 15,710 + 59,651 = 75,361 psi.

Allowable Bearing Stress = S_u, Flange = 94.2 ksi > 75.36 ksi... o.k.

2.10.10.7.5 Conclusion

From the above analysis, it is concluded that the maximum shear stresses in the flange threads and the maximum bearing stresses between lid and flange are within the code allowables for normal and accident load conditions. Consequently, the NUHOM®-MP197 lid and flange connection is structurally adequate.

2.10.10.8 References

1. ANSYS Computer Code and User's Manuals, Volumes 1-4, Rev. 5.6.
2. American Society of Mechanical Engineers, ASME Boiler and Pressure Vessel Code, Section II, Part D, 1998, including 1999 Addenda.
3. Helicoil Catalog, Bulletin 1000, Rev.4/98,"Screw Thread Inserts, Inch Series, Design & Production Manual".
4. Machinery Handbook, 21st Edition, Industrial Press, 1979.

Table 2.10.10-1
Individual Load Conditions

Run No.	Applicable Individual Loads	Load Used in Run
1	Bolt preload	-
2	Internal pressure	50 psig
3	External pressure	25 psig
4	Thermal stresses in 100°F hot ambient environment	-
5	Thermal stresses at –20° F cold ambient environment	-
6	3G lifting	3G
7	Rail Car Shock loads	4.7G – all directions
8	Rail car vibration loads	0.37G – vertical 0.19G –lateral 0.19G – longitudinal
9	1 foot end drop on lid end	30 G
10	1 foot end drop on bottom end	30 G
11	1 foot side drop	30 G
12	1G gravity loading	1 G

Table 2.10.10-2
Normal Condition Load Combinations

Run No.	Load Combination	Applicable Individual Loads Applied in the ANSYS Model								
		Bolt Pre-load	Gravity 1g	Int. Pres.	Ext. Pres.	Thermal Hot	Thermal Cold	Thermal -40°F Uniform	Rail Car Vib.	Rail Car shock
13	Hot Environment (100° F amb.)	x	x	x		x				
14	Cold Environment (-40° F amb.)	x	x		x			x		
15	Increased External Pressure	x	x		x		x			
16	Min. External Pressure	x	x	x		x				
17	Rail Car Vibration	x		x		x			x	
18		x			x		x		x	
19	Rail Car Shock	x		x		x				x
20		x			x		x			x

Run No.	Load Combination	Applicable Individual Loads Applied in the ANSYS Model							
		Bolt Pre-load	Internal Pres. (50 psi)	External Pres. (25 psi)	Thermal Hot	Thermal Cold	Lid End Drop	Bottom End Drop	Side drop
21	1 Ft End Drop on Lid End	x	x		x		x		
22		x		x		x	x		
23	1 Ft End Drop on Bottom End	x	x		x			x	
24		x		x		x		x	
25	1 Ft Side Drop	x	x		x				x
26		x		x		x			x

Table 2.10.10-3
Hypothetical Accident Condition Load Combinations

Run No.	Load Combination	Applicable Individual Loads Applied in the ANSYS Model							
		Bolt Pre-Load	Int. Pres. (50 psi)	Ext. Pres. (25 psi)	Thermal Hot	Thermal Cold	Lid End Drop	Bot. End Drop	Side Drop
27	30 Ft. End Drop on Bottom End	x	x		x			x	
28		x		x		x		x	
29	30 Ft. End Drop on Lid End	x	x		x		x		
30		x		x		x	x		
31	30 Ft. Side Drop	x	x		x				x
32		x		x		x			x

Run No.	Load Combination	Applicable Individual Loads Applied in the ANSYS Model							
		Bolt Pre-Load	Int. Pres. (50 psi)	Ext. Pres. (25 psi)	Thermal Hot	Thermal Cold	Corner Drop Lid End	Corner Drop Bot End	Oblique Drop Lid End
33	30 Ft. CG Over Corner Drop on Bottom End	x	x		x			x	
34		x		x		x		x	
35	30 Ft. CG Over Corner Drop on Lid End	x	x		x		x		
36		x		x		x	x		
37	30 Ft. 20° Oblique Impact on Lid End	x	x		x				x
38		x		x		x			x

Table 2.10.10-3
Hypothetical Accident Condition Load Combinations
(Continued)

Run No.	Load Combination	Applicable Individual Loads Applied in the ANSYS Model						
		Bolt Pre-load	Int. Pres. (50 psi)	Ext. Pres. (25 psi)	Thermal Hot	Thermal Cold	Oblique Drop Lid End	Oblique Drop Bottom End
39	30 Ft. 20° Oblique Impact on Bottom End	x	x		x			x
40		x		x		x		x

Run No.	Load Combination	Applicable Individual Loads Applied in the ANSYS Model						
		Bolt Pre-load	Int. Pres. (50 psi)	Ext. Pres. (25 psi)	Thermal Hot	Thermal Cold	Immersion Ext. Pres. (290 psi)	Fire
41	Immersion (290 psi)	x				x	x	
42	Fire Accident	x	x					x

Table 2.10.10-4
Maximum Component Stresses for Normal Conditions

Run No.	Description	Location	Maximum Stress Intensity (ksi)	Stress Type	Allowable Stress (ksi)**	Linearized nodes	Figure
13	Hot Environment (100° F amb.)	Lid	30.5	$P_m + P_b$	46.7		2.10.10-31
		Body Containment	17.7	$P_m + P_b$	31.4		
		Outer Shell	14.8	$P_m + P_b$	20.0		
14	Cold Environment (-40° F amb.)	Lid	27.9	$P_m + P_b$	46.7		2.10.10-32
		Body Containment	13.2	$P_m + P_b$	31.4		
		Outer Shell	12.3	$P_m + P_b$	20.0		
15	Increased External Pressure	Lid	27.5	$P_m + P_b$	46.7		2.10.10-33
		Body Containment	13.7	$P_m + P_b$	31.4		
		Outer Shell	12.5	$P_m + P_b$	20.0		
16	Min. External Pressure	Lid	30.5	$P_m + P_b$	46.7		2.10.10-34
		Body Containment	17.7	$P_m + P_b$	31.4		
		Outer Shell	14.8	$P_m + P_b$	20.0		
17	Rail Car Vibration, Hot Environment	Lid	30.3	$P_m + P_b$	46.7		2.10.10-35
		Body Containment	17.4	$P_m + P_b$	31.4		
		Outer Shell	15.2	$P_m + P_b$	20.0		
18	Rail Car Vibration, Cold Environment	Lid	27.2	$P_m + P_b$	46.7		2.10.10-36
		Body Containment	14.0	$P_m + P_b$	31.4		
		Outer Shell	12.9	$P_m + P_b$	20.0		
19	Rail Car Shock, Hot Environment	Lid	36.3	$P_m + P_b$	46.7		2.10.10-37
		Body Containment	26.0	$P_m + P_b$	31.4		
		Outer Shell	10.4	P_m	20.0	67 – 78	
			20.3	$P_m + P_b$	30.0		
20	Rail Car Shock, Cold Environment	Lid	33.6	$P_m + P_b$	46.7		2.10.10-38
		Body Containment	24.3	$P_m + P_b$	31.4		
		Outer Shell	12.0	P_m	20.0	76 – 78	
			20.3	$P_m + P_b$	30.0		
21	1 Ft Lid End Drop, Hot Environment	Lid	12.4	$P_m + P_b$	46.7		2.10.10-39
		Body Containment	20.2	$P_m + P_b$	31.4		
		Outer Shell	13.7	$P_m + P_b$	20.0		
22	1 Ft Lid End Drop, Cold Environment	Lid	12.6	$P_m + P_b$	46.7		2.10.10-40
		Body Containment	18.6	$P_m + P_b$	31.4		
		Outer Shell	11.6	$P_m + P_b$	20.0		
23	1 Ft Bottom End Drop, Hot Environment	Lid	12.3	$P_m + P_b$	46.7		2.10.10-41
		Body Containment	17.1	$P_m + P_b$	31.4		
		Outer Shell	13.8	$P_m + P_b$	20.0		
24	1 Ft Bottom End Drop, Cold Environment	Lid	14.0	$P_m + P_b$	46.7		2.10.10-42
		Body Containment	18.8	$P_m + P_b$	31.4		
		Outer Shell	11.7	$P_m + P_b$	20.0		
25	1 Ft Side Drop, Hot Environment	Lid	38.3	$P_m + P_b$	46.7		2.10.10-43
		Body Containment	20.3	P_m	31.4	281 – 276	
			33.5	$P_m + P_b$	47.1		
		Outer Shell	17.7	P_m	20.0	6,496 – 6500	
			28.2	$P_m + P_b$	30.0		
26	1 Ft Side Drop, Cold Environment	Lid	33.9	$P_m + P_b$	46.7		2.10.10-44
		Body Containment	21.1	P_m	31.4	281 – 176	
			35.0	$P_m + P_b$	47.1		
		Outer Shell	16.9	P_m	20.0	6,496 – 6,500	
			27.2	$P_m + P_b$	30.0		

**These are membrane stress intensity (P_m) allowables except where the stresses are linearized through the thickness, then P_m is compared to the P_m allowable and $P_m + P_b$ is compared to the $P_m + P_b$ allowable.

Table 2.10.10-5
Maximum Component Stresses for Accident Conditions

Run No.	Description	Location	Maximum Stress Intensity (ksi)	Stress Type	Allowable Stress (ksi)	Linearized nodes	Figure
27	30 Ft. End Drop on Bottom End, Hot Environment	Lid	16.5	$P_m + P_b$	98.0		2.10.10-45
		Body Containment	24.3	$P_m + P_b$	65.94		
		Outer Shell	14.8	$P_m + P_b$	48.0		
28	30 Ft. Bottom End Drop, Cold Environment	Lid	18.9	$P_m + P_b$	98.0		2.10.10-46
		Body Containment	24.5	$P_m + P_b$	65.94		
		Outer Shell	12.5	$P_m + P_b$	48.0		
29	30 Ft. End Drop on Lid End, Hot Environment	Lid	11.9	$P_m + P_b$	98.0		2.10.10-47
		Body Containment	29.8	$P_m + P_b$	65.94		
		Outer Shell	15.7	$P_m + P_b$	48.0		
30	30 Ft. End Drop on Lid End, Cold Environment	Lid	14.3	$P_m + P_b$	98.0		2.10.10-48
		Body Containment	28.4	$P_m + P_b$	65.94		
		Outer Shell	13.5	$P_m + P_b$	48.0		
31	30 Ft. Side Drop, Hot Environment	Lid	40.7	$P_m + P_b$	98.0		2.10.10-49
		Body Containment	50.5	P_m	65.94	276 – 281	
			82.8	$P_m + P_b$	94.2		
		Outer Shell	31.2	P_m	48.0	274 – 278	
			37.9	$P_m + P_b$	72.0		
32	30 Ft. Side Drop, Cold Environment	Lid	44.8	$P_m + P_b$	98.0		2.10.10-50
		Body Containment	51.3	P_m	65.94	276 – 281	
			84.5	$P_m + P_b$	94.2		
		Outer Shell	33.0	P_m	48.0	274 – 278	
			39.8	$P_m + P_b$	72.0		
33	30 Ft. CG Over Bottom Corner Drop, Hot Environment	Lid	39.1	$P_m + P_b$	98.0		2.10.10-51
		Body Containment	61.6	P_m	65.94	15,999 – 16,152	
			92.0	$P_m + P_b$	94.2		
		Outer Shell	20.9	$P_m + P_b$	48.0		
34	30 Ft. CG Over Bottom Corner Drop, Cold Environment	Lid	31.5	$P_m + P_b$	98.0		2.10.10-52
		Body Containment	45.7	P_m	65.94	17,239 – 17,241	
			91.5	$P_m + P_b$	94.2		
		Outer Shell	19.0	$P_m + P_b$	48.0		
35	30 Ft. CG Over Lid Corner Drop, Hot Environment	Lid	6.0	P_m	98.0	13,692 – 14,046	2.10.10-53
			115.7	$P_m + P_b$	140.0		
		Body Containment	55.9	$P_m + P_b$	65.94		
		Outer Shell	20.8	$P_m + P_b$	48.0		
36	30 Ft. CG Over Lid Corner Drop, Cold Environment	Lid	7.3	P_m	98.0	17,733 – 14,125	2.10.10-54
			112.8	$P_m + P_b$	140.0		
		Body Containment	64.0	$P_m + P_b$	65.94		
		Outer Shell	17.9	$P_m + P_b$	48.0		
37	30 Ft. 20° Lid Oblique Impact, Hot Environment	Lid	23.8	P_m	98.0	18,494 – 18,486	2.10.10-55
			63.8	$P_m + P_b$	140.0		
		Body Containment	56.7	P_m	65.94	25,418 – 25,407	
			78.6	$P_m + P_b$	94.2		
		Outer Shell	45.5	P_m	48.0	2,825 – 3,065	
			59.9	$P_m + P_b$	72.0		

Table 2.10.10-5 (continued)
Maximum Component Stresses for Accident Conditions

Run No.	Description	Location	Maximum Stress Intensity (ksi)	Stress Type	Allowable Stress (ksi)		Figure
38	30 Ft. 20° Lid Oblique Impact, Cold Environment	Lid	25.7	P_m	98.0	18,494 – 18,499	2.10.10-56
			70.5	$P_m + P_b$	140.0		
		Body Containment	57.3	P_m	65.94	2,827 – 3,067	
			82.1	$P_m + P_b$	94.2		
		Outer Shell	47.8	P_m	48.0	2,825 – 3,065	
			62.6	$P_m + P_b$	72.0		
39	30 Ft. 20° Bottom Oblique Impact, Hot Environment	Lid	40.3	$P_m + P_b$	98.0		2.10.10-57
		Body Containment	46.7	P_m	65.94	7,427 – 7,422	
			72.0	$P_m + P_b$	94.2		
		Outer Shell	42.0	P_m	48.0	7,617 – 7,533	
			59.0	$P_m + P_b$	72.0		
40	30 Ft. 20° Bottom Oblique Impact, Cold Environment	Lid	30.6	$P_m + P_b$	98.0		2.10.10-58
		Body Containment	47.7	P_m	65.94	7,427 – 7,422	
			74.0	$P_m + P_b$	94.2		
		Outer Shell	43.2	P_m	48.0	7,617 – 7,533	
			60.4	$P_m + P_b$	72.0		
41	Immersion (290 psi)	Lid	17.3	$P_m + P_b$	98.0		2.10.10-59
		Body Containment	24.0	$P_m + P_b$	65.94		
		Outer Shell	9.6	$P_m + P_b$	48.0		
42	Fire Accident	Lid	24.3	$P_m + P_b$	98.0		2.10.10-60
		Body Containment	28.4	$P_m + P_b$	65.94		
		Outer Shell	39.2	$P_m + P_b$	48.0		

Figure 2.10.10-28
Lid Finite Element Plot

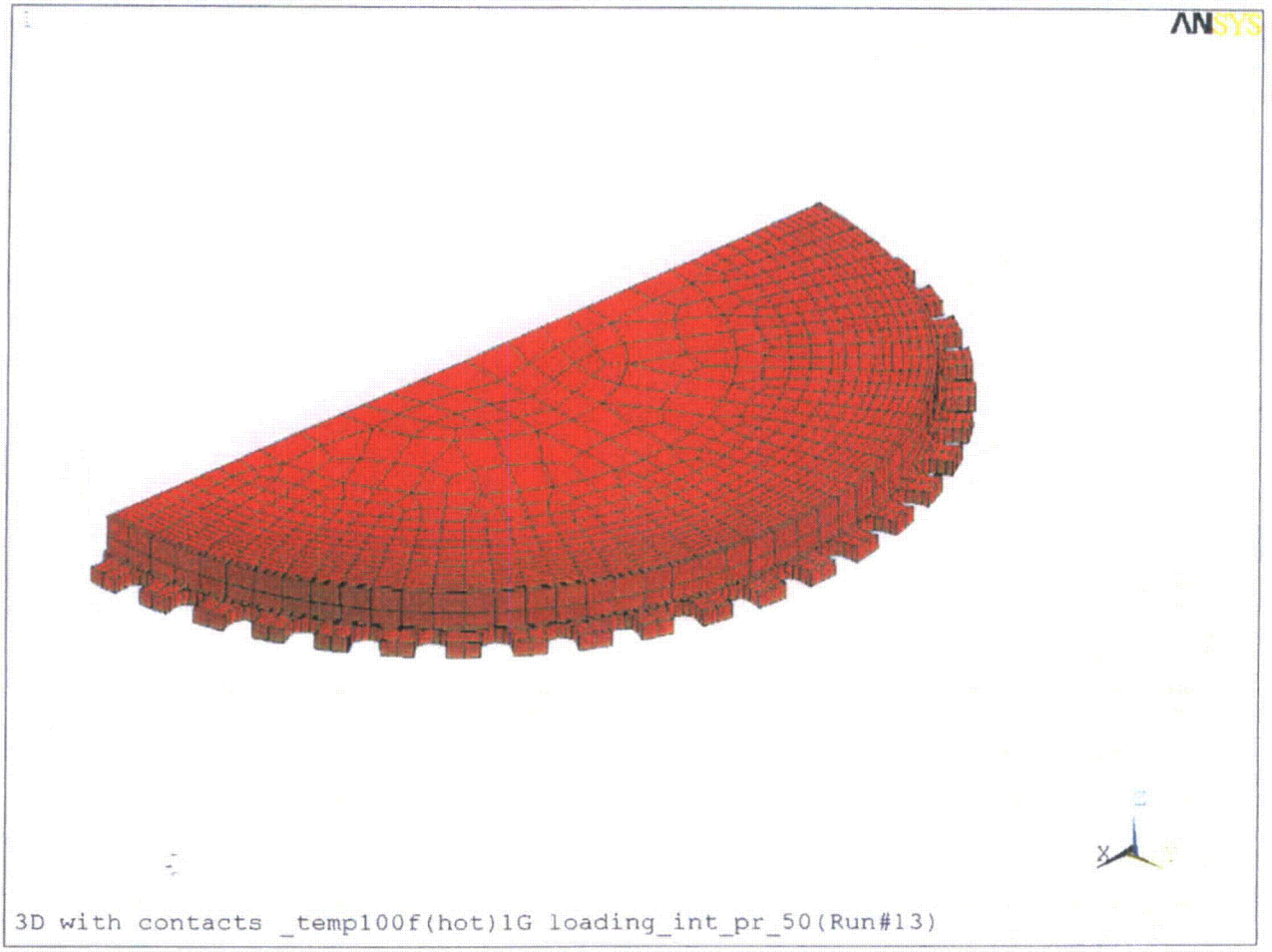

Figure 2.10.10-29
Containment Body Finite Element Plot

Figure 2.10.10-30
Outer Shell Finite Element Plot

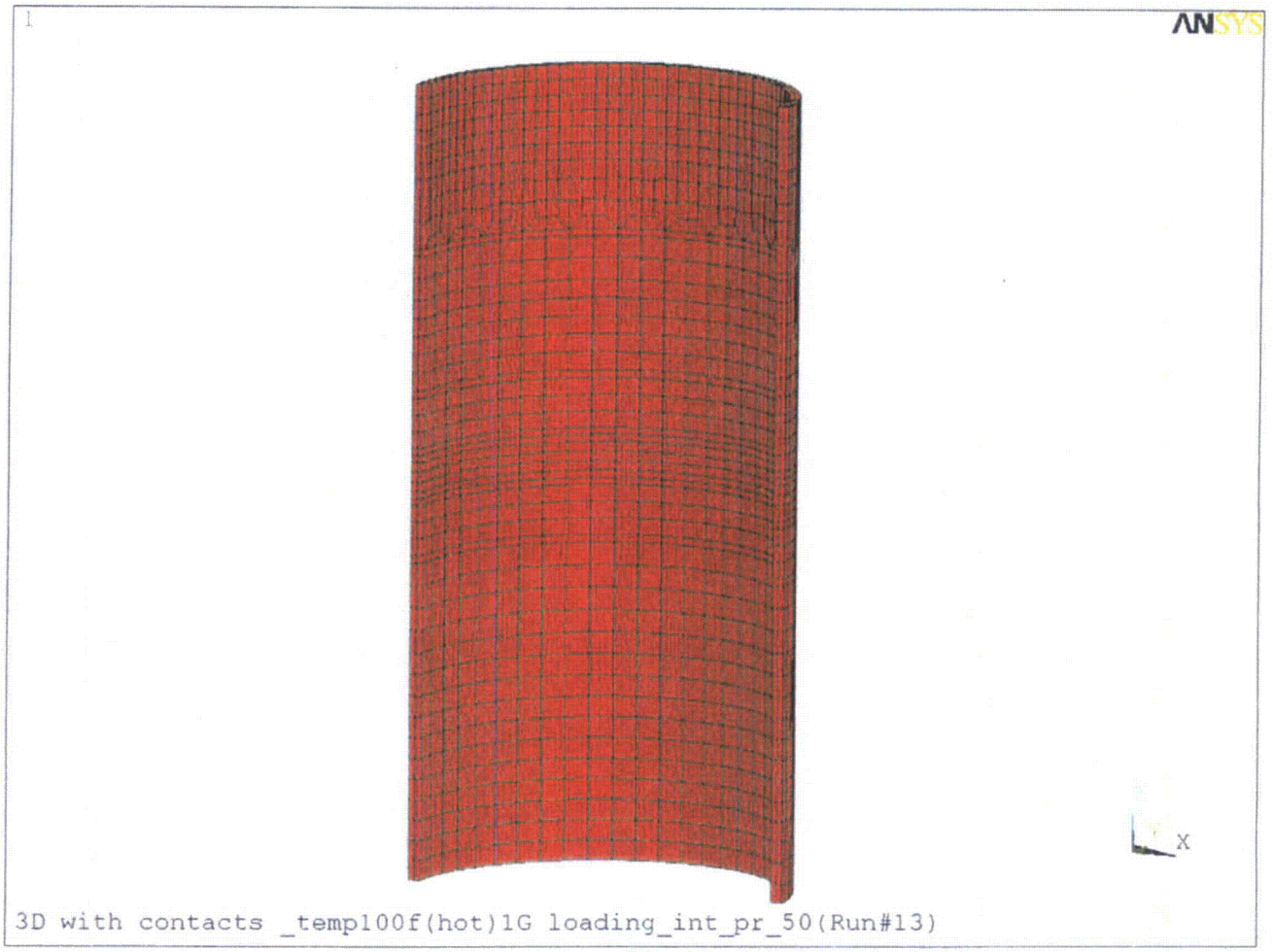

Figure 2.10.10-31
Run 13, Hot Environment (100°F ambient) Stress Intensity Plot

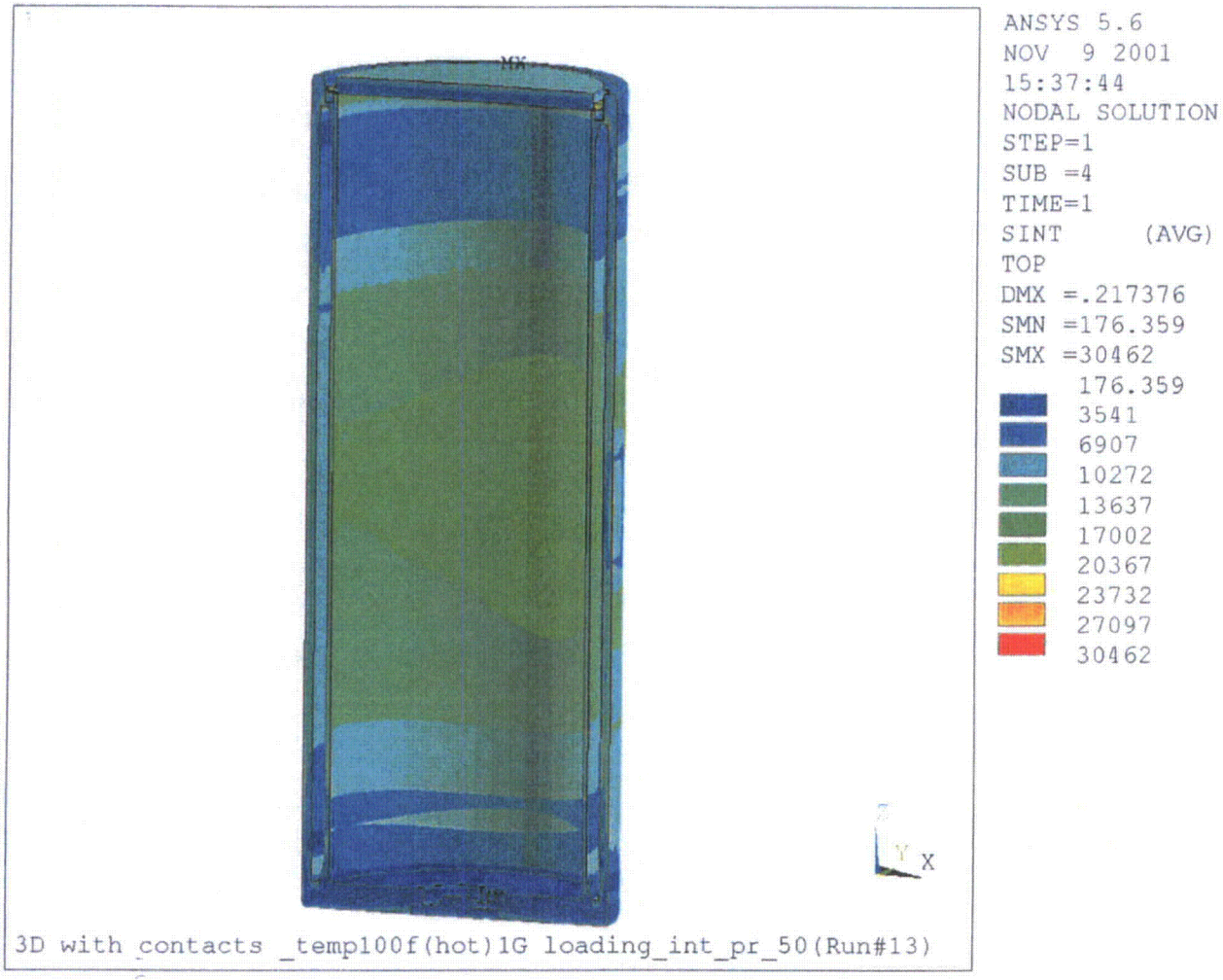

Figure 2.10.10-32
Run 14, Cold Environment (-40°F ambient) Stress Intensity Plot

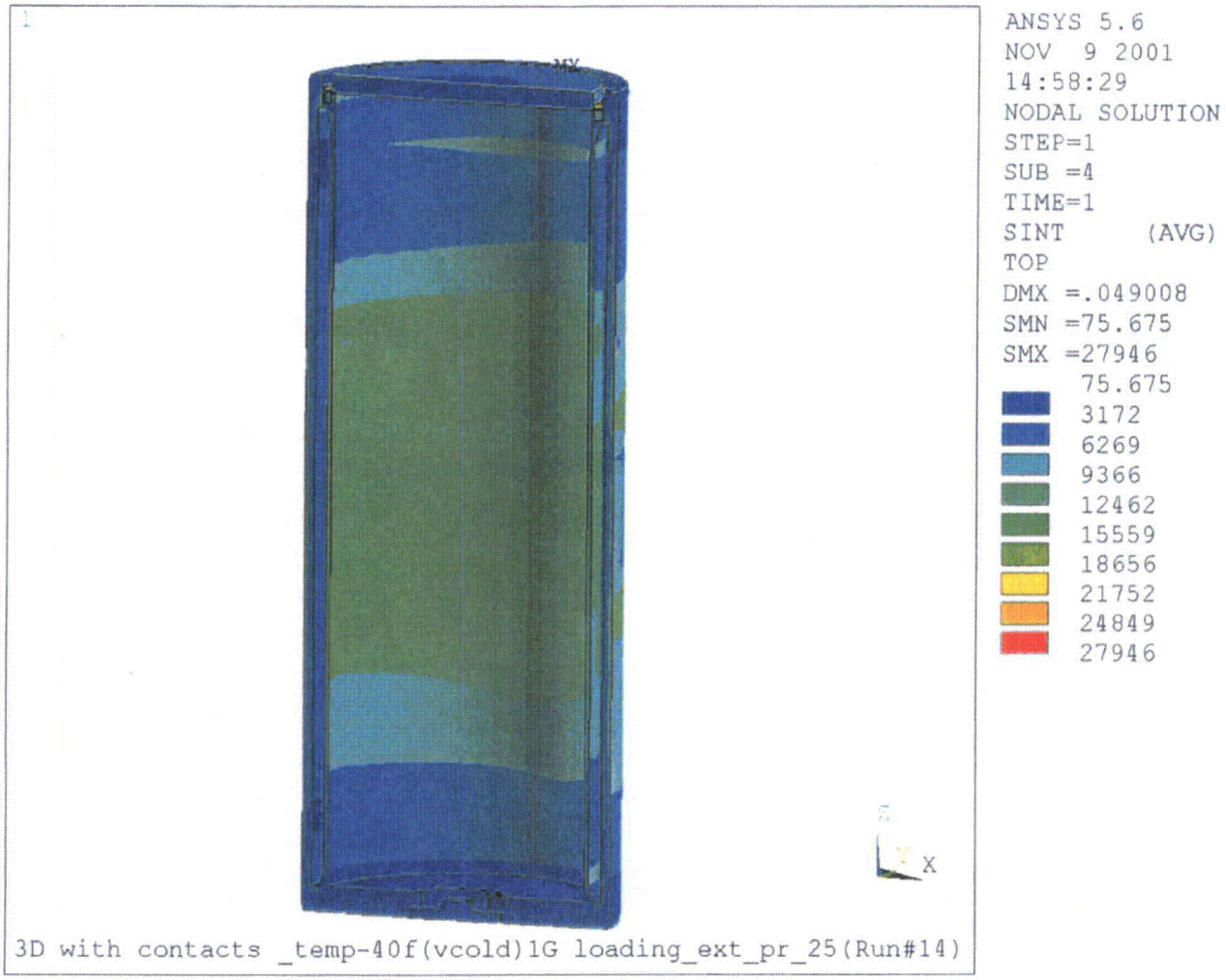

Figure 2.10.10-33
Run 15, Increased External Pressure Stress Intensity Plot

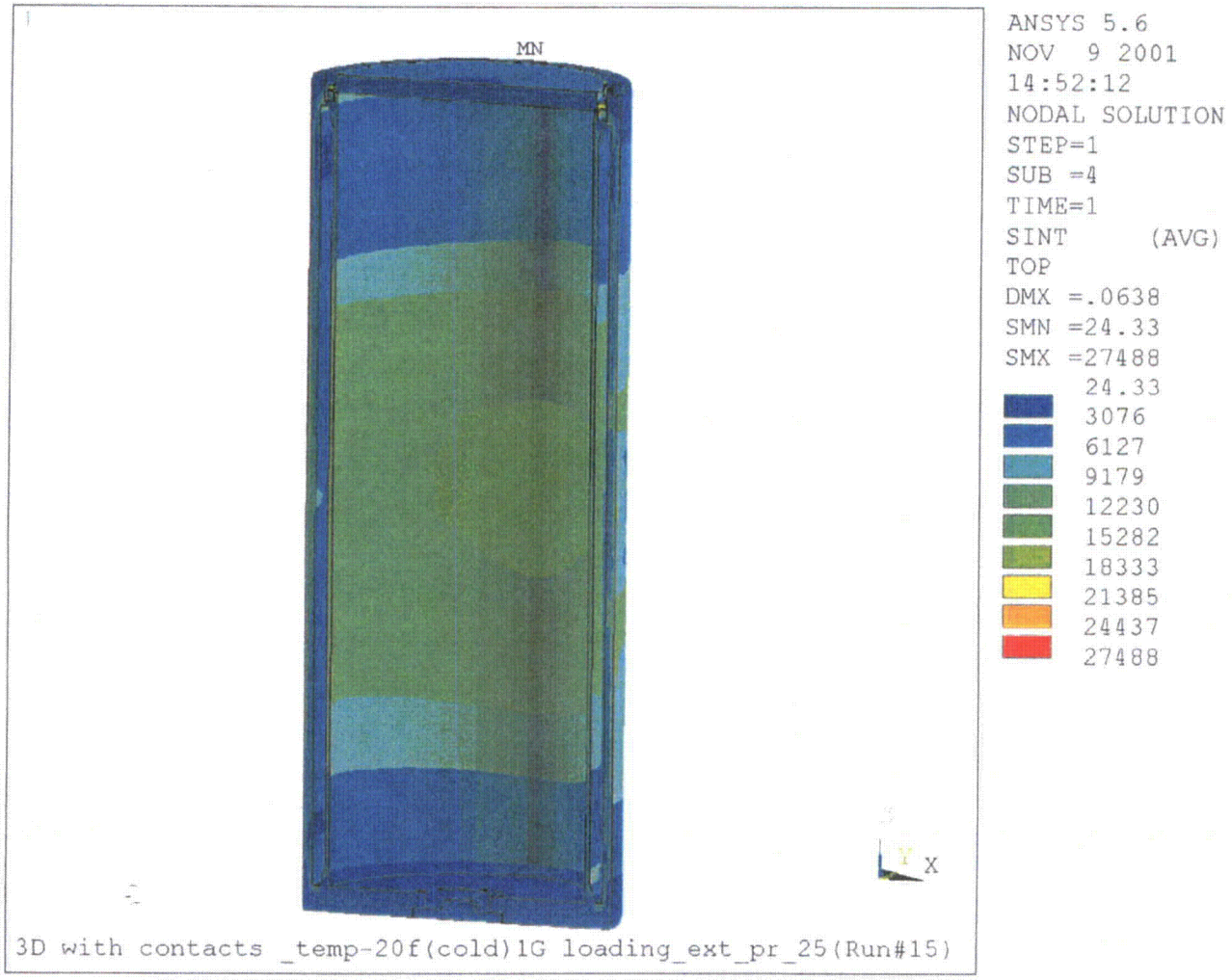

Figure 2.10.10-34
Run 16, Minimum External Pressure Stress Intensity Plot

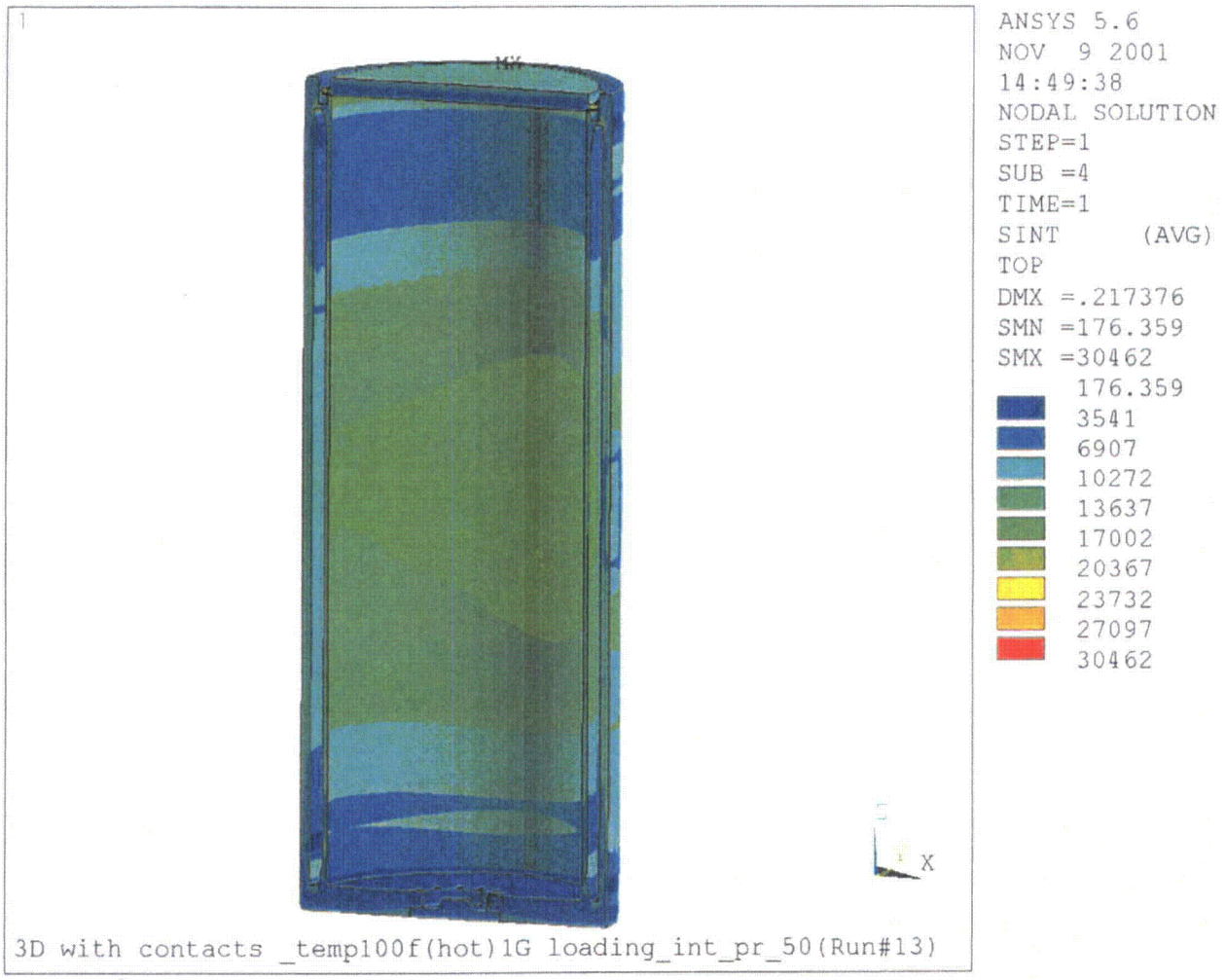

Figure 2.10.10-35
Run 17, Rail Car Vibration, Hot Environment Stress Intensity Plot

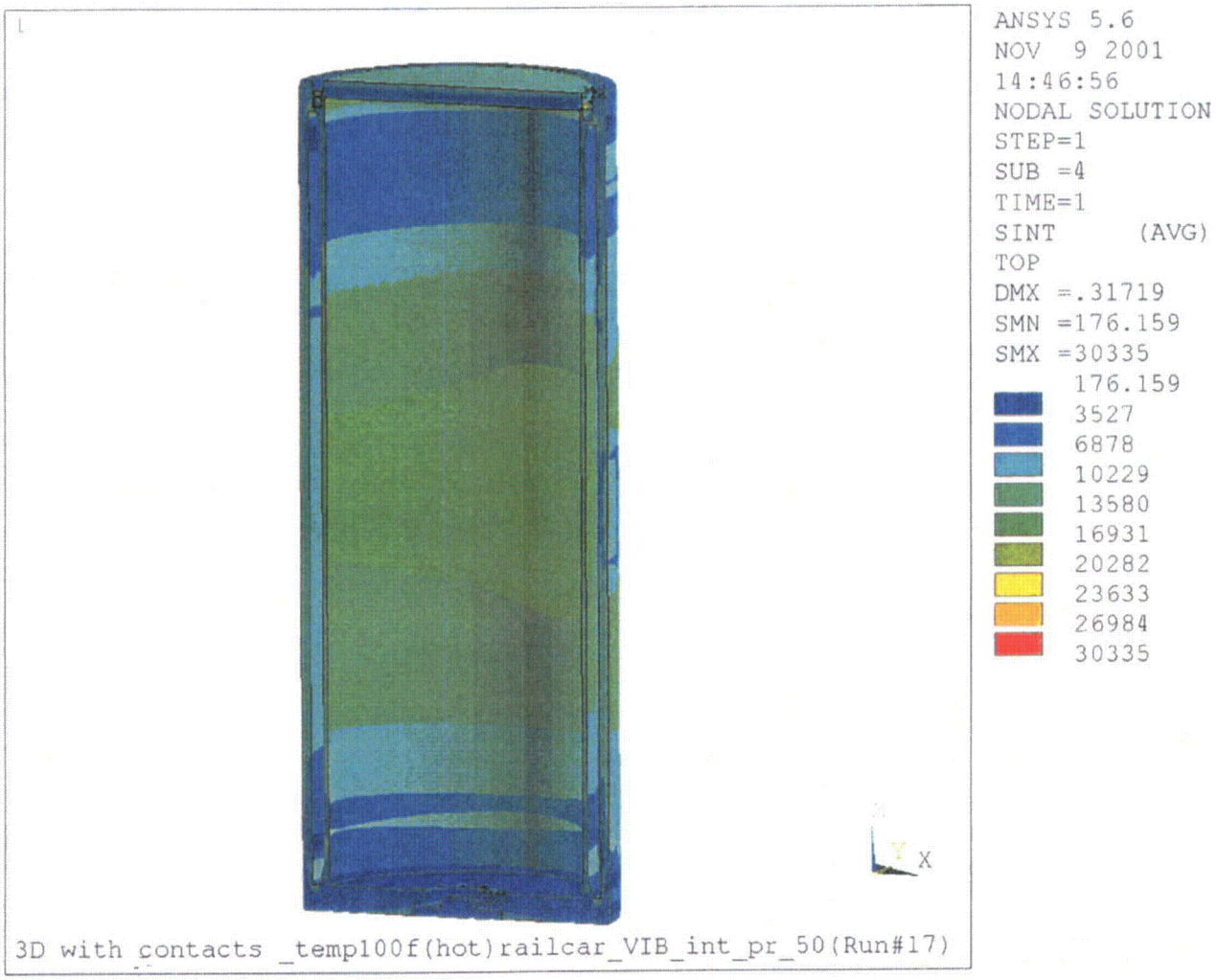

Figure 2.10.10-36
Run 18, Rail Car Vibration, Cold Environment Stress Intensity Plot

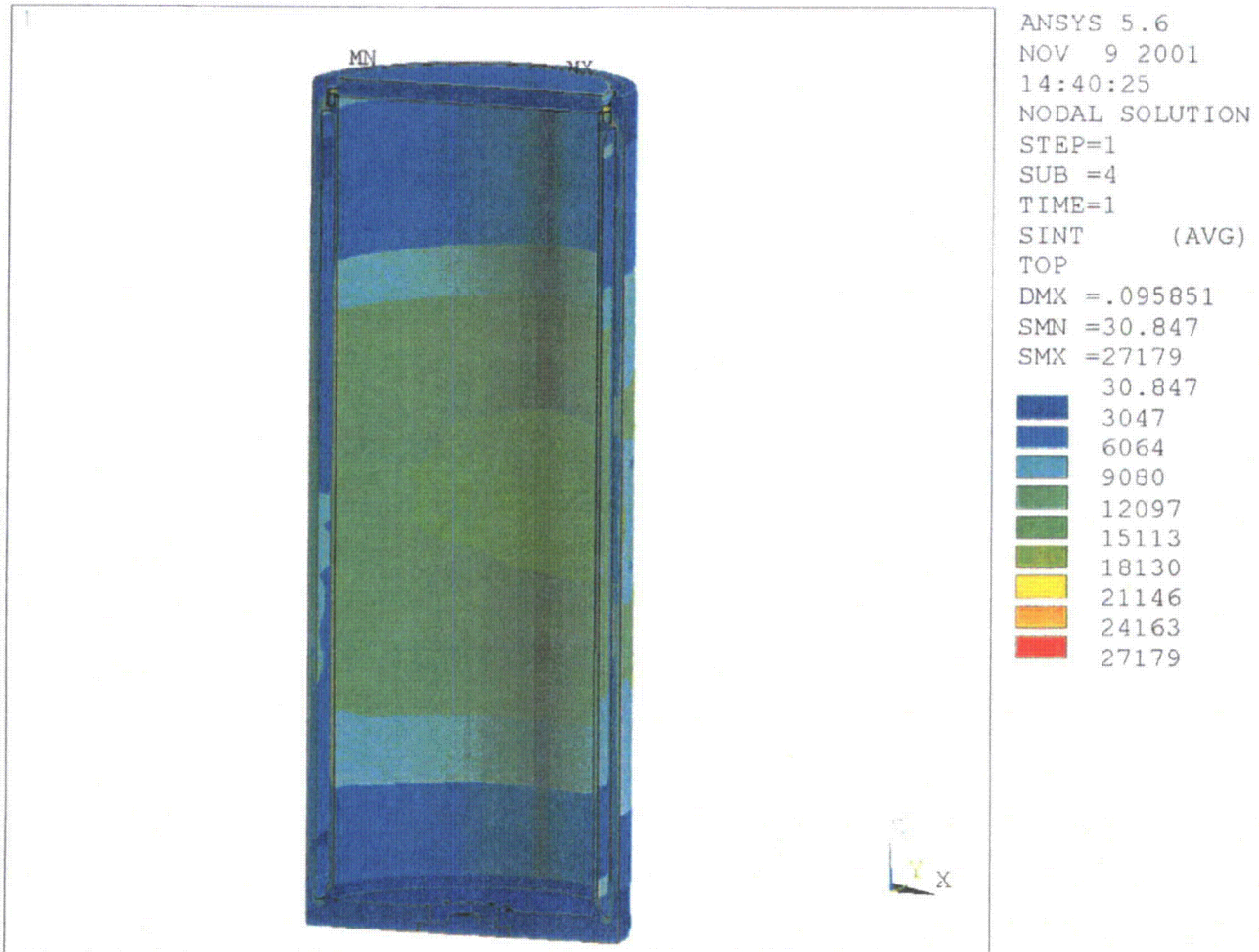

Figure 2.10.10-37
Run 19, Rail Car Shock, Hot Environment Stress Intensity Plot

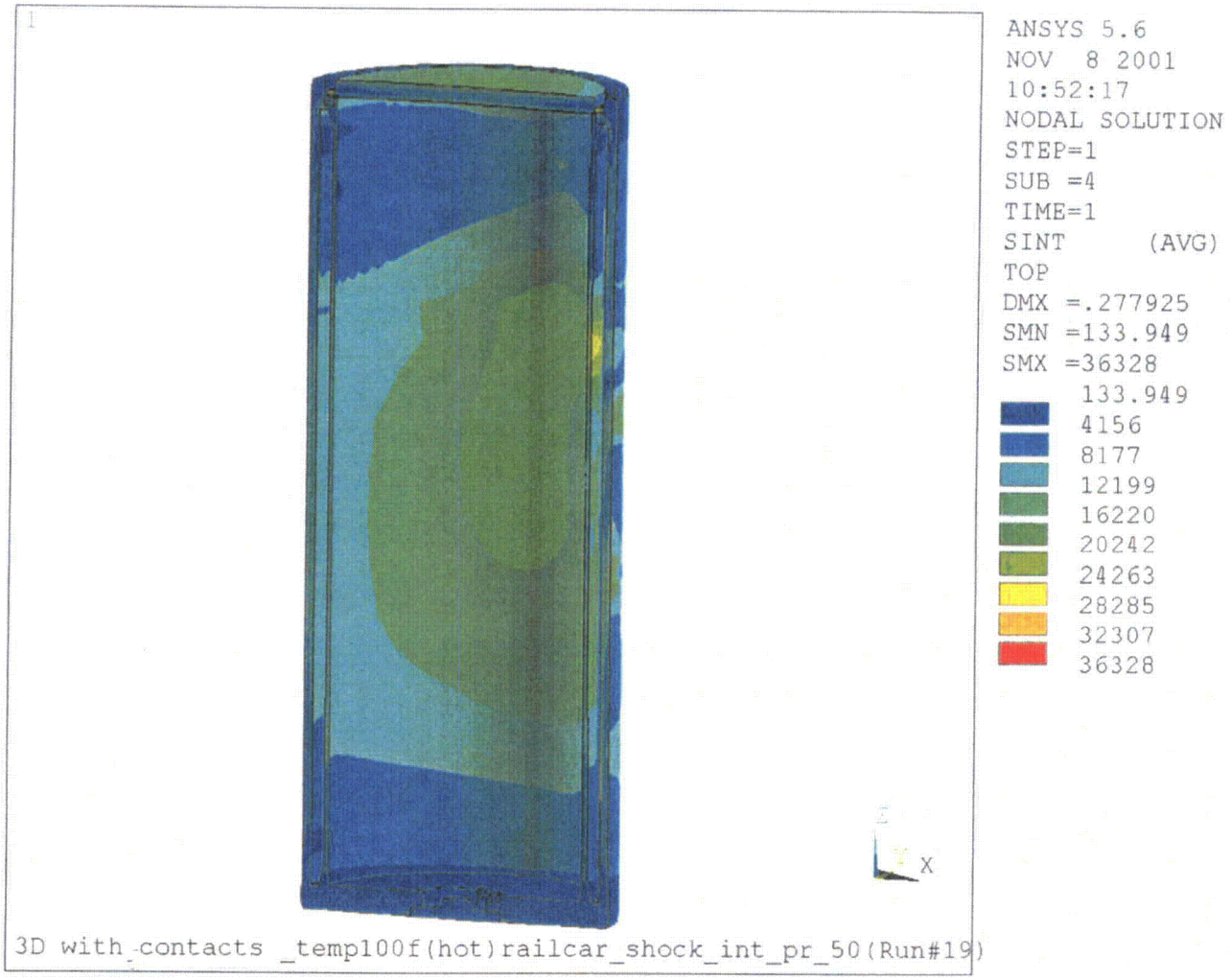

Figure 2.10.10-38
Run 20, Rail Car Shock, Cold Environment Stress Intensity Plot

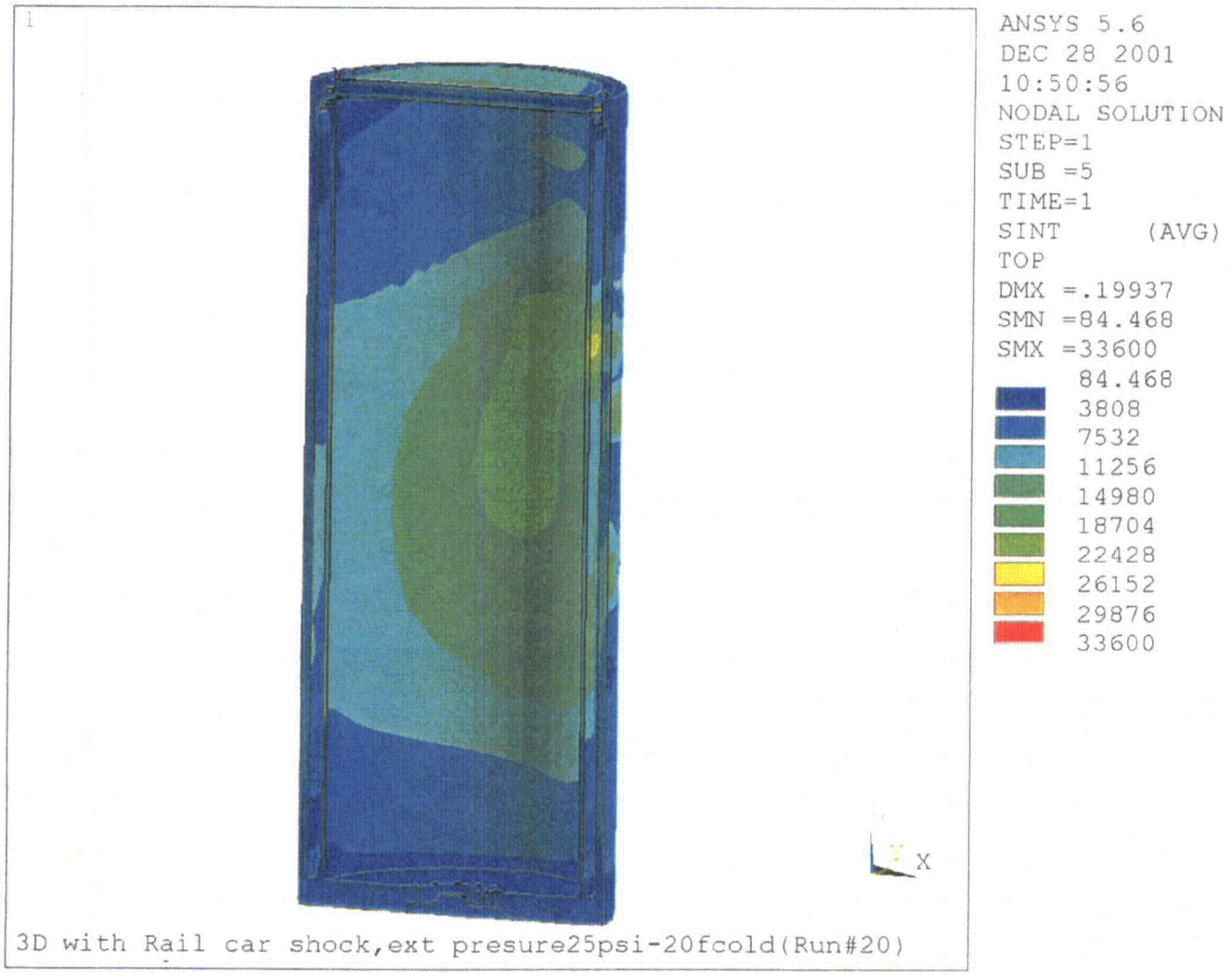

Figure 2.10.10-39
Run 21, 1 Foot Lid End Drop, Hot Environment Stress Intensity Plot

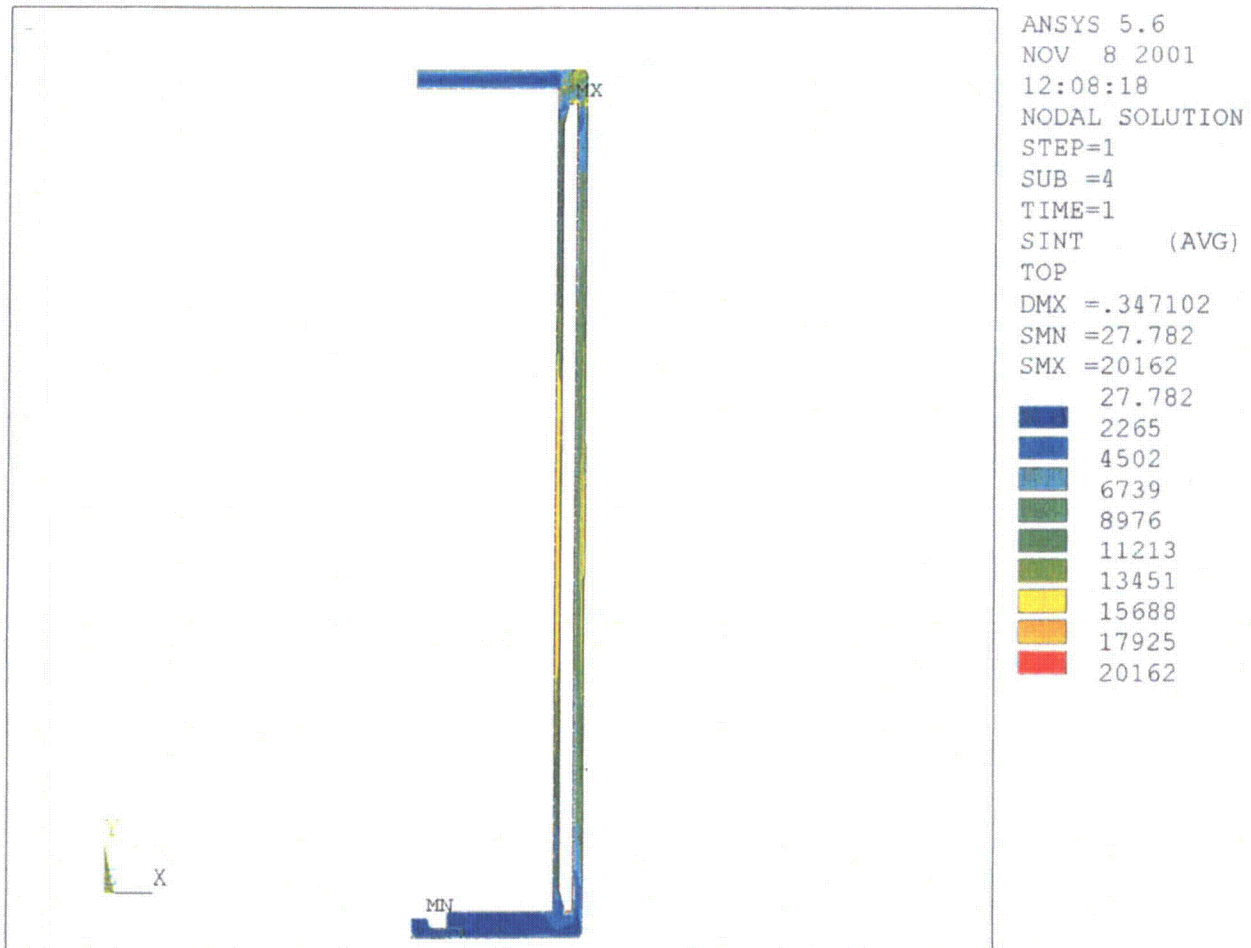

Figure 2.10.10-40
Run 22, 1 Foot Lid End Drop, Cold Environment Stress Intensity Plot

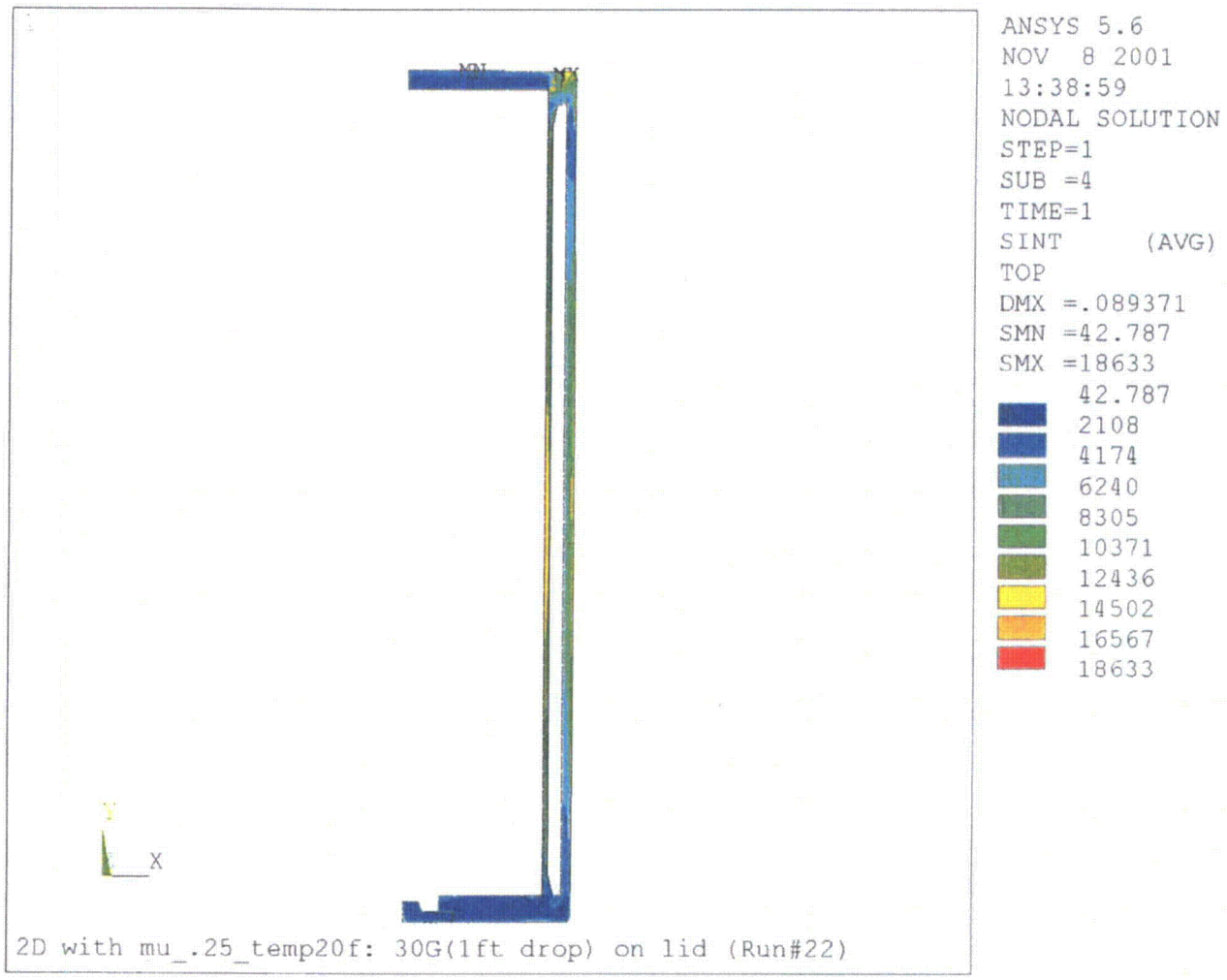

Figure 2.10.10-41
Run 23, 1 Foot Bottom End Drop, Hot Environment Stress Intensity Plot

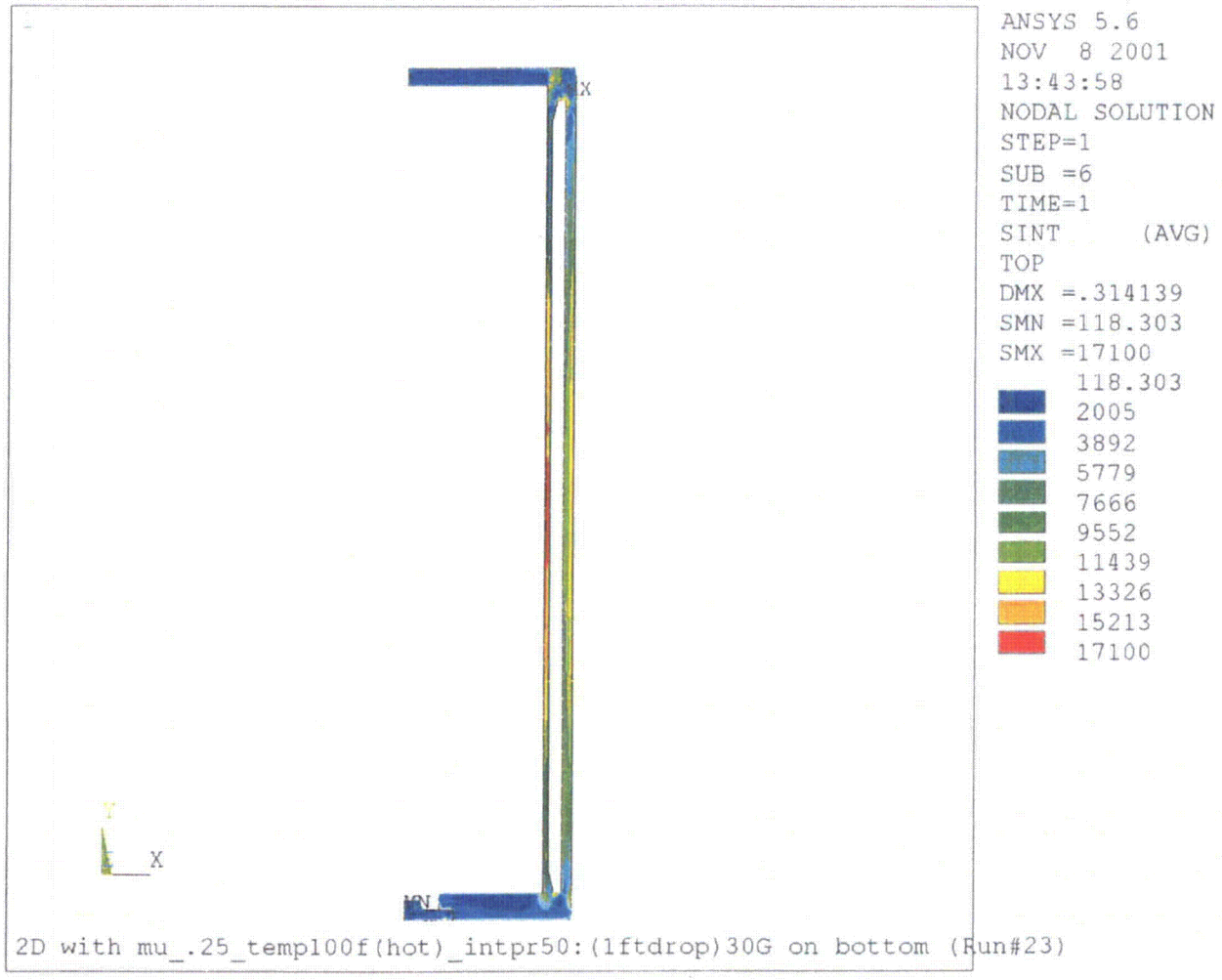

Figure 2.10.10-42
Run 24, 1 Foot Bottom End Drop, Cold Environment Stress Intensity Plot

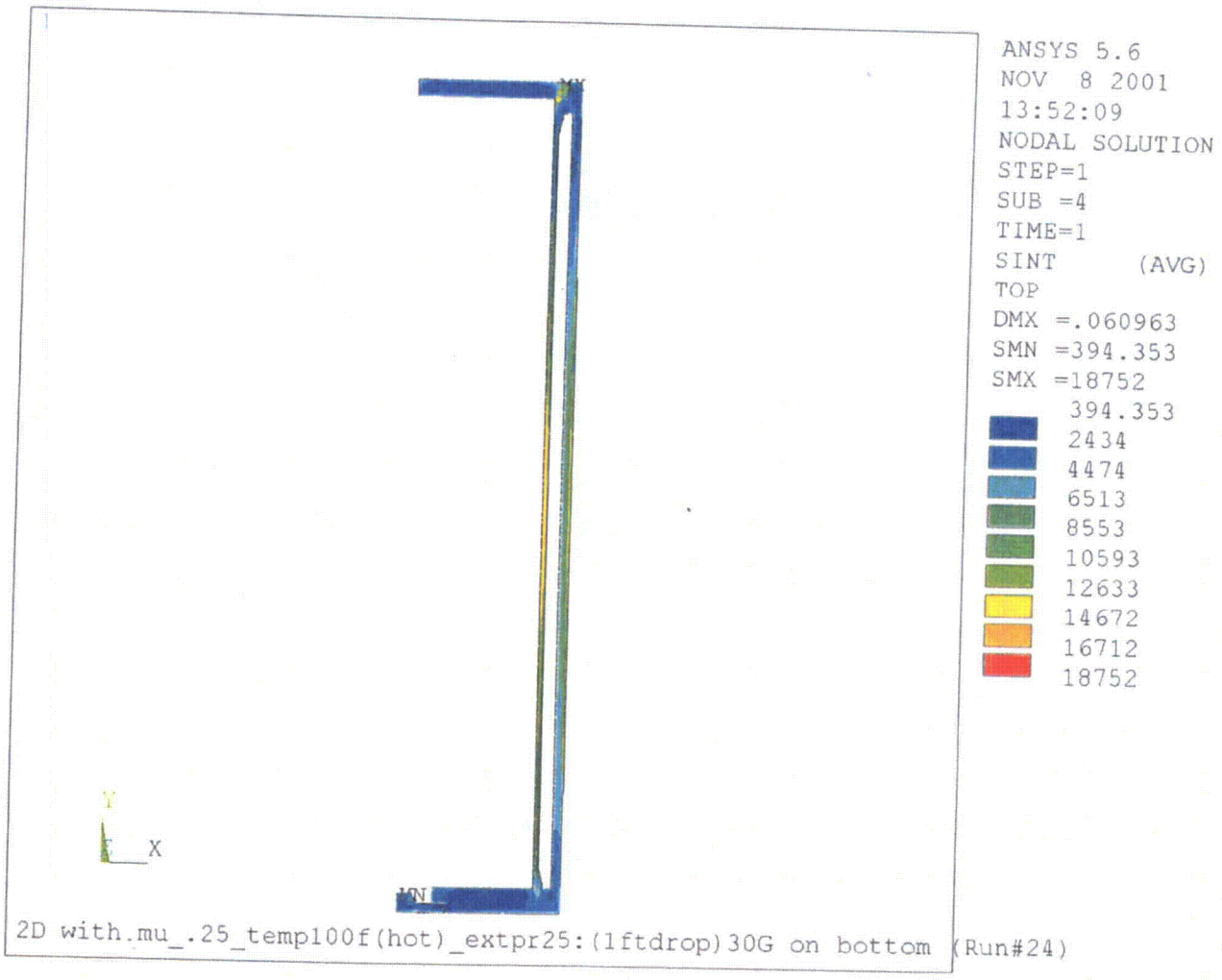

Figure 2.10.10-43
Run 25, 1 Foot Side Drop, Hot Environment Stress Intensity Plot

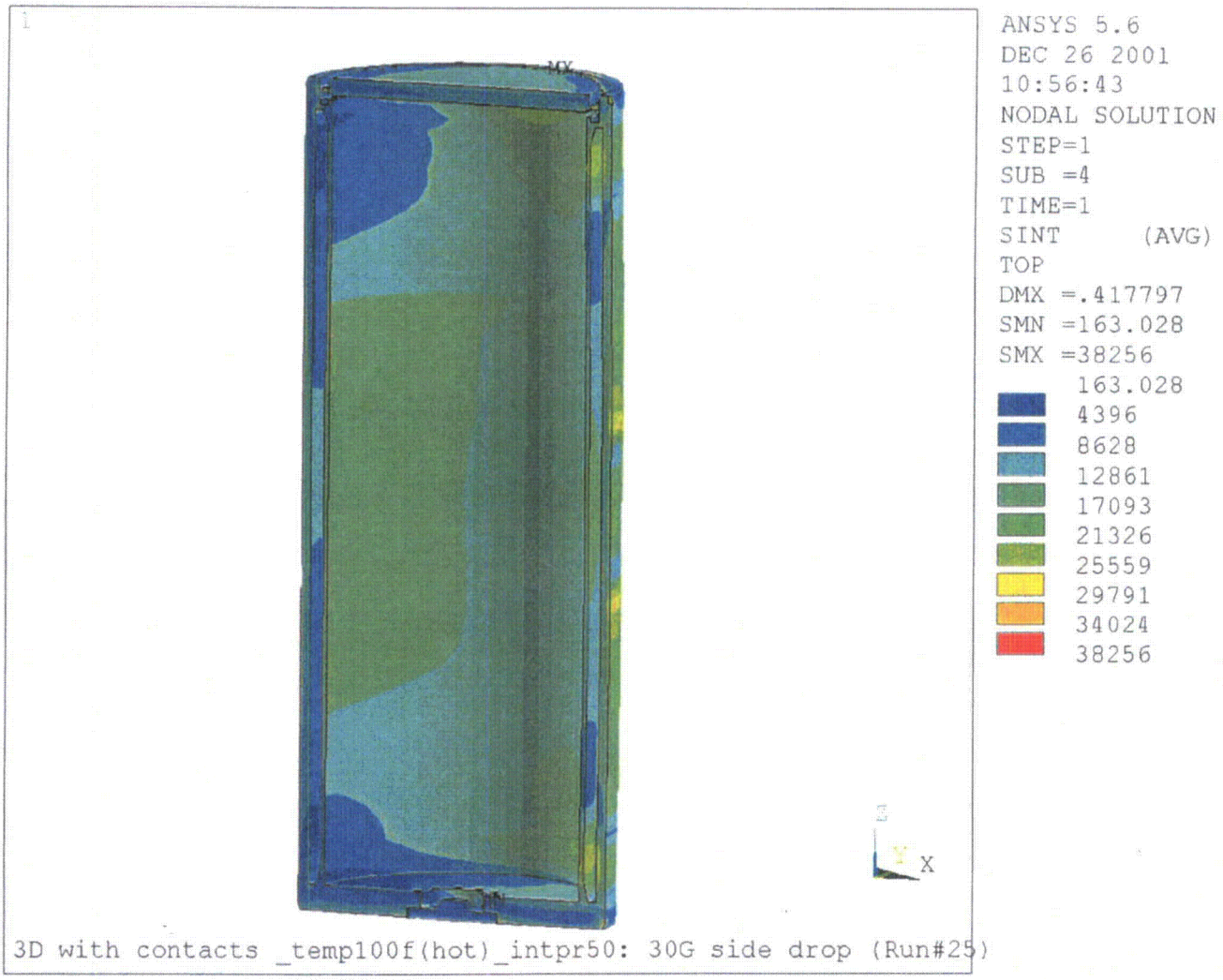

Figure 2.10.10-44
Run 26, 1 Foot Side Drop, Cold Environment Stress Intensity Plot

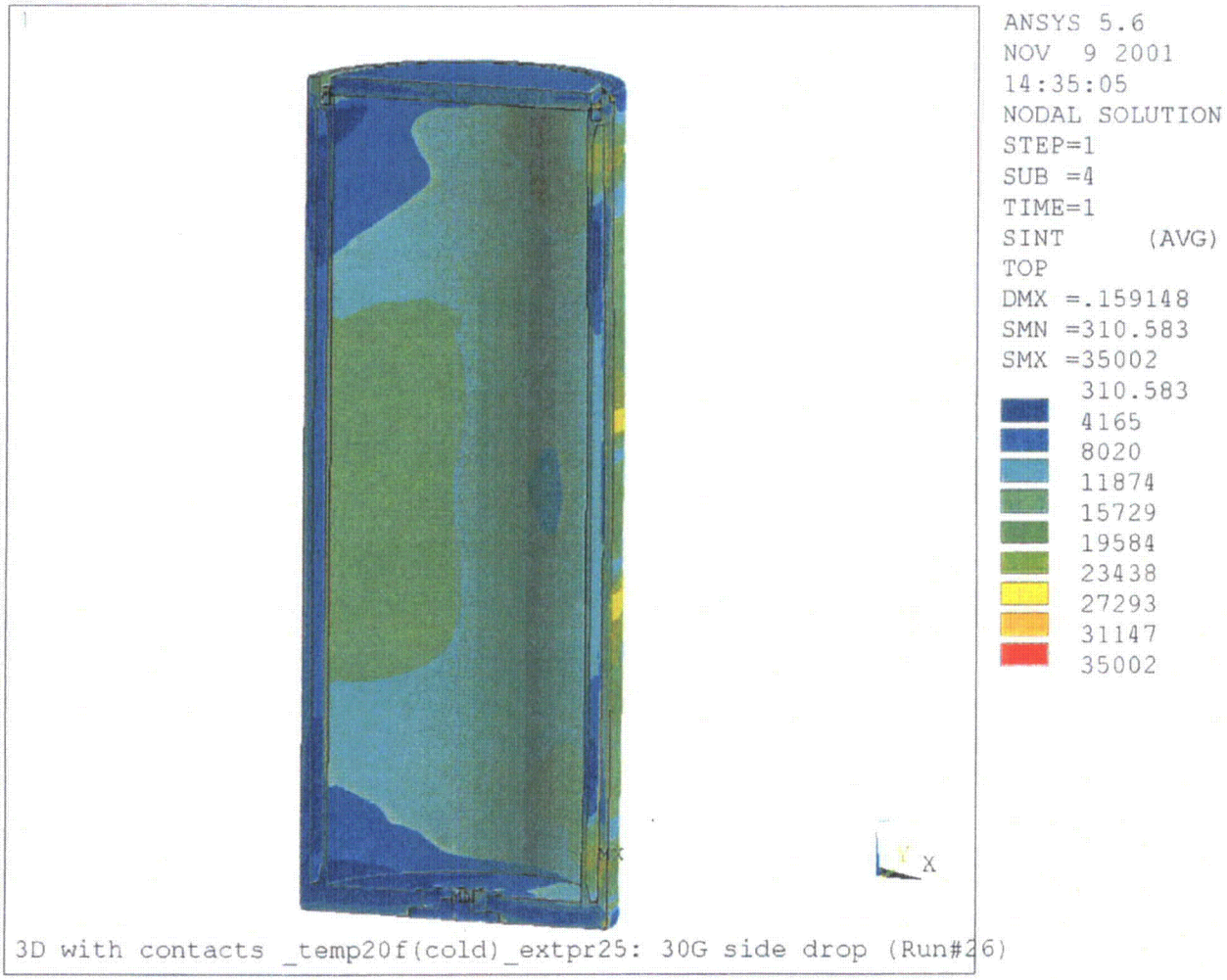

Figure 2.10.10-45
Run 27, 30 Foot Bottom End Drop, Hot Environment Stress Intensity Plot

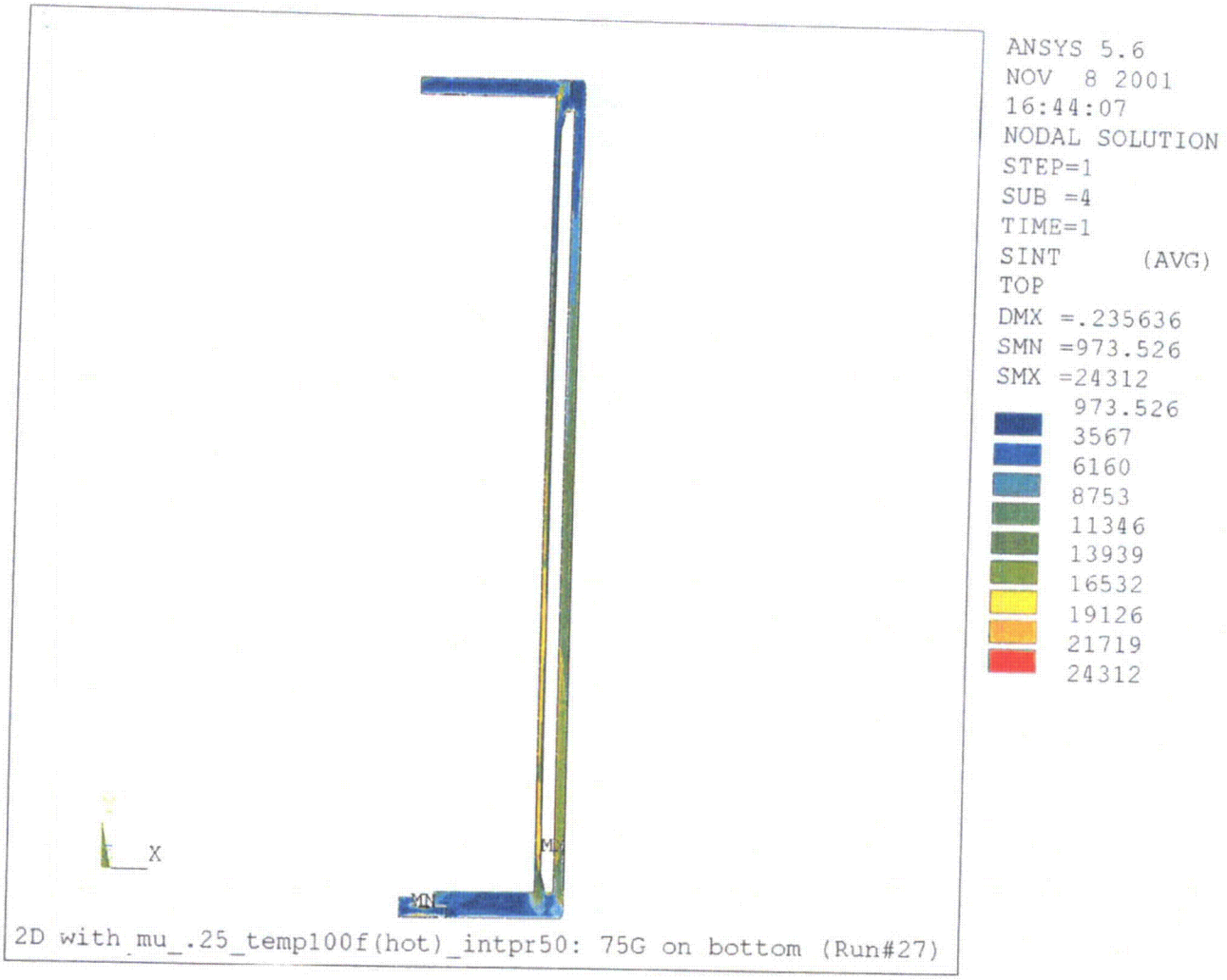

Figure 2.10.10-46
Run 28, 30 Foot Bottom End Drop, Cold Environment Stress Intensity Plot

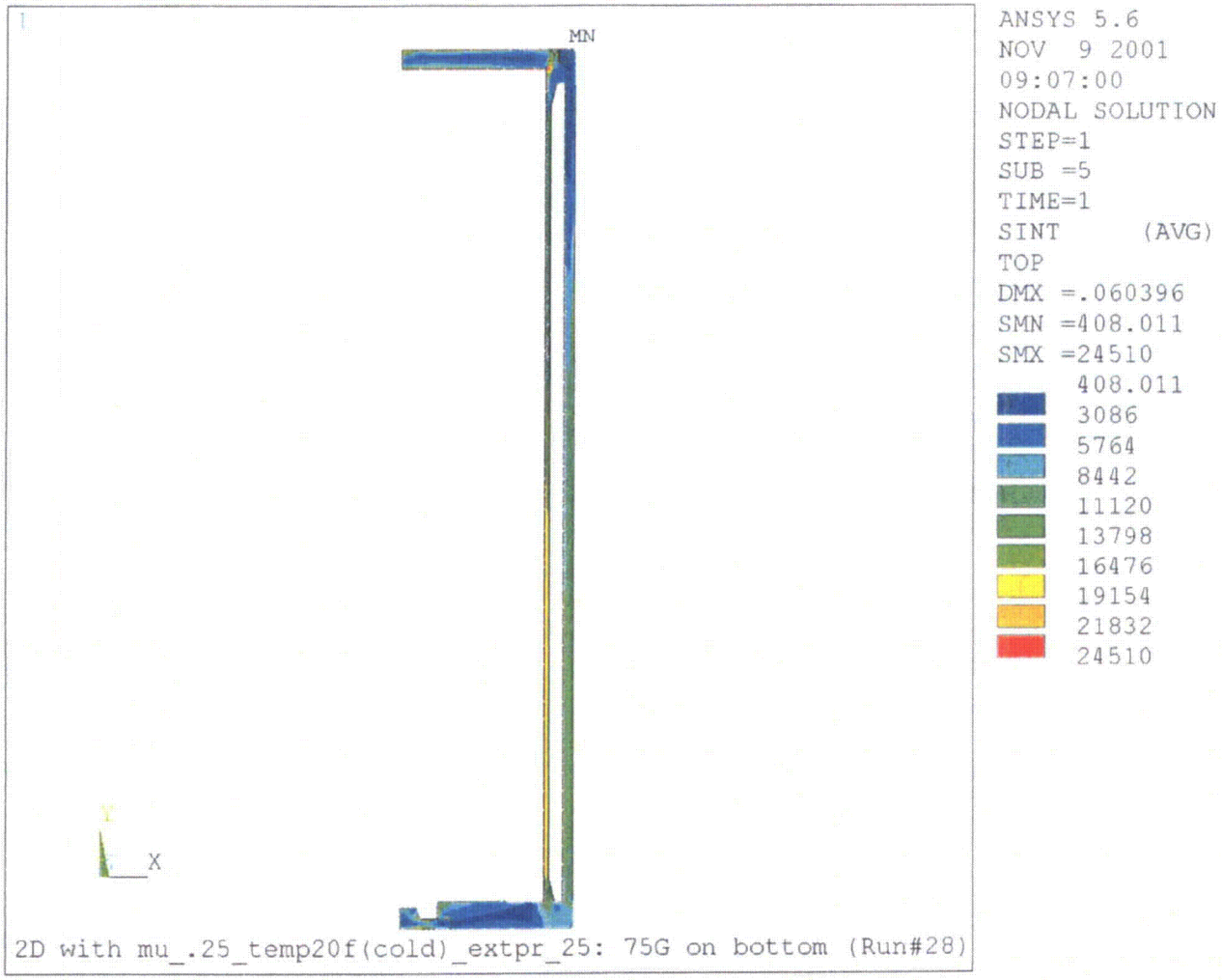

Figure 2.10.10-47
Run 29, 30 Foot Lid End Drop, Hot Environment Stress Intensity Plot

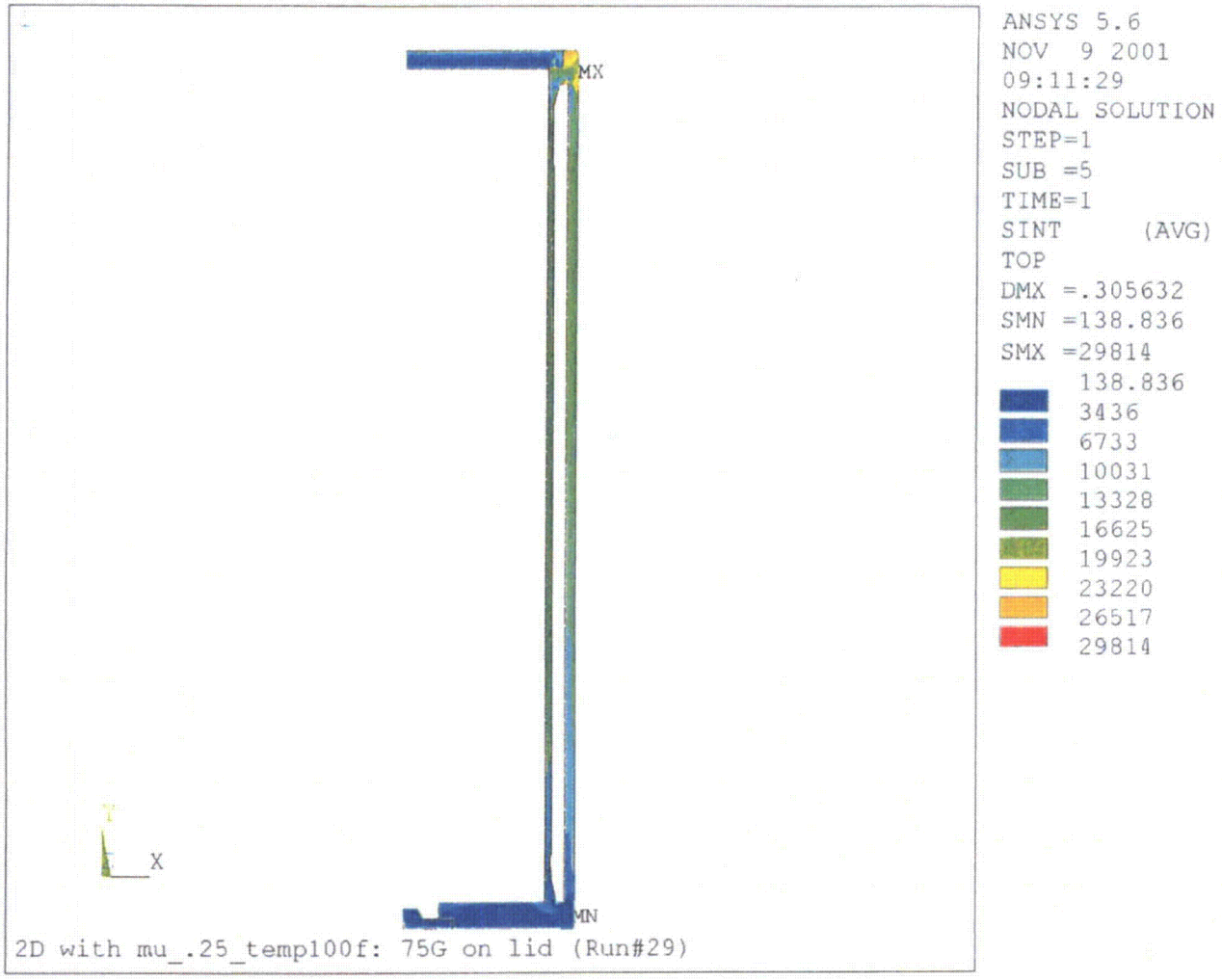

Figure 2.10.10-48
Run 30, 30 Foot Lid End Drop, Cold Environment Stress Intensity Plot

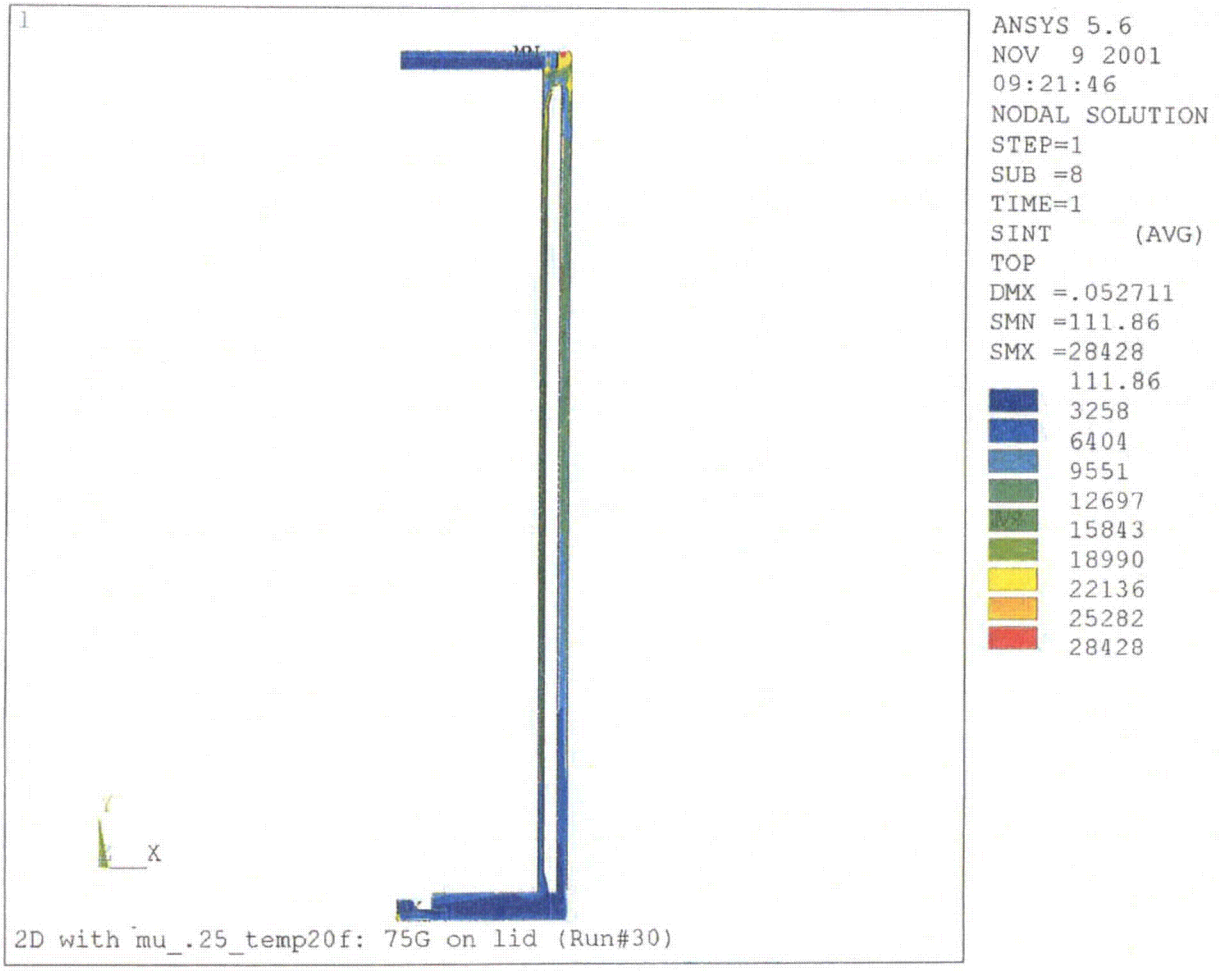

Figure 2.10.10-49
Run 31, 30 Foot Side Drop, Hot Environment Stress Intensity Plot

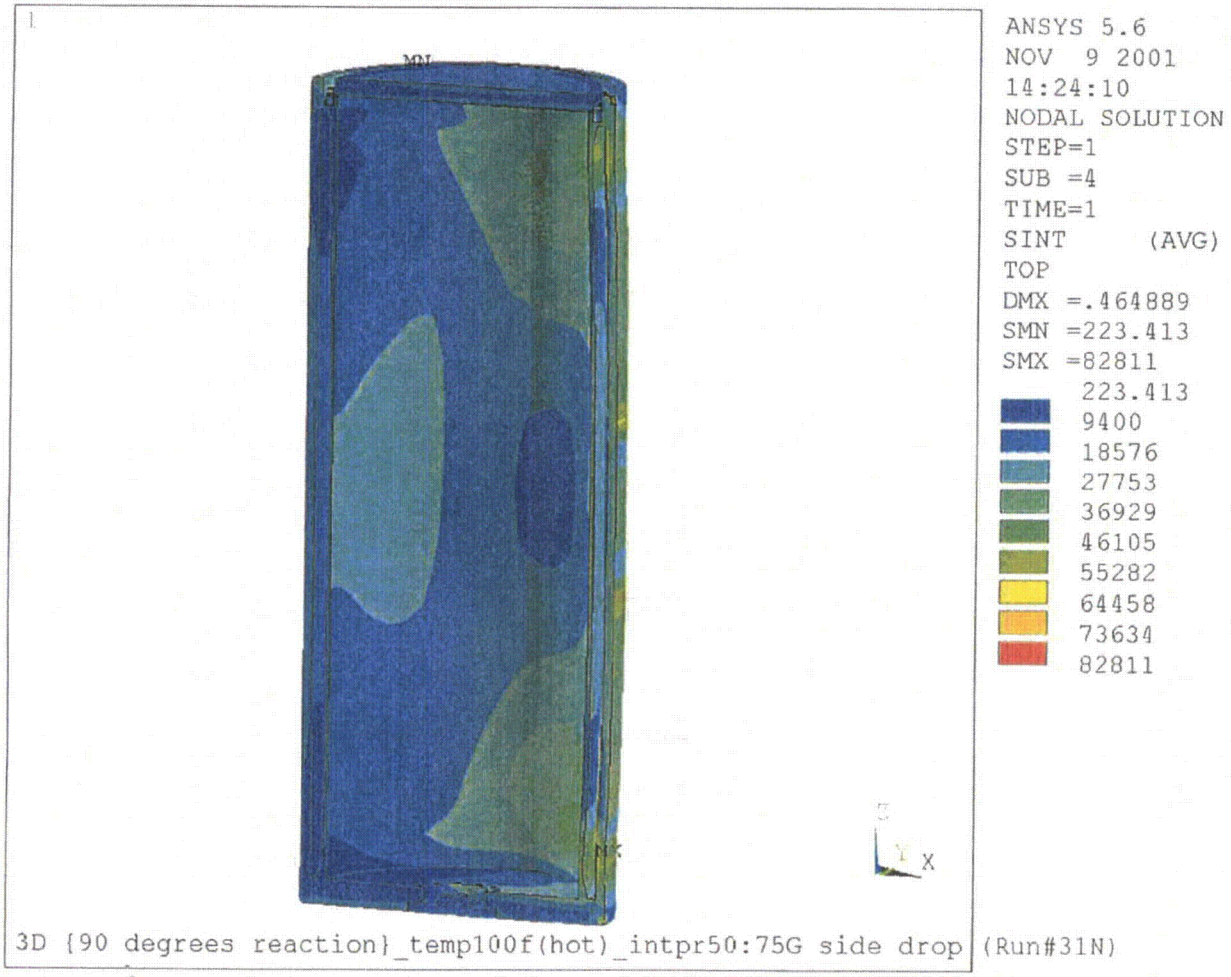

Figure 2.10.10-50
Run 32, 30 Foot Side Drop, Cold Environment Stress Intensity Plot

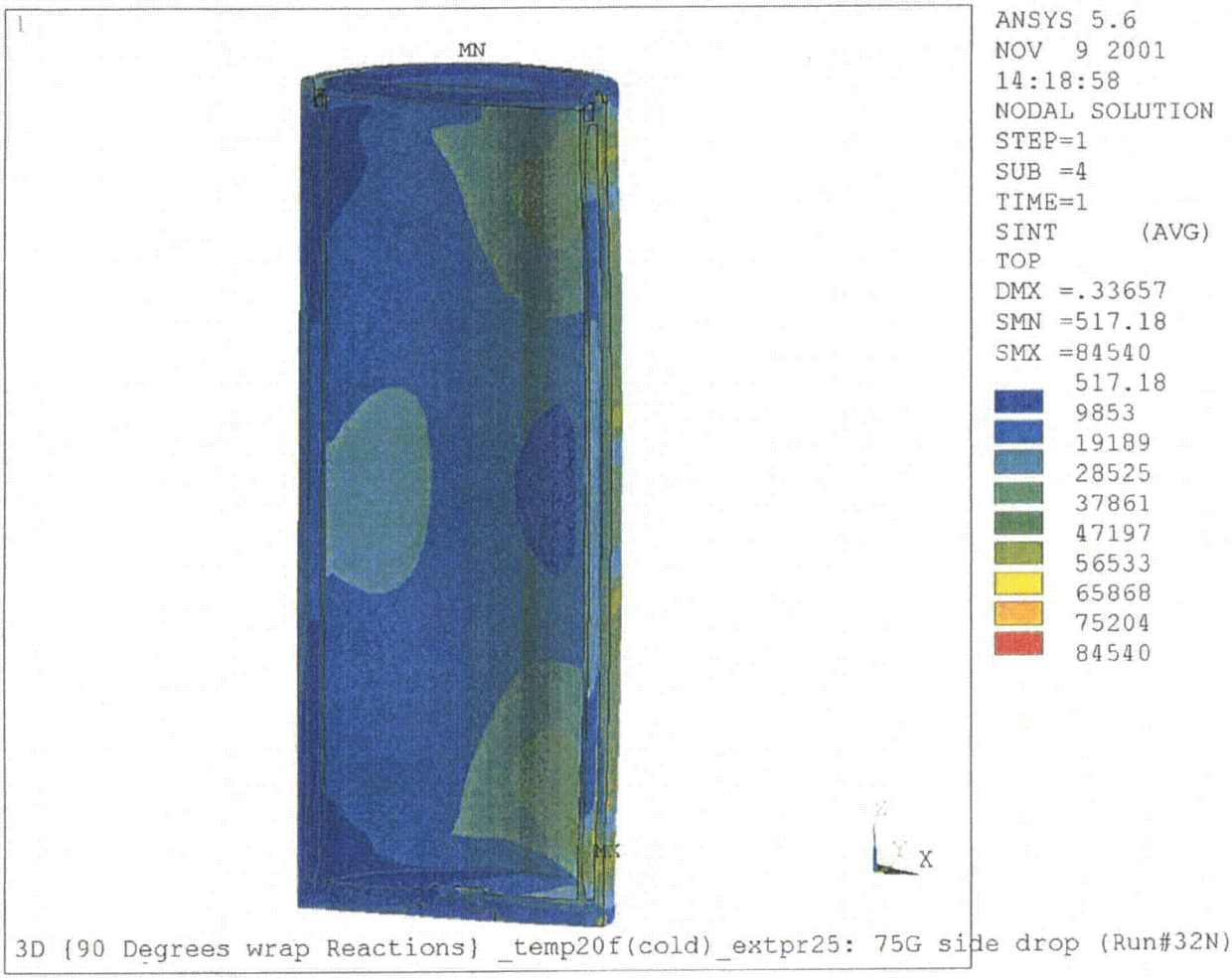

Figure 2.10.10-51
Run 33, 30 Foot CG Over Bottom Corner Drop, Hot Environment Stress Intensity Plot

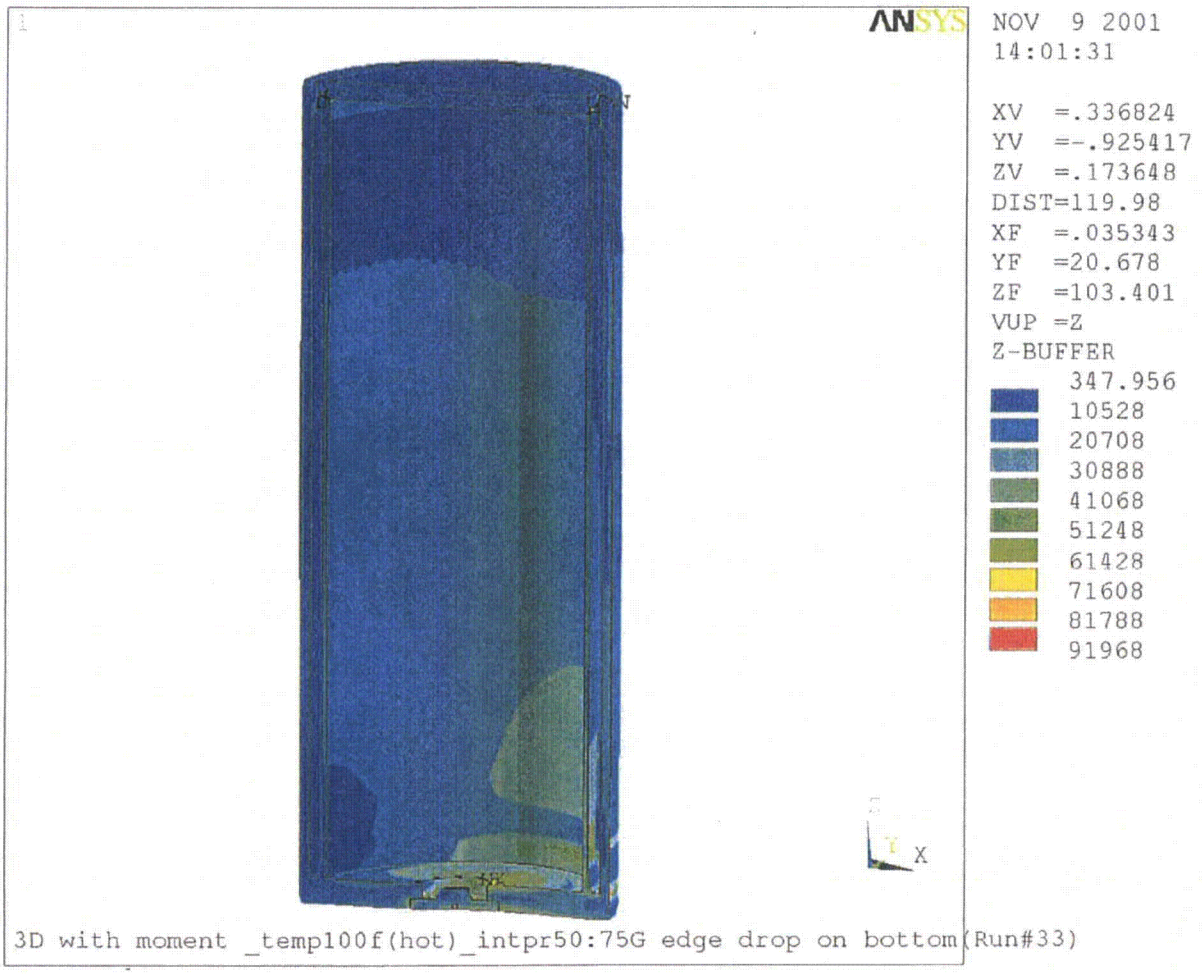

Figure 2.10.10-52
Run 34, 30 Foot CG Over Bottom Corner Drop, Cold Environment Stress Intensity Plot

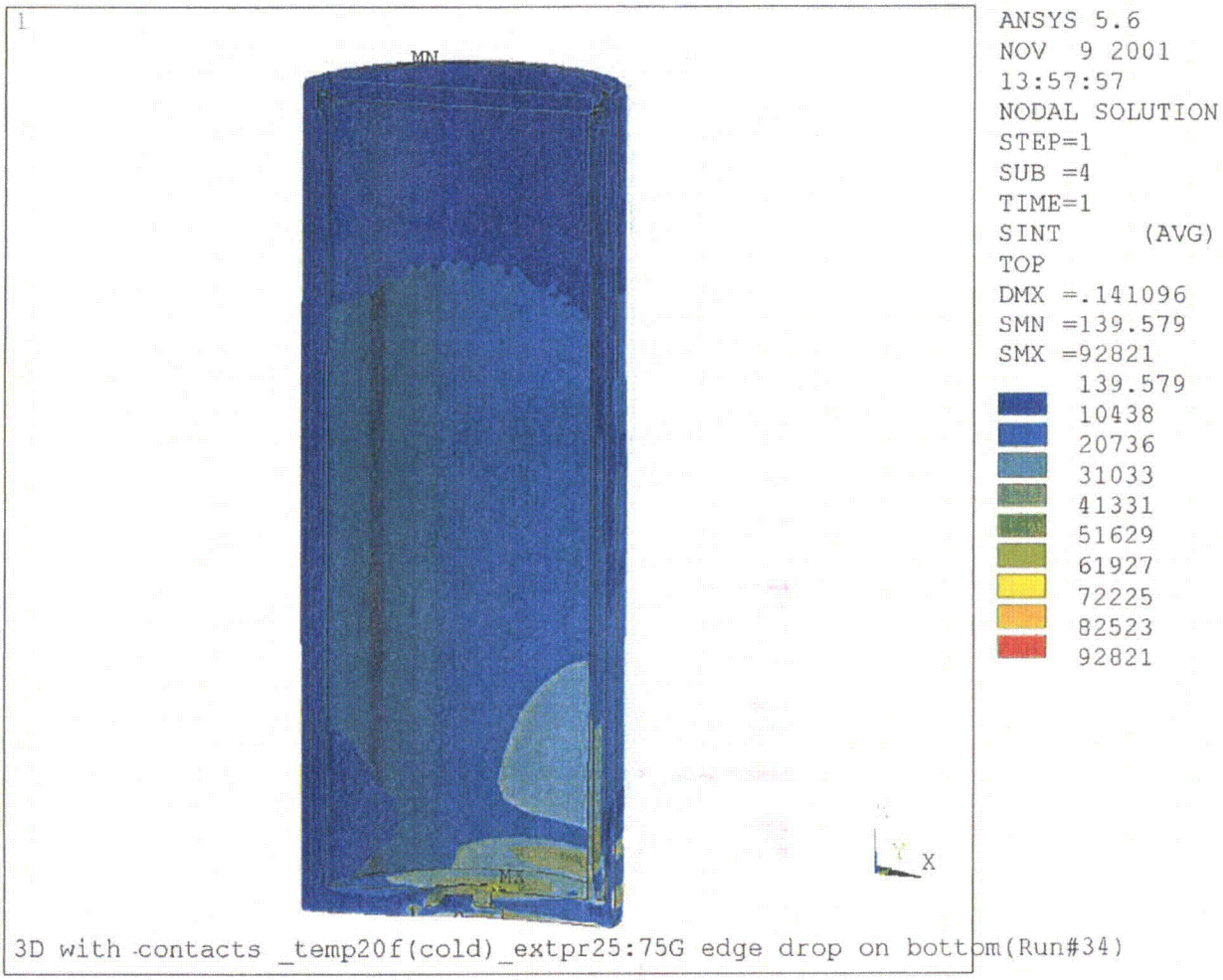

Figure 2.10.10-53
Run 35, 30 Foot CG Over Lid Corner Drop, Hot Environment Stress Intensity Plot

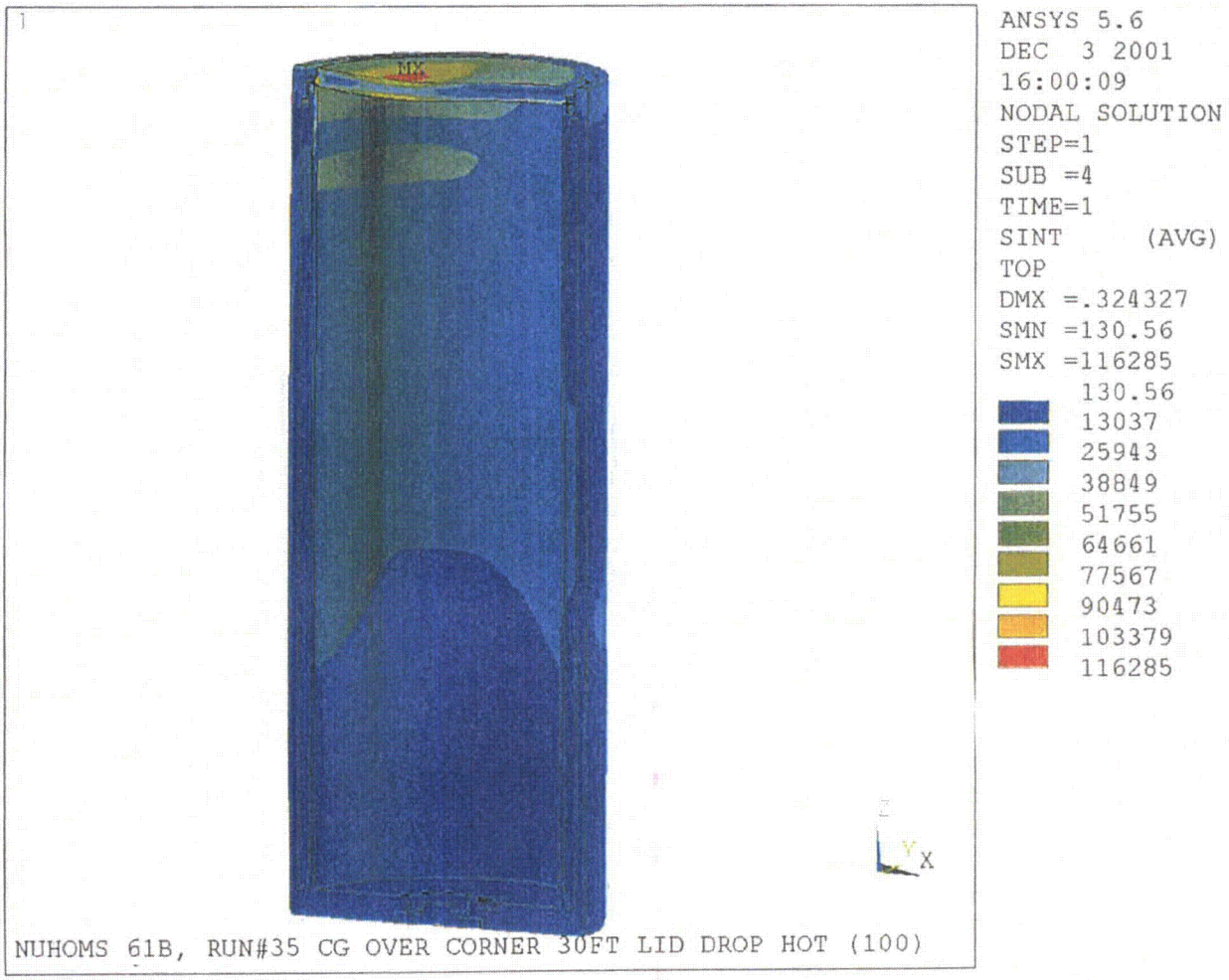

Figure 2.10.10-54
Run 36, 30 Foot CG Over Lid Corner Drop, Cold Environment Stress Intensity Plot

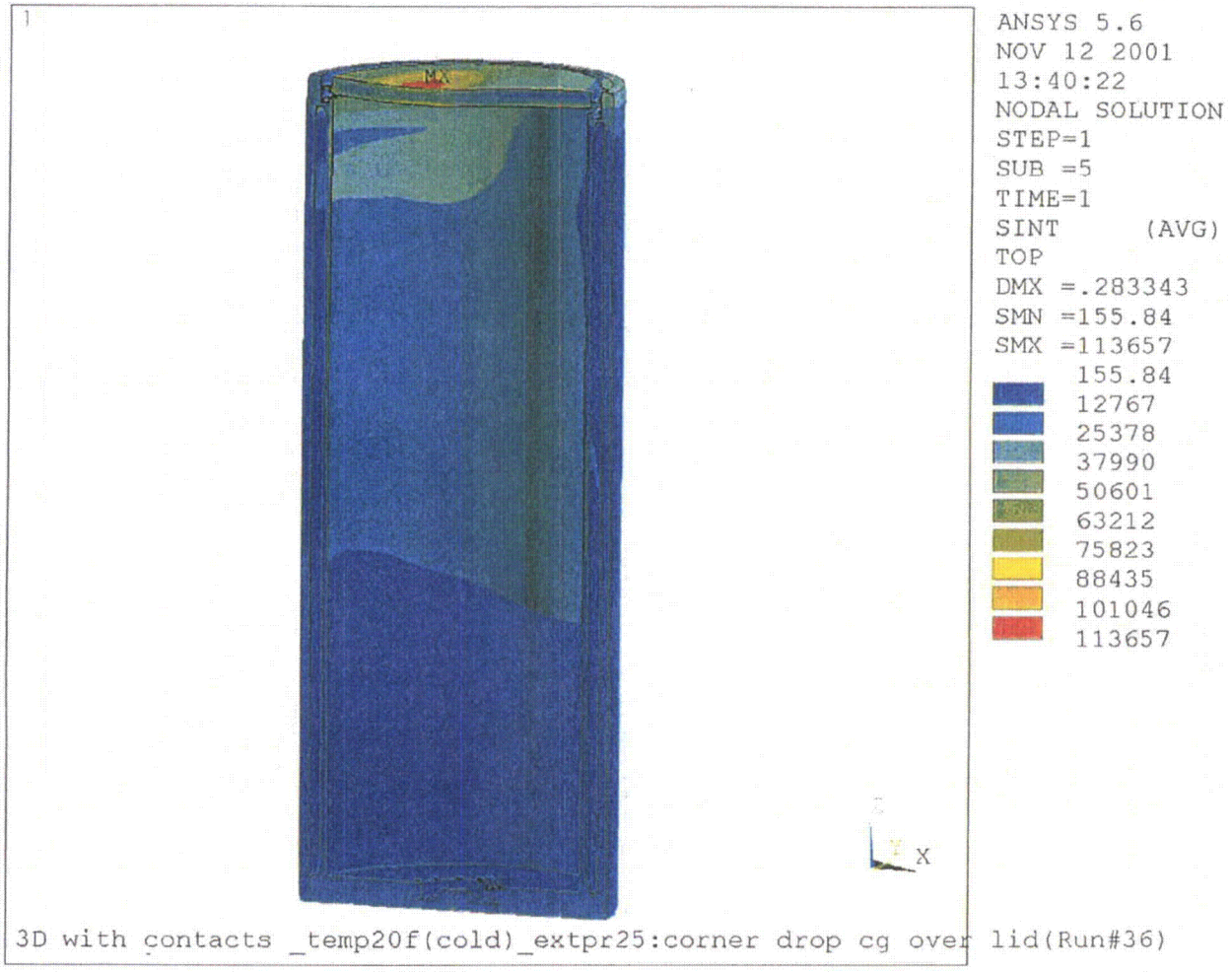

Figure 2.10.10-55
Run 37, 30 Foot 20° Lid End Slap Down Drop, Hot Environment Stress Intensity Plot

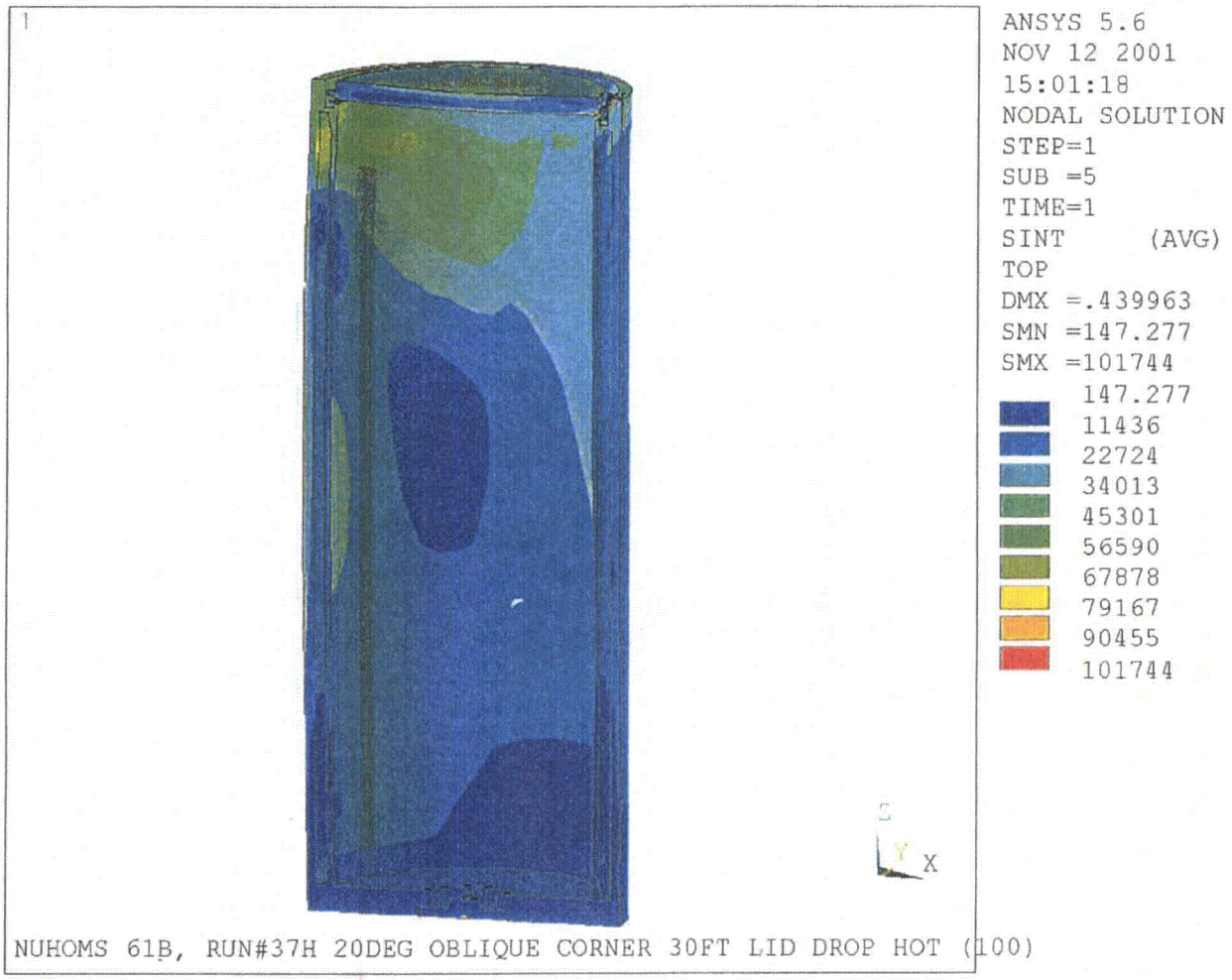

Figure 2.10.10-56
Run 38, 30 Foot 20° Lid End Slap Down Drop, Cold Environment Stress Intensity Plot

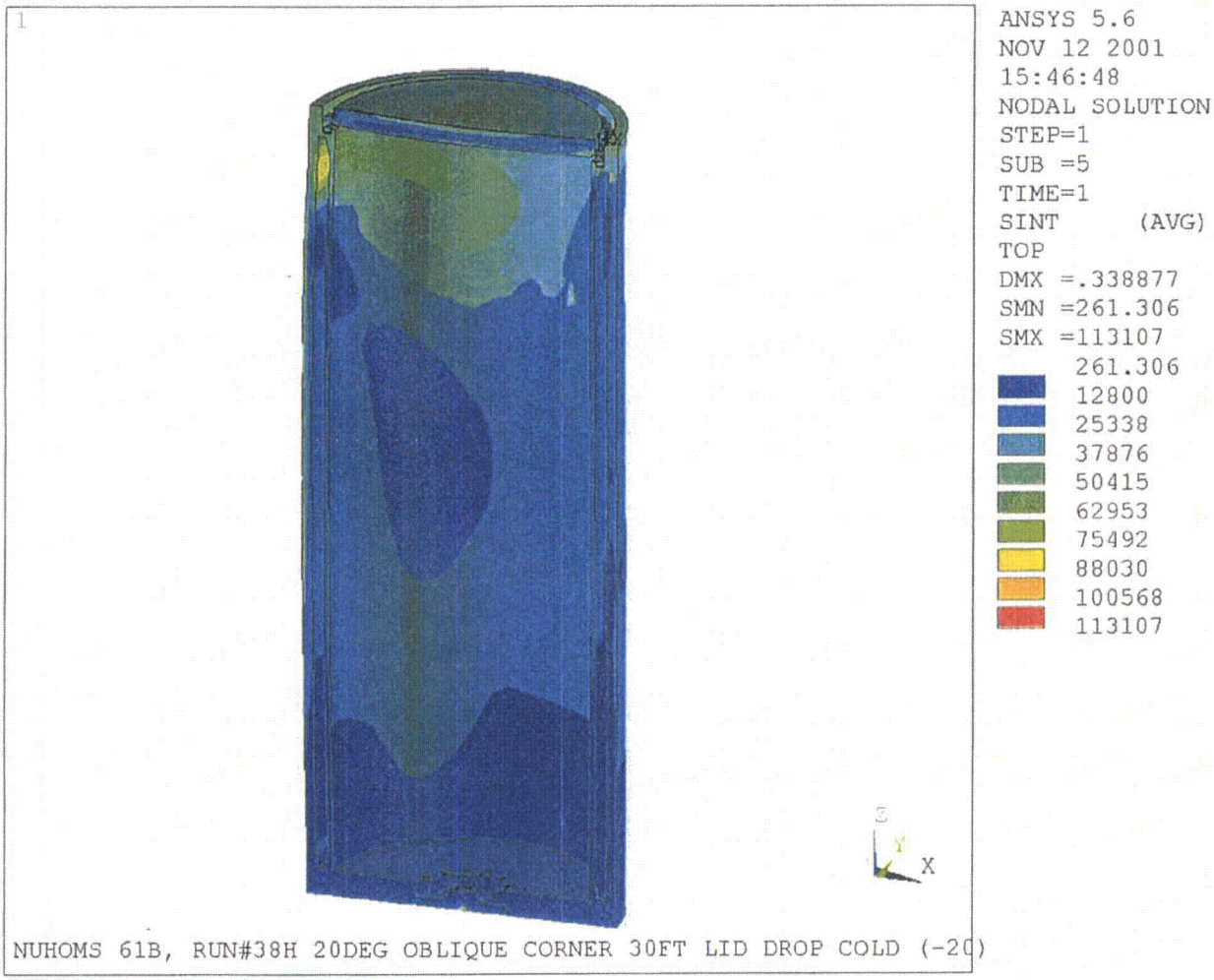

Figure 2.10.10-57
Run 39, 30 Foot 20° Bottom End Slap Down Drop, Hot Environment Stress Intensity Plot

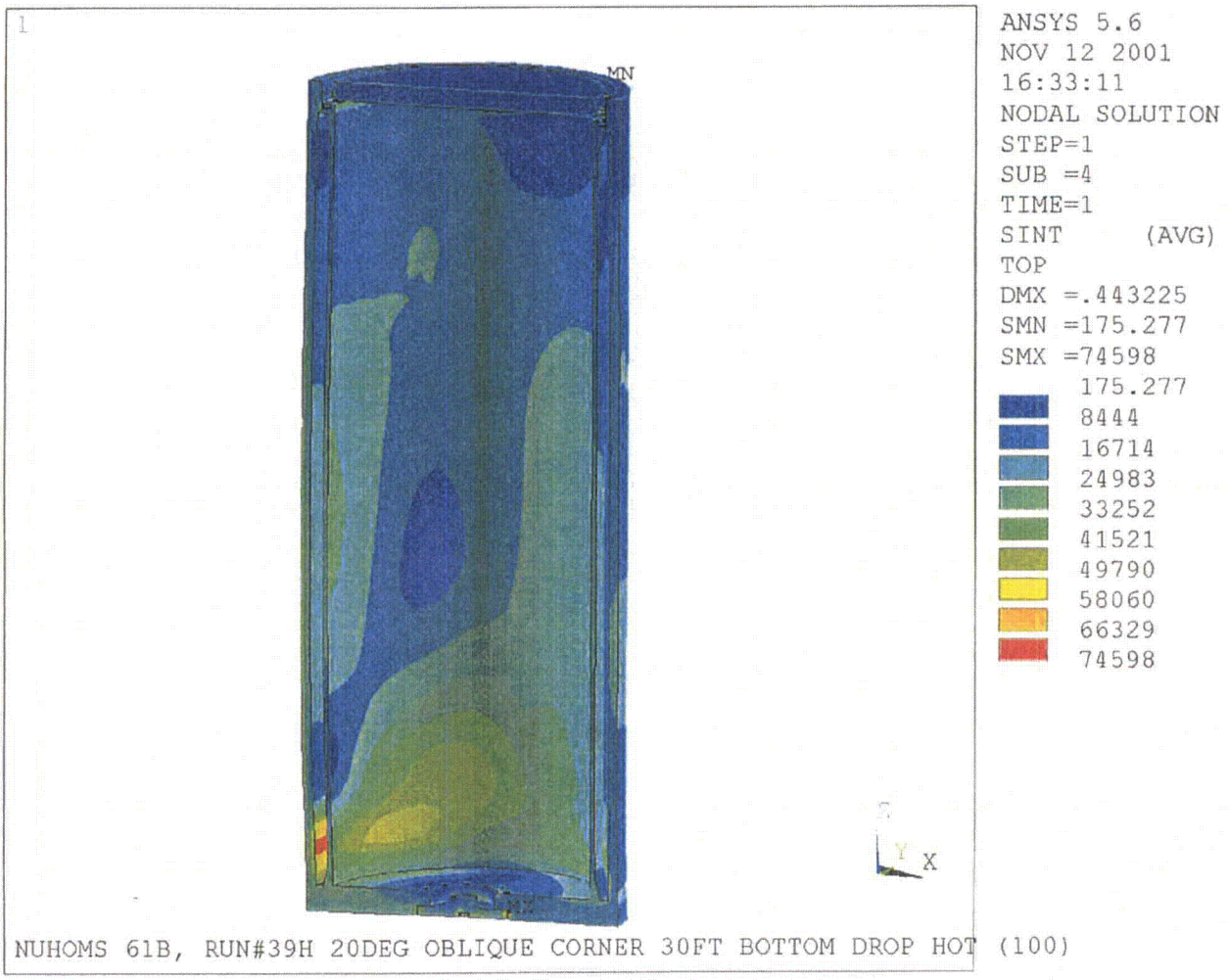

Figure 2.10.10-58
Run 40, 30 Foot 20° Bottom End Slap Down Drop, Cold Environment Stress Intensity Plot

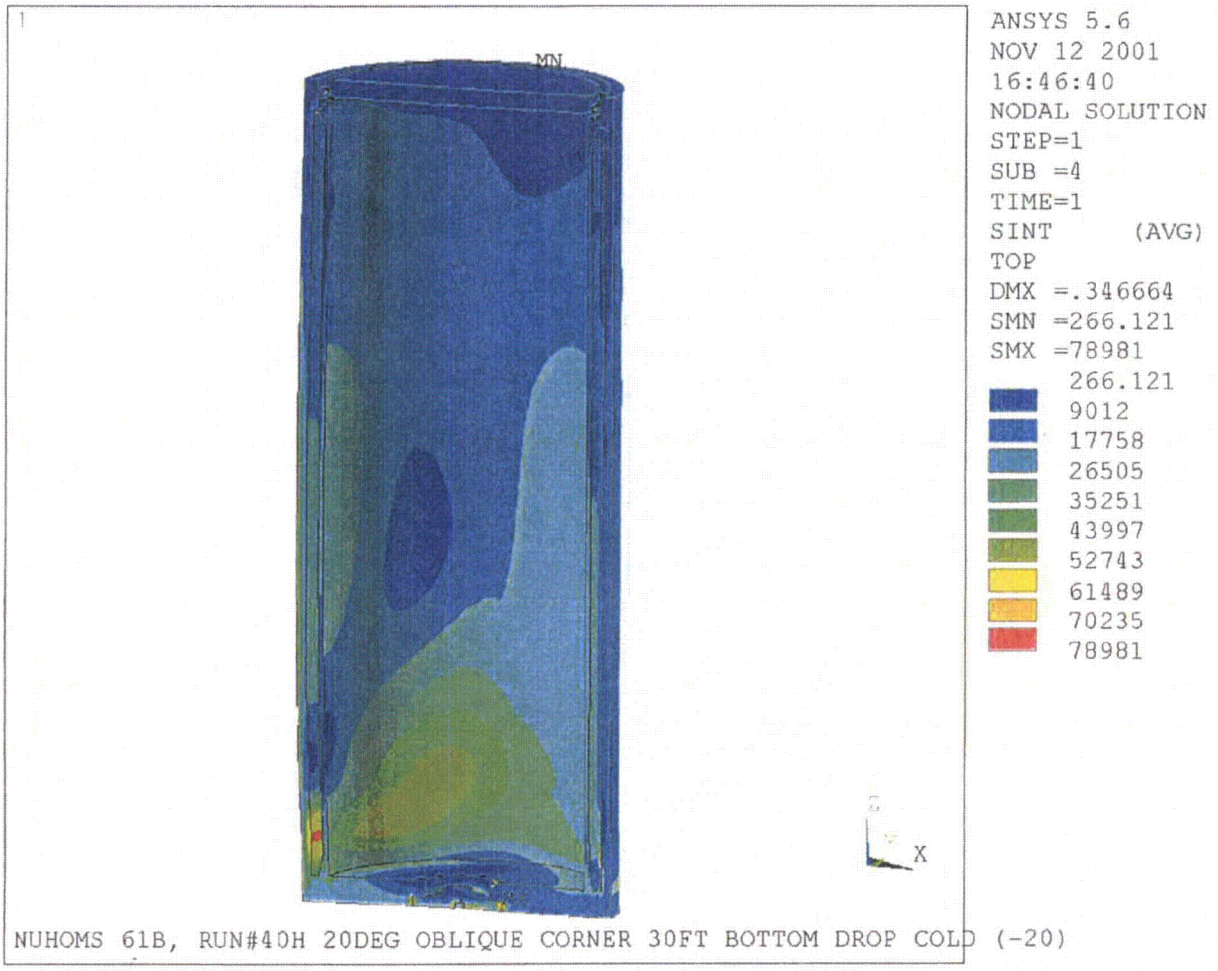

Figure 2.10.10-59
Run 41, Immersion (290 psi), Hot Environment Stress Intensity Plot

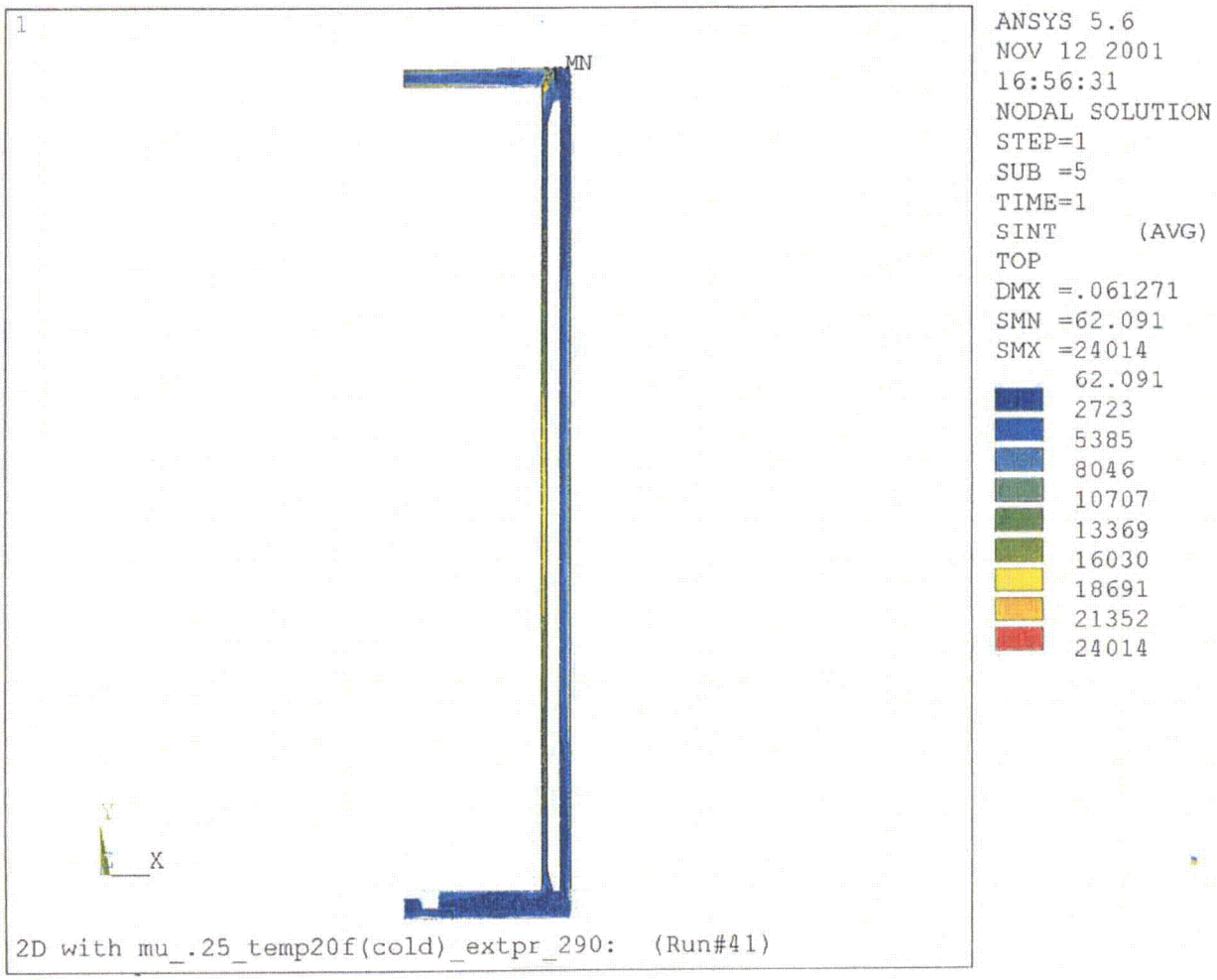

Figure 2.10.10-60
Run 42, Fire Accident, Cold Environment Stress Intensity Plot

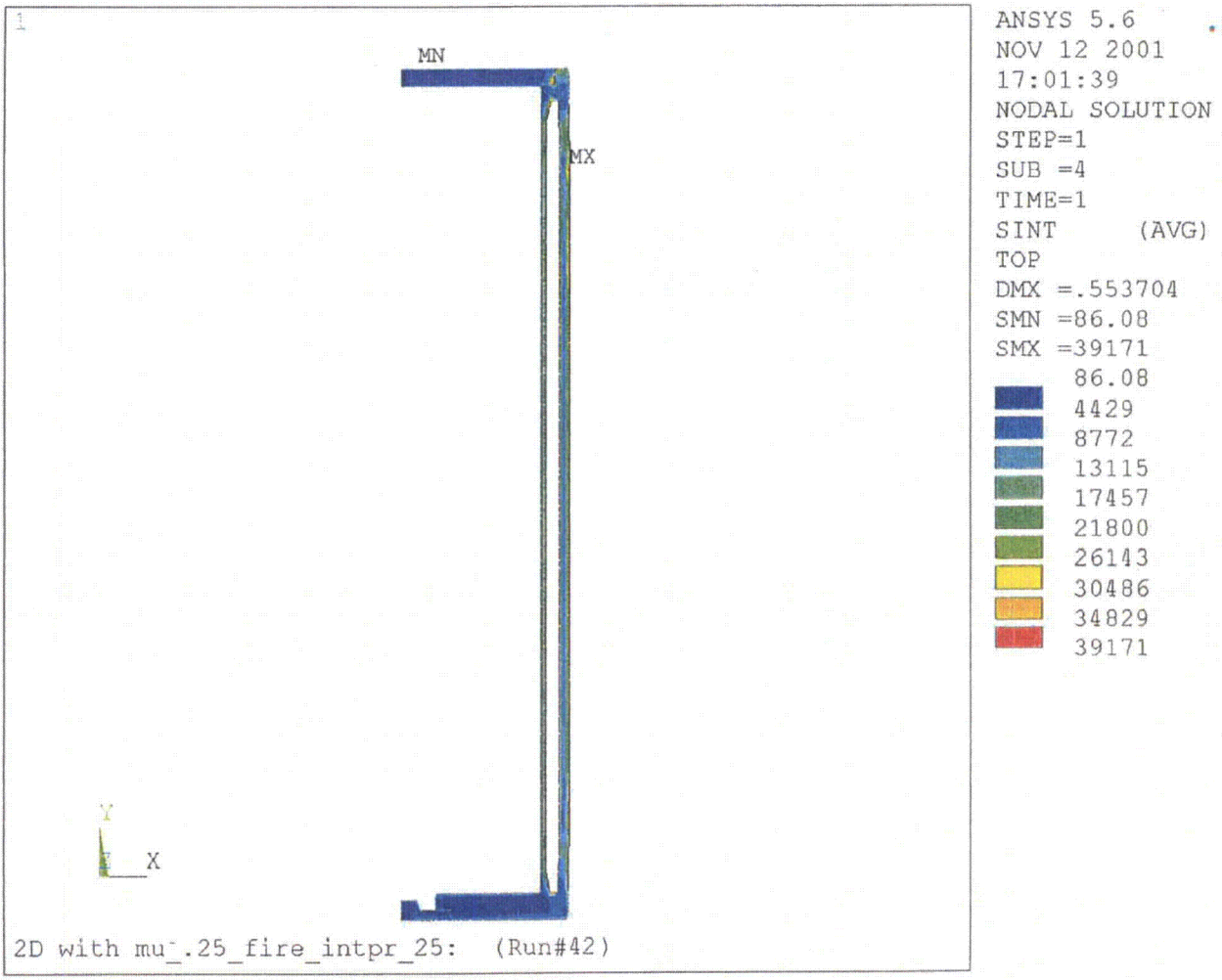

NUHOMS®-MP197 TRANSPORT PACKAGING

CHAPTER 3

TABLE OF CONTENTS

LIST OF TABLES

LIST OF FIGURES

CHAPTER 3

THERMAL EVALUATION

3.1 Discussion

The NUHOMS®-MP197 packaging is designed to passively reject decay heat under normal conditions of transport and hypothetical accident conditions while maintaining appropriate packaging temperatures and pressures within specified limits. Objectives of the thermal analyses performed for this evaluation include:

- limits to ensure components perform their intended safety functions;
- Determination of temperature distributions to support the calculation of thermal stresses;
- Determination of the cask and the DSC cavity gas pressures;
- Determination of the maximum fuel cladding temperature. Determination of maximum and minimum temperatures with respect to cask materials

To establish the heat removal capability, several thermal design criteria are established for the packaging. These are:

- Containment of radioactive material and gases is a major design requirement. Seal temperatures must be maintained within specified limits to satisfy the containment function during normal transport and hypothetical accident conditions. A maximum long-term seal temperature limit of 400 °F is set for the Flourocarbon O-Rings [8] & [15].
- Maximum temperatures of the containment structural components must not adversely affect the containment function.
- To maintain the stability of the neutron shield resin during normal transport conditions, an allowable temperature range of -40 to 300 °F (-40 to 149 °C) is set for the neutron shield.
- In accordance with 10CFR71.43(g) the maximum temperature of accessible package surfaces in the shade is limited to 185 °F (85 °C).
- A maximum fuel cladding temperature limit of 570 °C (1058 °F) is set for the fuel assemblies with an inert cover gas [9].
- A maximum temperature limit of 327 °C (620 °F) is set for the lead, corresponding to the melting point [11].

The ambient temperature range for normal transport is –20 to 100 °F (-29 to 38 °C) per 10CFR71(b). In general, all the thermal criteria are associated with maximum temperature limits and not minimum temperatures. All materials can be subjected to a minimum environment temperature of -40 °F (-40 °C) without adverse effects, as required by 10CFR71(c)(2).

The NUHOMS®-MP197 is analyzed based on a maximum heat load of 15.86 kW from 61 fuel assemblies. The analyses consider the effect of the decay heat load varying axially along a fuel assembly. The decay heat profile for a fuel assembly with a peak power factor of 1.2 and an active length of 144 in. is used for the evaluation. A description of the detailed analyses performed for normal transport conditions is provided in Section 3.4 and accident conditions in Section 3.5. A thermal analysis performed for vacuum drying conditions is described in Appendix 3.7.4. A summary of the analysis is provided in Table 3-1. The thermal evaluation concludes that with this design heat load, all design criteria are satisfied.

3.2 Summary of Thermal Properties of Materials

The analyses use interpolated values when appropriate for intermediate temperatures where the temperature dependency of a specific parameter is deemed significant. The interpolation assumes a linear relationship between the reported values.

1. BWR Fuel

Temperature (°F)	Thermal Conductivity (Btu/hr-in-°F)		Specific Heat (Btu/lbm-F)	Density (lbm/in^3)
	Transverse	Axial		
116.804	0.0137	0.0437	0.0574	0.105
214.424	0.0160	...	...	...
312.419	0.0186	...	...	...
410.726	0.0215	...	...	...
509.254	0.0249	...	...	...
608.009	0.0288	...	...	...
707.002	0.0329	...	...	...
806.149	0.0375	...	...	...
905.419	0.0425	...	...	...
1005.000	0.0461	0.0437	0.0574	0.105

The fuel conductivity analysis, including determination of specific heat and density values, is presented in Appendix 3.7.1.

2. Helium

Temperature		Conductivity	
(K) [2]	(°F)	(W/m-K) [2]	(Btu/hr-in-°F)
100	-280	0.0073	0.0004
150	-190	0.0095	0.0005
200	-100	0.1151	0.0055
250	-10	0.1338	0.0064
300	80	0.1500	0.0072
400	260	0.1800	0.0087
500	440	0.2110	0.0102
600	620	0.2470	0.0119
800	980	0.3070	0.0148
1000	1340	0.3630	0.0175

3. Neutron Shielding (Polyester Resin)

Thermal Conductivity (Btu/hr-in-°F) [3]	Specific Heat (Btu/lbm-°F) [3]	Density (lbm/in^3) [3]
0.0087	0.3107	0.051

4. SA-240, Type 304 Stainless Steel

Temperature [1] (°F)	Thermal Conductivity [1] (Btu/hr-ft-°F)	Thermal Conductivity (Btu/hr-in-°F)	Diffusivity [1] (ft^2/hr)	Specific Heat (Btu/lbm-°F)	Density [1] (lbm/in^3)
70	8.6	0.717	0.151	0.117	0.282
100	8.7	0.725	0.152	0.117	...
150	9.0	0.750	0.154	0.120	...
200	9.3	0.775	0.156	0.122	...
250	9.6	0.800	0.158	0.125	...
300	9.8	0.817	0.160	0.126	...
350	10.1	0.842	0.162	0.128	...
400	10.4	0.867	0.165	0.129	...
450	10.6	0.883	0.167	0.130	...
500	10.9	0.908	0.170	0.131	...
550	11.1	0.925	0.172	0.132	...
600	11.3	0.942	0.174	0.133	...
650	11.6	0.967	0.177	0.134	...
700	11.8	0.983	0.179	0.135	...
750	12.0	1.000	0.181	0.136	...
800	12.2	1.017	0.184	0.136	...
850	12.5	1.042	0.186	0.138	...
900	12.7	1.058	0.189	0.138	...
950	12.9	1.075	0.191	0.138	...
1000	13.2	1.100	0.194	0.139	...
1050	13.4	1.117	0.196	0.140	...
1100	13.6	1.133	0.198	0.141	...
1150	13.8	1.150	0.201	0.141	...
1200	14.0	1.167	0.203	0.141	...
1250	14.3	1.192	0.205	0.143	...
1300	14.5	1.208	0.208	0.143	...
1350	14.7	1.225	0.210	0.143	...
1400	14.9	1.242	0.212	0.144	...
1450	15.1	1.258	0.214	0.145	...
1500	15.3	1.275	0.216	0.145	0.282

5. SA-36 Carbon Steel

Temperature[1] (°F)	Thermal Conductivity [1] (Btu/hr-ft-°F)	Thermal Conductivity (Btu/hr-in-°F)	Diffusivity [1] (ft^2/hr)	Specific Heat (Btu/lbm-°F)	Density [1] (lbm/in^3)
70	23.6	1.967	0.454	0.107	0.282
100	23.9	1.992	0.443	0.111	...
150	24.2	2.017	0.433	0.115	...
200	24.4	2.033	0.422	0.118	...
250	24.4	2.033	0.414	0.121	...
300	24.4	2.033	0.406	0.123	...
350	24.3	2.025	0.396	0.126	...
400	24.2	2.017	0.386	0.128	...
450	23.9	1.992	0.375	0.131	...
500	23.7	1.975	0.364	0.133	...
550	23.4	1.950	0.355	0.135	...
600	23.1	1.925	0.346	0.137	...
650	22.7	1.892	0.333	0.140	...
700	22.4	1.867	0.320	0.143	...
750	22.0	1.833	0.308	0.146	...
800	21.7	1.808	0.298	0.149	...
850	21.2	1.767	0.286	0.152	...
900	20.9	1.742	0.274	0.156	...
950	20.5	1.708	0.262	0.160	...
1000	20.0	1.667	0.248	0.165	...
1050	19.6	1.633	0.237	0.169	...
1100	19.2	1.600	0.228	0.173	...
1150	18.7	1.558	0.213	0.180	...
1200	18.2	1.517	0.197	0.189	...
1250	17.5	1.458	0.179	0.200	...
1300	16.7	1.392	0.155	0.221	...
1350	15.8	1.317	0.119	0.272	...
1400	15.3	1.275	0.077	0.407	...
1450	15.1	1.258	0.154	0.201	...
1500	15.1	1.258	0.169	0.183	0.282

6. SA-705, Type 630 Stainless Steel

Temperature[1] (°F)	Thermal Conductivity [1] (Btu/hr-ft-°F)	Thermal Conductivity (Btu/hr-in-°F)	Diffusivity [1] (ft^2/hr)	Specific Heat (Btu/lbm-°F)	Density [1] (lbm/in^3)
70	9.9	0.825	0.188	0.108	0.282
100	10.1	0.842	0.189	0.110	...
150	10.4	0.867	0.189	0.113	...
200	10.6	0.883	0.189	0.115	...
250	10.9	0.908	0.190	0.118	...
300	11.2	0.933	0.190	0.121	...
350	11.4	0.950	0.191	0.122	...
400	11.7	0.975	0.191	0.126	...
450	12.0	1.000	0.191	0.129	...
500	12.2	1.017	0.190	0.132	...
550	12.5	1.042	0.190	0.135	...
600	12.7	1.058	0.190	0.137	...
650	13.0	1.083	0.188	0.142	...
700	13.2	1.100	0.186	0.145	...
750	13.4	1.117	0.183	0.150	...
800	13.5	1.125	0.180	0.154	...
850	13.6	1.133	0.176	0.158	...
900	13.7	1.142	0.172	0.163	...
950	13.8	1.150	0.167	0.169	...
1000	13.8	1.150	0.160	0.177	...
1050	13.9	1.158	0.153	0.186	...
1100	14.0	1.167	0.146	0.196	...
1150	14.1	1.175	0.134	0.216	...
1200	14.2	1.183	0.129	0.226	...
1250	14.4	1.200	0.140	0.211	...
1300	14.6	1.217	0.152	0.197	...
1350	14.8	1.233	0.171	0.177	...
1400	15.0	1.250	0.185	0.166	...
1450	15.2	1.267	0.194	0.161	...
1500	15.4	1.283	0.201	0.157	0.282

7. Air

Temperature		ν [2]	μ [2]	Pr [2]	Conductivity		Kin. Visc.
(K) [2]	(°F)	(m^3/kg)	(Pa-s)	(---)	(W/m-K)(2)	(Btu/hr-ft-°F)	(ft^2/s)
200	-100	0.573	1.33E-5	0.740	0.0181	0.0105	8.203E-05
300	80	0.861	1.85E-5	0.708	0.0263	0.0152	1.715E-04
400	260	1.148	2.30E-5	0.694	0.0336	0.0194	2.842E-04
500	440	1.436	2.70E-5	0.688	0.0404	0.0233	4.173E-04
600	620	1.723	3.06E-5	0.690	0.0466	0.0269	5.675E-04
800	980	2.298	3.70E-5	0.705	0.0577	0.0333	9.152E-04
1000	1340	2.872	4.24E-5	0.707	0.0681	0.0393	1.311E-03

8. Wood

Thermal Conductivity (i) (Btu/hr-in-°F)	
Min.	Max.
0.0019	0.0378

(i) The conductivity of wood is affected by a number of basic factors e.g., density, moisture content, and grain direction. The wood conductivity decreases for lower moisture content and lower specific gravity.

The lowest wood conductivity reported in Reference 4 is 0.275 Btu-in/hr-ft^2-°F. This value is measured perpendicular to wood grains in a wood with 0% moisture content and 0.08 specific gravity. Specific gravity of dry balsa is 0.13, and specific gravity of red wood is 0.35-0.4 (Reference 4). The lowest wood conductivity is used to analyze the thermal performance under normal transport conditions, and during the pre- and post-fire accident condition.

The wood conductivity parallel to the grain is 2.0 to 2.8 times greater than the value perpendicular to the grains. The highest conductivity perpendicular to wood grains with 30% moisture content and a specific gravity of 0.8 is 1.950 Btu-in/hr-ft^2-°F (Reference 4). Multiplying this value by 2.8 results in the greatest wood conductivity (5.46 Btu-in/hr-ft^2-°F). The maximum wood conductivity is used during the fire accident condition.

The values in Reference 5 are also bounded y the minimum and the maxim thermal conductivities given in the above table.

(ii) Wood is conservatively given no thermal mass (ρ=0, C_p = 0)

9. Poison Plates

Specific Heat	Density
Btu/lbm-°F	lbm/in^3
0.214	0.098

Properties are from Reference 2 for aluminum. The thermal conductivities are specified in Section 3.3 for the neutron poison plates and will be verified via testing.

10. Aluminum Alloy 6063-T5

Temperature[1] (°F)	Thermal Conductivity [1] (Btu/hr-ft-°F)	Thermal Conductivity (Btu/hr-in-°F)	Diffusivity [1] (ft^2/hr)	Specific Heat (Btu/lbm-°F)	Density [1] (lbm/in^3)
70	120.8	10.067	3.34	0.216	0.097
100	120.3	10.025	3.30	0.217	...
150	119.7	9.975	3.23	0.221	...
200	119.1	9.925	3.18	0.223	...
250	118.3	9.858	3.13	0.225	...
300	118.3	9.858	3.09	0.228	...
350	117.9	9.825	3.04	0.231	...
400	117.6	9.800	3.00	0.234	0.097

11. Lead

Temperature		Conductivity		Specific Heat		Density	
(K) [2]	(°F)	(W/m-K) [2]	(Btu/hr-in-°F)	(kJ/kg-K) [2]	(Btu/lbm-°F)	(kg/m^3) [2]	(lbm/in^3)
200	-100	36.7	1.767	0.125	0.030	11,330	0.409
250	-10	36.0	1.733	0.127	0.030	...	...
300	80	35.3	1.700	0.129	0.031	...	...
400	260	34.0	1.637	0.132	0.032	...	...
500	440	32.8	1.579	0.137	0.033	...	...
600	620	31.4	1.512	0.142	0.034	11,330	0.409

12. Emissivities and Absorptivities

Thermal radiation effects at the external surfaces of the packaging are considered. Impact limiter external surfaces are painted white. The emissivity of white paint varies between 0.93-0.95 and the solar absorptivity varies between 0.12-0.18 ([2] & [6]). To account for dust and dirt, the thermal analysis uses a solar absorptivity of 0.30 and an emissivity of 0.90 for the exterior surfaces of the impact limiters.

The external surface of the cask body is weathered stainless steel (emissivity = 0.85, [6]). To account for dust and dirt and to bound the problem, the thermal analysis uses a solar absorptivity of 0.9 and an emissivity of 0.8 for the cask body external surface.

After a fire, the cask surface will be partially covered in soot (emissivity = 0.95, [7]). Painted surfaces are given a post-fire emissivity of 0.90. The cask body surfaces are given a post-fire emissivity of 0.80. To bound the problem all surfaces are given a solar absorptivity of unity after the fire accident condition.

3.3 Technical Specifications for Components

The neutron poison plates will have the following minimum conductivity:

Temperature		Conductivity	
(°C)	(°F)	(W/m-°C)	(Btu/hr-in-°F)
20	68	120	5.78
100	212	145	6.98
250	482	150	7.22
300	571	150	7.22

3.4 Thermal Evaluation for Normal Conditions of Transport

The normal conditions of transport are used for determination of the maximum fuel cladding temperature, NUHOMS®-MP197 component temperatures, confinement pressures and thermal stresses. These steady state environmental conditions correspond to the maximum daily averaged ambient temperature of 100 °F and the 10CFR Part 71.71(c) insolation averaged over a 24 hour period.

3.4.1 Thermal Models

The finite element models are developed using the ANSYS computer code [10]. ANSYS is a comprehensive thermal, structural, and fluid flow analysis package. It is a finite element analysis code capable of solving steady-state and transient thermal analysis problems in one, two, and three dimensions. Heat transfer via a combination of conduction, radiation, and convection can be modeled by ANSYS. The three-dimensional geometry of the packaging was modeled. Solid entities were modeled by SOLID70 three-dimensional thermal elements. SURF152 surface effect elements were used for the application of the solar heat load.

Two finite element models are used for the normal conditions of transport evaluation:

- A cask body model to determine temperature distributions within the cask body, impact limiters, and thermal shield.

- A basket model to determine temperature distributions within the DSC and it's contents. This model also includes the helium gap between the DSC and the cask cavity inner surfaces.

The interior nodes of the cask body model line up with the exterior nodes of the basket model. The analysis is performed by first running the cask body model. The temperatures on the inner cavity surfaces are then applied as a boundary condition to the exterior nodes of the basket model. This approach allowed the modeling of sufficient detail within the packaging while keeping the overall size of the individual models reasonable.

3.4.1.1 Cask Body Model

To determine component temperatures within the cask body during normal conditions of transport, a finite element model of the cask body is developed. The three-dimensional model represents a 90° symmetric section of the packaging and includes the geometry and material properties of the impact limiters, thermal shield, the cask body, lead, neutron shielding (resin in aluminum containers), and outer shell.

The neutron shielding consists of 60 long slender resin-filled aluminum containers placed between the cask body and outer stainless steel shell. The aluminum containers are confined between the cask body and outer shell, and butt against the adjacent shells. For conservatism, an air gap of 0.01 in. at thermal equilibrium is assumed to be present between the resin boxes and adjacent shells. Radiation across these gaps is conservatively neglected. The redwood and balsa

within the impact limiters are modeled as an isotropic material containing bounding material properties as described in Section 3.2 for wood.

The finite element plot of the cask body model is shown in Figure 3-1.

Generally, good surface contact is expected between adjacent components. However, to bound the heat conductance uncertainty between adjacent components, the following gaps at thermal equilibrium are assumed:

- 0.0100" radial gaps between resin boxes and adjacent shells
- 0.0300" radial gap between lead and cask body
- 0.0600" radial gap between cask lid and cask body
- 0.0625" axial gap between cask lid and cask body
- 0.0600" radial and axial gaps between ram plate and cask body
- 0.0625" axial gap between rear impact limiter and thermal shield
- 0.0625" axial gap between thermal shield and cask body
- 0.1250" axial gap between front impact limiter and cask body
- 0.0625" axial gap between thermal shield and impact limiter

All heat transfer across the gaps is by gaseous conduction. Other modes of heat transfer are neglected.

Heat Dissipation

Heat is dissipated from the surface of the packaging by a combination of radiation and natural convection.

Heat dissipation by natural convection is described by the following equations for the average Nusselt number [11]:

$$\overline{N}_{u_L} = \overline{H}_c \frac{L}{k} = 0.13(Gr_L Pr)^{1/3} \quad \text{for } Pr\,Gr_L > 10^9 \qquad \text{(Horizontal cylinders and vertical surfaces)}$$

$$\overline{N}_{u_L} = \overline{H}_c \frac{L}{k} = 0.59(Gr_L Pr)^{1/4} \quad \text{for } 10^4 < Pr\,Gr_L < 10^9 \qquad \text{(vertical surfaces)}$$

where,

Gr_L = Grashof number = $\rho^2 g\beta(T_s-T_a)L^3/\mu^2$
ρ = density, lb/ft^3
g = acceleration due to gravity, ft/sec^2
β = temperature coefficient of volume expansion, 1/R
μ = absolute viscosity, lb/ft-sec
L = characteristic length, ft
Pr = Prandtl number
H_c = natural convection coefficient

The heat transfer coefficient, H_r, for heat dissipation by radiation, is given by the equation:

$$H_r = G_{12}\left[\frac{\sigma(T_1^4 - T_2^4)}{T_1 - T_2}\right] Btu/hr - ft^2 - {}^oF$$

where,

G_{12} = the gray body exchange coefficient
= (surface emissivity) (view factor)
T_1 = ambient temperature, °R
T_2 = surface temperature, °R

The total heat transfer coefficient $H_t = H_r + H_c$, is applied as a boundary condition on the outer surfaces of the finite element model.

3.4.1.2 Basket Model

To determine component temperatures within the canister and its contents during normal conditions of transport a finite element model is developed. The three-dimensional model represents a 90° symmetric section of the packaging and includes the geometry and material properties of the canister, basket, fuel assembly active lengths, basket peripheral inserts, and the helium between the canister and the cask body.

The finite element plot of the basket model is shown in Figure 3-2.

To bound the heat conductance uncertainty between adjacent packaging components the following gaps at thermal equilibrium are assumed:

- 0.0100" surrounding outside of the fuel compartments
- 0.0100" between the fuel compartment wrap and plates parallel to the wrap
- 0.0400" between the fuel compartment wrap and plates perpendicular to the wrap
- 0.0950" between perpendicular plates
- 0.0100" between plates and basket rails
- 0.1250" axial gap between bottom of canister and cask body

Maximum Fuel Cladding Temperature

The finite element model includes a representation of the spent nuclear fuel that is based on a fuel effective conductivity model. The decay heat of the fuel with a peaking factor of 1.2 was applied directly to the fuel elements. The maximum fuel temperature reported is based on the results of the temperature distribution in the fuel region of the model. As described in Appendix 3.7.1, the homogenized fuel properties are chosen to match both the temperature drop between basket walls and fuel assembly center pin, and the effective conductivity of the fuel assemblies.

Average Cavity Gas Temperature

The cavity gas temperatures are calculated using maximum component temperatures under normal and hypothetical accident conditions of transport. For simplicity and conservatism, the average gas temperature within the canister is assumed to be the average of the maximum fuel cladding and canister wall temperatures. Within the cask body the average cavity gas temperature is taken to be the average of the maximum cask body and canister wall temperatures.

3.4.1.3 Decay Heat Load

The decay heat load corresponds to a total heat load of 15.86 kW from 61 assemblies (0.260 kW/assy.) with a peaking factor of 1.2. A typical heat profile for spent BWR fuel with an axial peaking factor of 1.2 was used to distribute the decay heat load in the axial direction within the active length regions of the models. This heat profile is shown below. Within the basket model, the decay heat load is applied as volumetric heat generation in the elements that represent the homogenized fuel. Within the Cask Body model the heat is applied as heat fluxes into the elements that model the cask cavity wall.

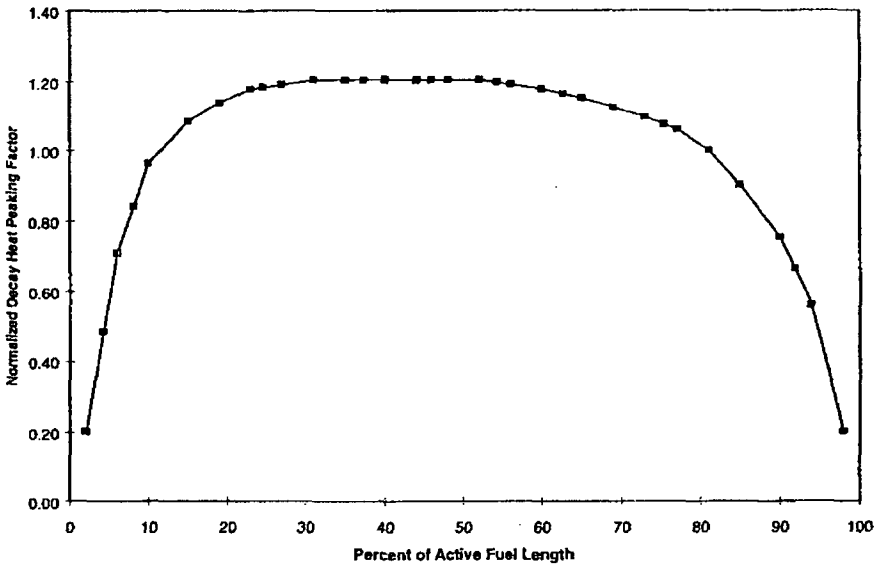

The elements representing the homogenized fuel assemblies are divide into 12 equal size intervals. Every interval is 12" long. Average peaking factors are calculated for these intervals based on the typical heat profile. Heat generating rate per unit volume of the homogenized fuel assembly is calculated as follows:

$$Q''' = \frac{Q}{V} = \frac{Q}{a \times a \times L_a} = \frac{0.26 \times 3412.3}{6.0 \times 6.0 \times 144} = 0.171 \qquad \text{Btu/in}^3$$

Where,

Q = Decay heat load per assembly = 0.26 kW

V = Volume of one homogenized assembly considering active fuel length
a = width of homogenized fuel assembly = 6.0"
L_a = Active fuel length = 144"

The volumetric heat generating value is multiplied by the average peaking factor of each interval. The average peaking factors and the resultant heat generating rates are listed in the following table.

Interval No. from Top of Active Fuel	Average Peaking Factor	Heat Generating Rate (Btu/in^3)
1	0.51	0.087
2	1.07	0.183
3	1.17	0.200
4	1.20	0.205
5	1.20	0.205
6	1.19	0.204
7	1.17	0.200
8	1.14	0.195
9	1.10	0.188
10	1.02	0.175
11	0.84	0.144
12	0.41	0.070

3.4.1.4 Solar Heat Load

The total insolation for a 12-hour period in a day is 1475 Btu/ft^2 for curved surfaces and 738 Btu/ft^2 for flat surfaces not transported horizontally as per 10CFR Part 71.71(c). This insolation is averaged over a 24-hr period (daily averaged value) and applied as a constant heat flux to the external surfaces of the cask body model. Daily averaging of the solar heat load is justified based on the large thermal inertia of the NUHOMS®-MP197 packaging. Solar absorptivities of 0.30 and 0.9 are used for the painted and stainless steel surfaces of the packaging, respectively. Multiplying the total insolation by the solar absorptivity values gives the maximum amount of insolation that can be absorbed on each surface. The following table shows the applied solar heat fluxes in the finite element models.

Location in FE-Model	Surface Shape	Total Insolance Per 10CFR 71.71 ($gcal/cm^2$) / (Btu/ft^2)	Conditions	Surface Absoptivity	Solar Heat Flux applied over Surface Effect Elements ($Btu/hr\text{-}in^2$)
Radial Surface of Impact Limiter	Curved	400 / 1475	Steady State (Pre Fire)	0.3	0.128
			Post Fire	1.0	0.427
Top & Bottom Surfaces of Impact Limiter	Flat, Vertical	200 / 738	Steady State (Pre Fire)	0.3	0.064
			Post Fire	1.0	0.216
Radial Surface of Cask Body	Curved	400 / 1475	Steady State (Pre Fire)	0.9	0.384
			Post Fire	1.0	0.427

3.4.2 Maximum Temperatures

Steady state thermal analyses are performed using the maximum decay heat load of 0.260 kW per assembly (15.86 kW total), 100°F ambient temperature and the maximum insolation. The temperature distributions within the cask body and basket models are shown in Figures 3-3 and 3-4, respectively. The temperature distribution within the basket is shown in Figure 3-5. The fuel assembly temperature distribution is shown in Figure 3-6. A summary of the calculated cask component temperatures is listed in Table 3-1.

3.4.3 Maximum Accessible Surface Temperature in the Shade

The accessible surfaces of the NUHOMS®-MP197 packaging consist of the personnel barrier and outermost vertical and radial surfaces of the impact limiters. The cask body model is run without insolation to determine the accessible surface temperature of the impact limiters in the shade. The maximum accessible surface temperature of the impact limiters in the shade does not exceed 110 °F.

The personnel barrier surrounds approximately one fourth of the cask body and has an open area of at least 80%. Heat transfer between the cask and barrier will be minimal due to the small radiation view factor between the cask and barrier. The personnel barrier rises 90 in. above the base of the transport frame and limits the accessible packaging surfaces to only the impact limiter surfaces. Accessible surfaces of the packaging remain below the design criteria of 185 °F (85 °C).

3.4.4 Minimum Temperatures

Under the minimum temperature condition of -40°F (-40°C) ambient, the resulting packaging component temperatures will approach -40°F if no credit is taken for the decay heat load. Since the package materials, including containment structures and the seals, continue to function at this temperature, the minimum temperature condition has no adverse effect on the performance of the NUHOMS®-MP197.

Temperature distributions under the minimum ambient temperatures of –20°F and -40°F with no insolation and the maximum design heat load are determined. Table 3-2 lists the results of these analyses.

3.4.5 Maximum Internal Operating Pressure

The maximum internal pressures within the NUHOMS®-MP197 cask body and DSC during normal conditions of transport are calculated within Appendix 3.7.3.

3.4.6 Maximum Thermal Stresses

The maximum thermal stresses during normal conditions of transport are calculated in Chapter 2.

3.4.7 Evaluation of Cask Performance for Normal Conditions of Transport

The thermal analysis for normal transport concludes that the NUHOMS®-MP197 packaging design meets all applicable requirements. The maximum component temperatures calculated using conservative assumptions are low. The maximum seal temperature (217°F, 103°C) during normal transport is well below the 400°F long-term limit specified for continued seal function. The maximum neutron shield temperature is below 300°F (149°C) and no degradation of the neutron shielding is expected. The predicted maximum fuel cladding temperature is well within allowable fuel temperature limit of 1058°F (570°C). The comparison of the results with the allowable ranges is tabulated below:

	Temperature, °F		
Component	**Maximum**	**Minimum**	**Allowable Range**
Seal	217	-40	-40 to 400
Neutron Shield	249	-40	-40 to 300
Fuel Cladding	598	-40	1058 max.
Lead	299	-40	620 max.

3.5 Thermal Evaluation for Accident Conditions

The NUHOMS®-MP197 packaging is evaluated under the hypothetical accident sequence of 10CFR71.73. In order to demonstrate that the seal, fuel cladding, and lead temperatures remain below thermal design requirements, four analytical models are developed as discussed below.

3.5.1 Fire Accident Evaluation

The fire thermal evaluation is performed primarily to demonstrate the containment integrity of the packaging. This is assured as long as the containment seals remain below 400°F and the cavity pressure is less than 50 psig (4.4 atm absolute pressure). Four models are used for the evaluation:

- A cask cross-section model for the determination of the peak fuel cladding temperature.
- A cask body model to evaluate the performance of the seals under hypothetical accident conditions.
- A trunnion-region model to demonstrate that lead remains below its melting point during hypothetical accident conditions.
- A bearing block-region model to demonstrate that lead remains below its melting point during hypothetical accident conditions.

During the free drop and puncture conditions, the steel encased wood impact limiters are locally deformed but remain firmly attached to the cask. Because of the very low conductivity of wood, a minimal amount of wood is required to provide adequate insulation during the fire accident condition. Therefore, there is a negligible change in the thermal performance of the impact limiters due to dimensional changes caused by the hypothetical accident conditions of 10CFR71.73. Under exposure to the thermal accident environment the wood at the periphery of the impact limiter shell would char but not burn.

An average convective heat transfer coefficient of 2.75 Btu/hr-ft^2-°F is utilized for the fire accident evaluation as calculated in Appendix 3.7.2.

3.5.2 Cask Cross Section Model

To demonstrate that the peak fuel cladding temperature remains below thermal design limits, a cask cross-section finite element model of the NUHOMS®-MP197 packaging was developed. The three-dimensions, quarter-symmetry model includes the cask body, canister, basket, and fuel along the 144" active fuel length. To bound the heat conductance uncertainty between adjacent packaging components the same gap assumptions made in sections 3.4.1.1 and 3.4.1.2 are applied to the model.

During the pre-fire condition, convection and radiation from the external surface of this model are as in normal conditions of transport (100°F ambient). During the fire phase, a constant convective heat transfer coefficient of 2.75 Btu/hr-ft^2-°F is used. As per 10CFR71.73, a 30 minute 1,475°F flame temperature with an emittance of 0.9 and a surface absorptivity of 0.8 is used during the fire accident condition. During the fire accident condition, gaps within the cask body and basket were removed to maximize heat input into the model from the fire. These gaps are included during the pre- and post-fire accident conditions. See Section 3.4.1 for a detailed description of the model including the method used to calculate the maximum fuel cladding temperature and the average cavity gas temperature. The decay heat load is applied as per Section 3.4.1.3.

The Cask Cross Section finite element model and the temperature distribution at the end of the fire accident condition are shown in Figures 3-7 and 3-9, respectively. The maximum temperature distribution within the fuel assemblies is shown in Figure 3-10.

3.5.3 Cask Body Model

To demonstrate the integrity of the seals during the fire accident, the cask body finite element model of the NUHOMS®-MP197 packaging developed in Section 3.4.1.1 was run under hypothetical accident conditions. Pre-Fire, Fire accident, and Post-Fire cool-down boundary conditions are determined as per Section 3.5.2. During the fire accident condition, gaps within the packaging were removed to maximize heat input into the model from the fire. These gaps are included during the pre- and post-fire accident conditions. The decay heat load is applied as per Section 3.4.1.3.

The Cask Body finite element model and the temperature distribution at the end of the fire accident condition are shown in Figures 3-1 and 3-8, respectively.

3.5.4 Trunnion Region Model

To determine the peak transient lead temperature in the region of the trunnions, a trunnion region finite element model was developed. The two-dimensional, axisymmetric model represents the geometry and material properties of the trunnion block, trunnion plug, and cask body in the region of the trunnion.

To bound the heat conductance uncertainty between adjacent packaging components the following gaps at thermal equilibrium are assumed:

- 0.0100" between the trunnion plug and the neutron absorbing resin
- 0.0100" between the trunnion plug and the trunnion block
- 0.0100" between the resin and the cask outer shell
- 0.0100" between the trunnion block and the cask outer shell
- 0.0300" radial gap between lead and cask body

Pre-Fire, Fire accident, and Post-Fire cool-down boundary conditions are determined as per Section 3.5.2. During the fire accident condition, gaps within the packaging were removed to

maximize heat input into the model from the fire. These gaps are included during the pre- and post-fire accident conditions. The decay heat load is applied as a flux including a peaking factor of 1.2.

The trunnion region finite element model and the temperature distribution at the time of peak lead temperature are shown in Figures 3-11 and 3-12, respectively.

3.5.5 Bearing Block Region Model

To determine the peak transient lead temperature in the region of the bearing block, a bearing block region finite element model was developed. A three-dimensional quarter-symmetry finite element model was created of the bearing block including the geometry and material properties of the adjacent neutron shielding and the corresponding portion of the cask body. Solid entities were modeled by SOLID70 three-dimensional thermal elements.

To bound the heat conductance uncertainty between adjacent packaging components the following gaps at thermal equilibrium are assumed:

- 0.0100" radial gaps between resin boxes and adjacent shells
- 0.0300" radial gap between lead and cask body
- 0.0600" gap between the bearing block and the resin/resin boxes in radial, axial, and circumfrential directions

Pre-Fire, Fire accident, and Post-Fire cool-down boundary conditions are determined as per Section 3.5.2. During the fire accident condition, gaps within the packaging were removed to maximize heat input into the model from the fire. These gaps are included during the pre- and post-fire accident conditions. The decay heat load is applied as a flux including a peaking factor of 1.2.

The bearing block region finite element model and the temperature distribution at the time of peak lead temperature are shown in Figures 3-13 and 3-14, respectively.

3.5.6 Maximum Internal Operating Pressure

The maximum internal pressures within the NUHOMS®-MP197 cask body and DSC during hypothetical accident conditions of transport are calculated within Appendix 3.7.3.

3.5.7 Summary of Results

Table 3-3 presents the maximum temperatures of the cask components during the fire event. The maximum temperatures calculated for the seals and the fuel cladding are 279°F and 680°F, respectively.

3.5.8 Evaluation of Package Performance during Fire Accident Conditions

It is concluded that the NUHOMS®-MP197 packaging maintains containment during the postulated accident conditions. The maximum seal temperature is below the 400°F limit specified for seal function and the fuel cladding temperature is well below the limit of 1058°F (570°C).

A comparison of the results with the temperature limits is tabulated below:

Component	Temperature, °F	
	Maximum	**Limit**
Seal	279	400 max.
Fuel Cladding	680	1058 max.
Lead	478	620 max.

3.6 References

1. *ASME Boiler and Pressure Vessel Code*, American Society of Mechanical Engineers, Section II, 1998.

2. *Handbook of Heat Transfer Fundamentals*, W. Rohsenhow and J. Harnett, McGraw-Hill Publishing, New York, 1985.

3. *TN-24 Dry Storage Cask Topical Report*, Transnuclear, Inc., Revision 2A, Hawthorne, NY, 1989.

4. *Wood Handbook: Wood as an Engineering Material*, U.S. Department of Agriculture, Forest Service, March 1999.

5. NUREG/CR-0200, Vol. 3, Rev. 6, SCALE, A Modular Code System for Performing Standardized Computer Analyses for Licensing Evaluation.

6. *Principles of Heat Transfer, Fourth Edition*, Kreith et. al., Harper & Row, Publishers, New York, 1986.

7. *Standard Handbook for Mechanical Engineers, Seventh Edition*, Baumeister & Marks, McGraw-Hill Book Co., New York, 1969

8. *Parker O-Ring Handbook 5700*, Y2000 Edition, 1999

9. PNL-4835, Johnson et. al., Technical Basic for Storage of Zircalloy-Clad Spent Fuel in Inert Gases, Pacific Northwest Laboratory, 1983.

10. ANSYS Engineering Analysis System, *User's Manual for ANSYS Revision 5.6*, ANSYS, Inc., Houston, PA.

11. *Chemical Engineers' Handbook, Fifth Edition*, Perry P.H. and Chilton C.H., McGraw-Hill Book Co., New York, 1973.

12. *TN-68 Dry Storage Cask Final Safety Analysis Report*, Transnuclear Inc., Revision 0, Hawthorne, NY, 2000.

13. *Standard Review Plan for Transportation Packages for Spent Nuclear Fuel*, NUREG-1617, 2000.

14. NUHOMS COC 1004 Amendment No. 3, 2000

15. Material Report Number KJ0835, Parker O-Ring Division, 1989.

TABLE 3-1

COMPONENT TEMPERATURES IN THE NUHOMS®-MP197 PACKAGING

Component	Normal Transport			Fire Accident	
	Maximum (°F)	Minimum* (°F)	Allowable Range(°F)	Peak(°F)	Allowable Range(°F)
Thermal Shield	186	-40	**	1172	**
Impact Limiters	195	-40	**	1456	N/A
Resin	249	-40	-40 to 300	N/A	N/A
Lead	299	-40	620 max.	478	620 max.
Cask Body	302	-40	**	535	**
Outer Shell	263	-40	**	N/A	**
Flourocarbon Seals, Ram Plate	217	-40	-40 to 400	270	-40 to 400
Flourocarbon Seals, Lid	204	-40	-40 to 400	279	-40 to 400
Canister	388	-40	**	485	**
Basket Peripheral Inserts	482	-40	**	564	**
Basket	578	-40	**	661	**
Fuel Cladding	598	-40	1058 max.	680	1058 max.
Average Cavity Gas (Cask Body)	345	-40	N/A	504	N/A
Average Cavity Gas (Canister)	493	-40	N/A	583	N/A

* Assuming no credit for decay heat and an ambient temperature of -40°F
** The components perform their intended safety function within the operating range.

TABLE 3-2

TEMPERATURE DISTRIBUTION IN THE NUHOMS®-MP197 PACKAGE
(MINIMUM AMBIENT TEMPERATURES)

Component	Maximum Component Temperature	
	-20 °F Ambient	-40 °F Ambient
Thermal Shield	65	47
Impact Limiters	73	56
Resin	128	111
Lead	183	167
Cask Body	187	170
Flourocarbon Seals, Ram Plate	187*	170*
Flourocarbon Seals, Lid	187*	170*
Canister	282	267
Basket Peripheral Inserts	381	367
Basket	482	468
Fuel Cladding	505	492

* Taken to be the maximum temperature within cask body and lid.

TABLE 3-3

MAXIMUM TRANSIENT TEMPERATURES DURING FIRE ACCIDENT

Component	Maximum Transient
Thermal Shield	1172 (End of Fire)
Lead	478 (4.7 Hours)
Cask Body	535 (End of Fire)
Flourocarbon Seals, Ram Plate	270 (31.0 Hours)
Flourocarbon Seals, Lid	279 (12.0 Hours)
Canister	485 (4.9 Hours)
Basket Peripheral Inserts	564 (15.9 Hours)
Basket	661 (24.9 Hours)
Fuel Cladding	680 (27.9 Hours)
Average Cavity Gas (Cask Body)	504
Average Cavity Gas (Canister)	583

FIGURE 3-1

FINITE ELEMENT PLOT,
CASK BODY MODEL

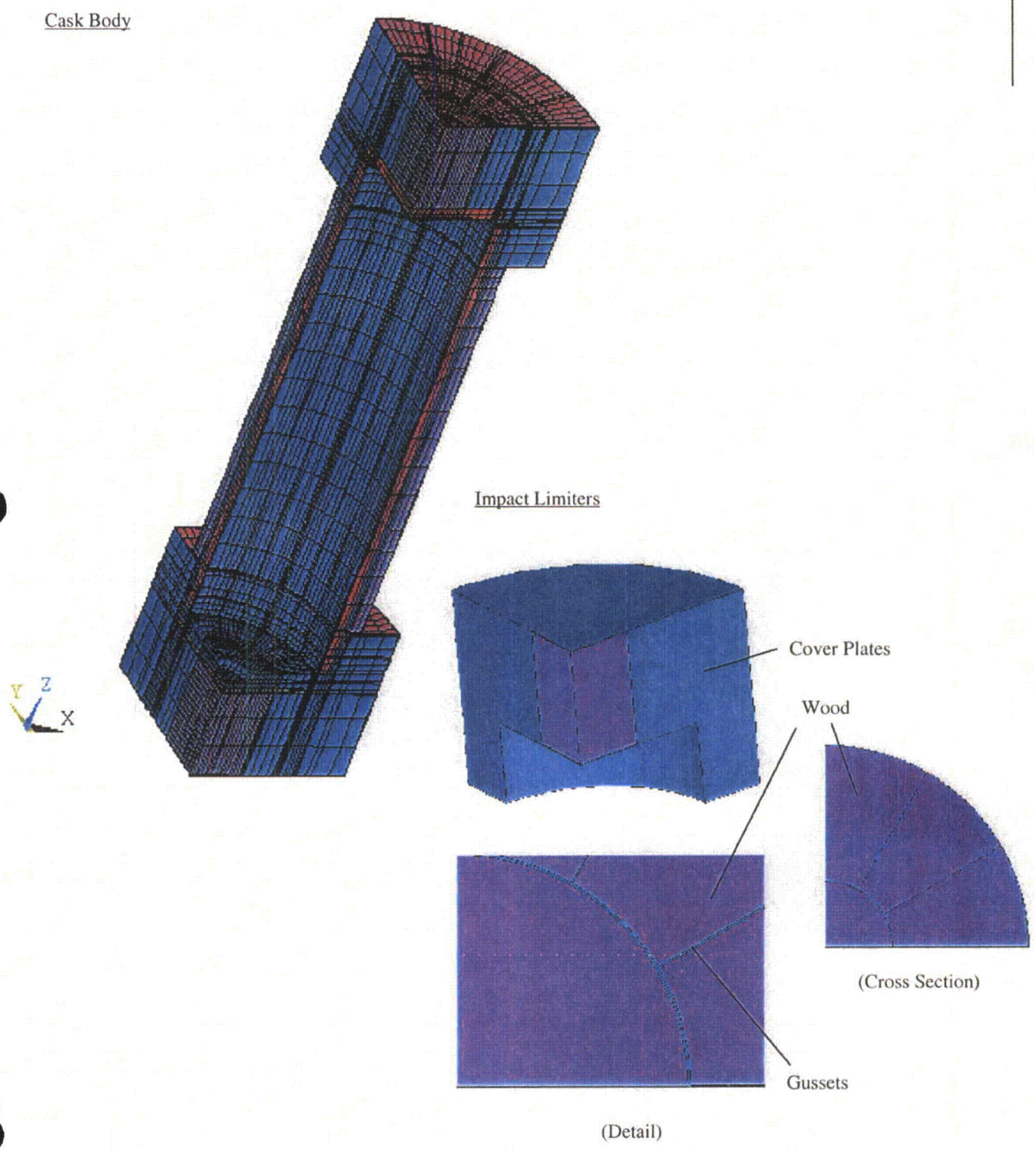

FIGURE 3-2

FINITE ELEMENT PLOT,
BASKET AND CANISTER MODEL

FIGURE 3-3

TEMPERATURE DISTRIBUTION,
CASK BODY MODEL
(NORMAL CONDITIONS OF TRANSPORT)

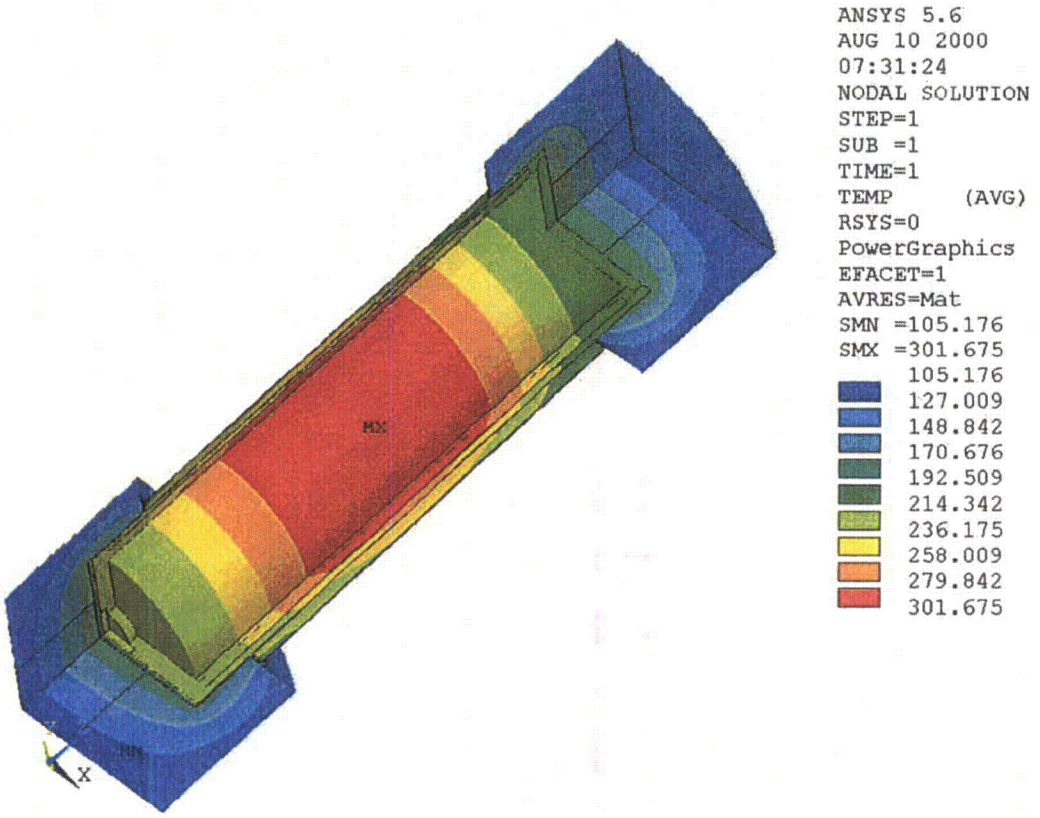

FIGURE 3-4

TEMPERATURE DISTRIBUTION,
BASKET AND CANISTER MODEL
(NORMAL CONDITIONS OF TRANSPORT)

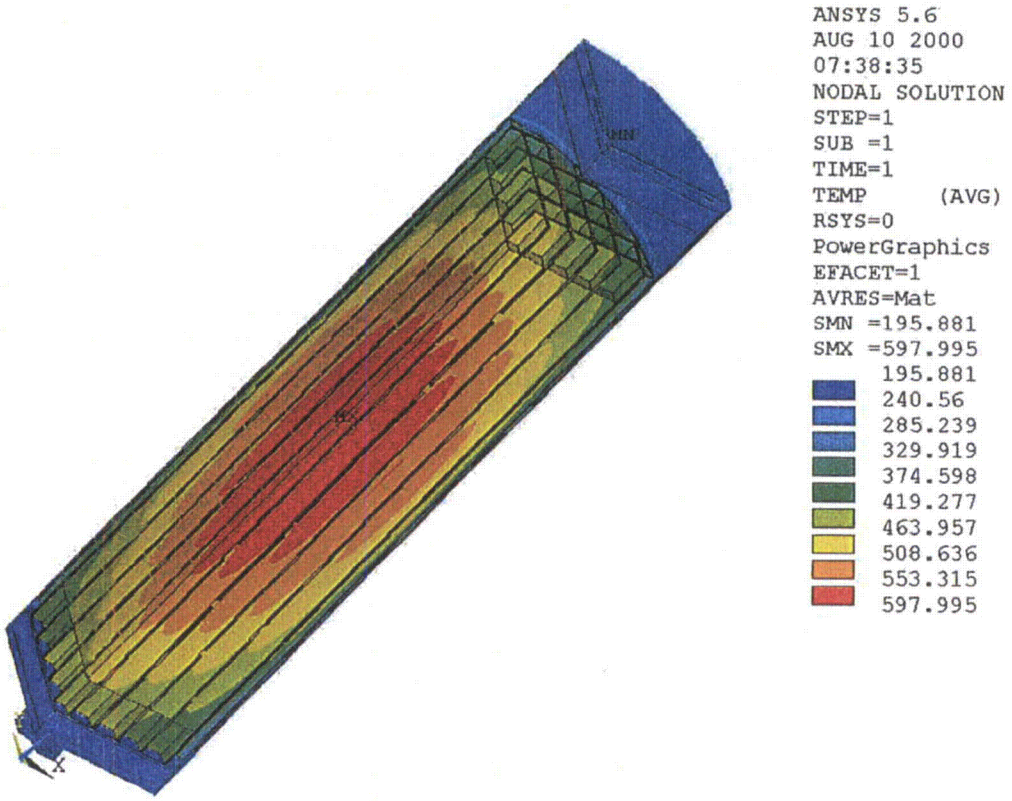

FIGURE 3-5

TEMPERATURE DISTRIBUTION,
BASKET
(NORMAL CONDITIONS OF TRANSPORT)

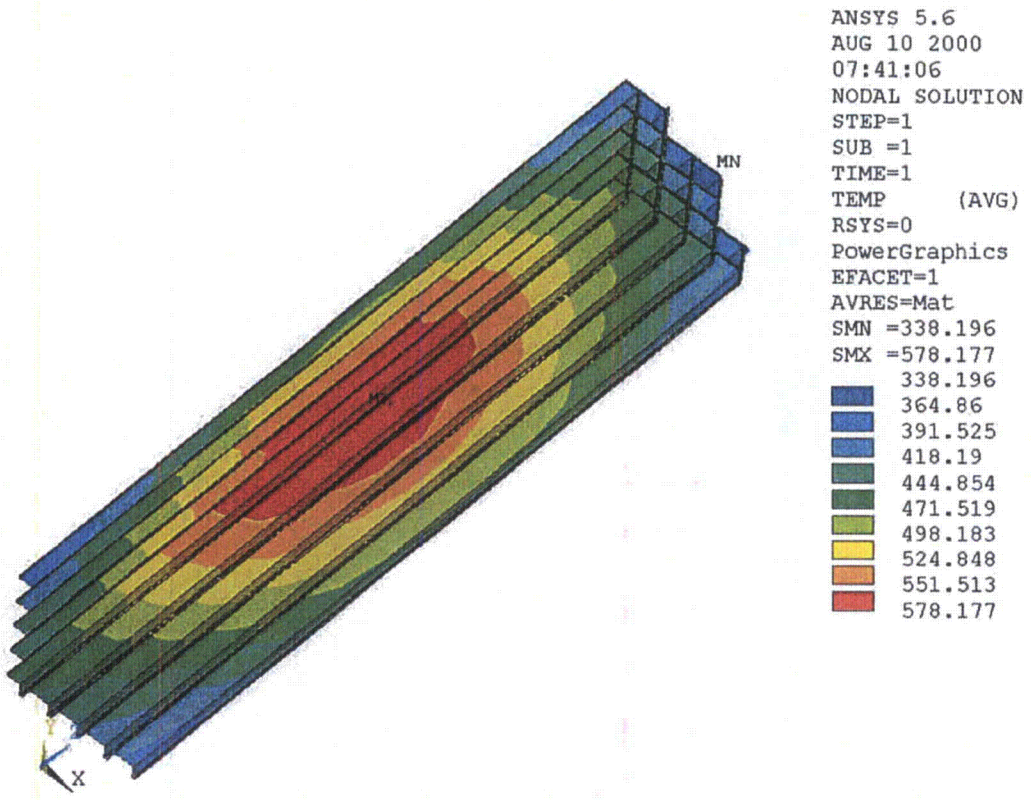

FIGURE 3-6

TEMPERATURE DISTRIBUTION,
FUEL ASSEMBLIES
(NORMAL CONDITIONS OF TRANSPORT)

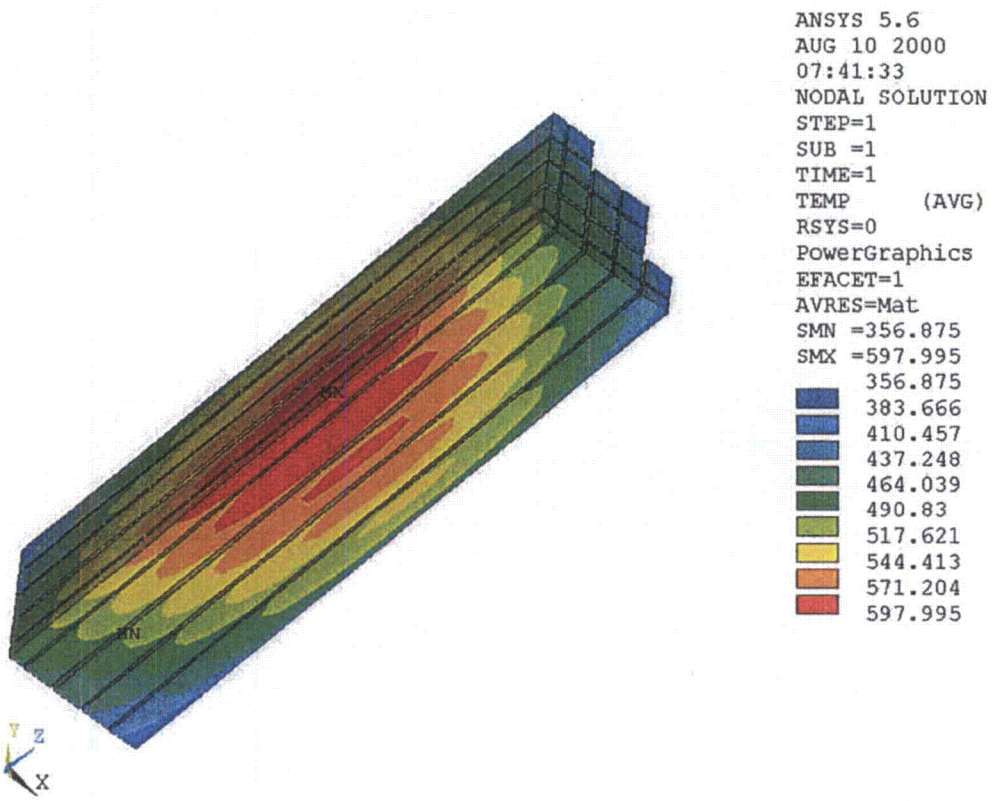

FIGURE 3-7

FINITE ELEMENT PLOT,
CASK CROSS-SECTION MODEL

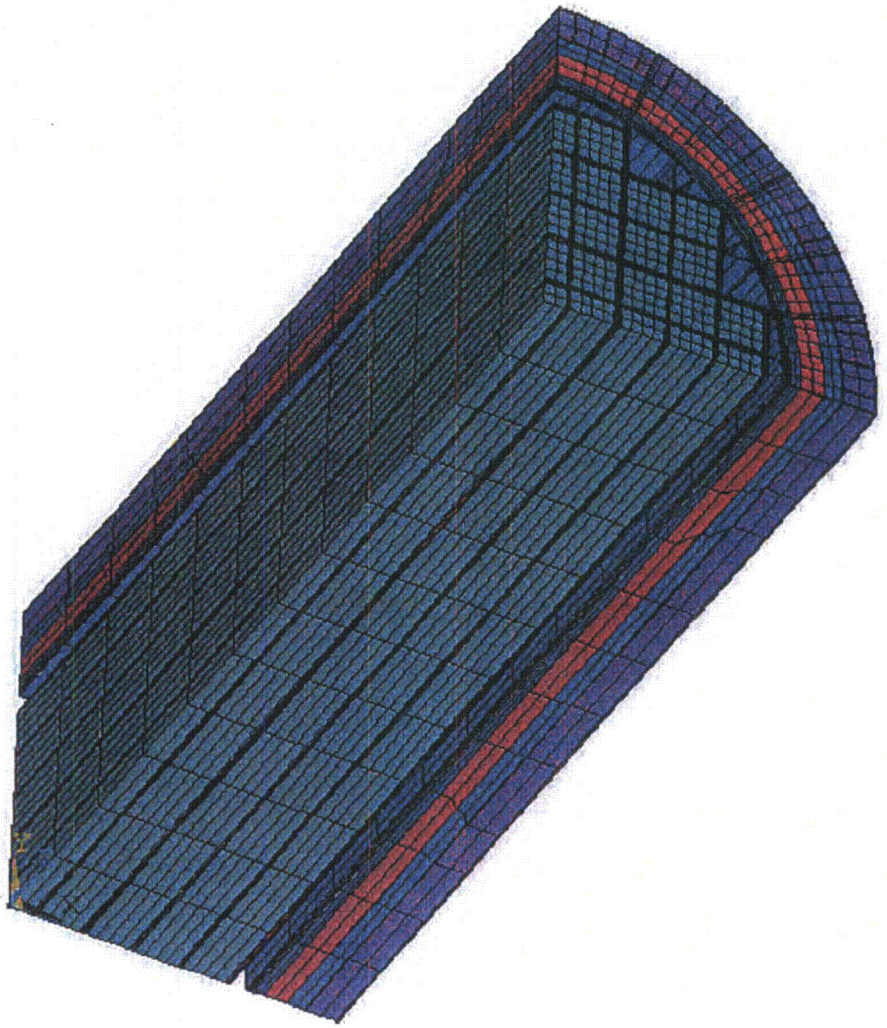

FIGURE 3-8

TEMPERATURE DISTRIBUTION,
CASK BODY MODEL, END OF FIRE
(HYPOTHETICAL ACCIDENT CONDITIONS)

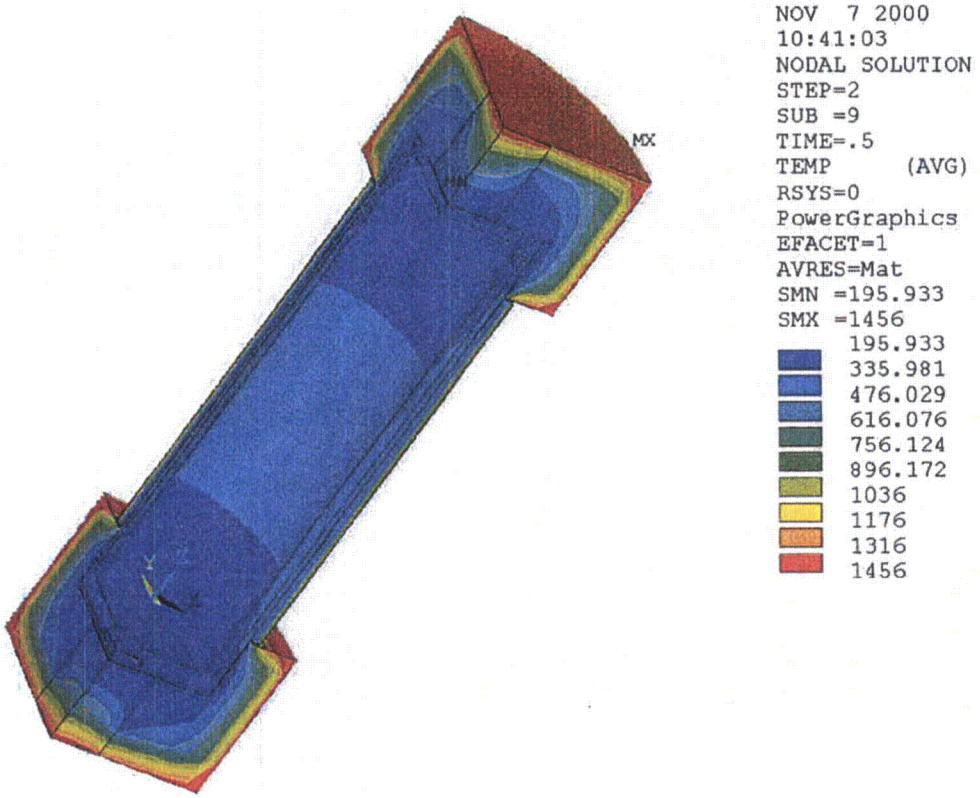

FIGURE 3-9

TEMPERATURE DISTRIBUTION,
CASK CROSS SECTION MODEL, END OF FIRE
(HYPOTHETICAL ACCIDENT CONDITIONS)

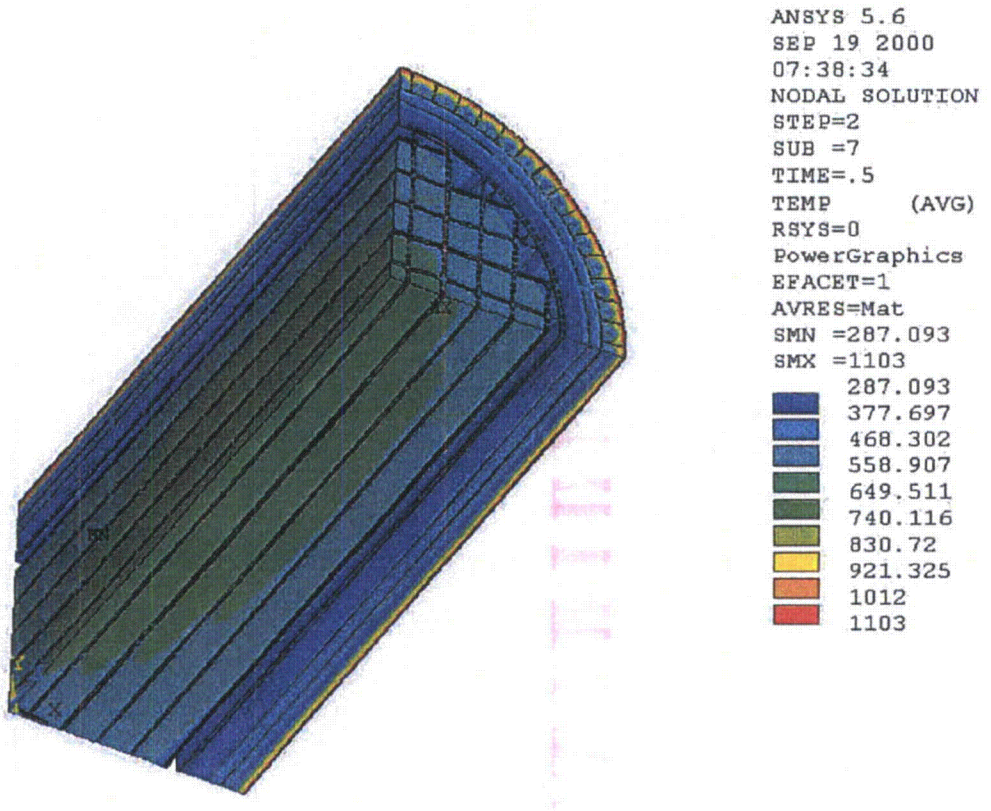

FIGURE 3-10

TEMPERATURE DISTRIBUTION,
FUEL ASSEMBLIES, PEAK TEMPERATURES
(HYPOTHETICAL ACCIDENT CONDITIONS)

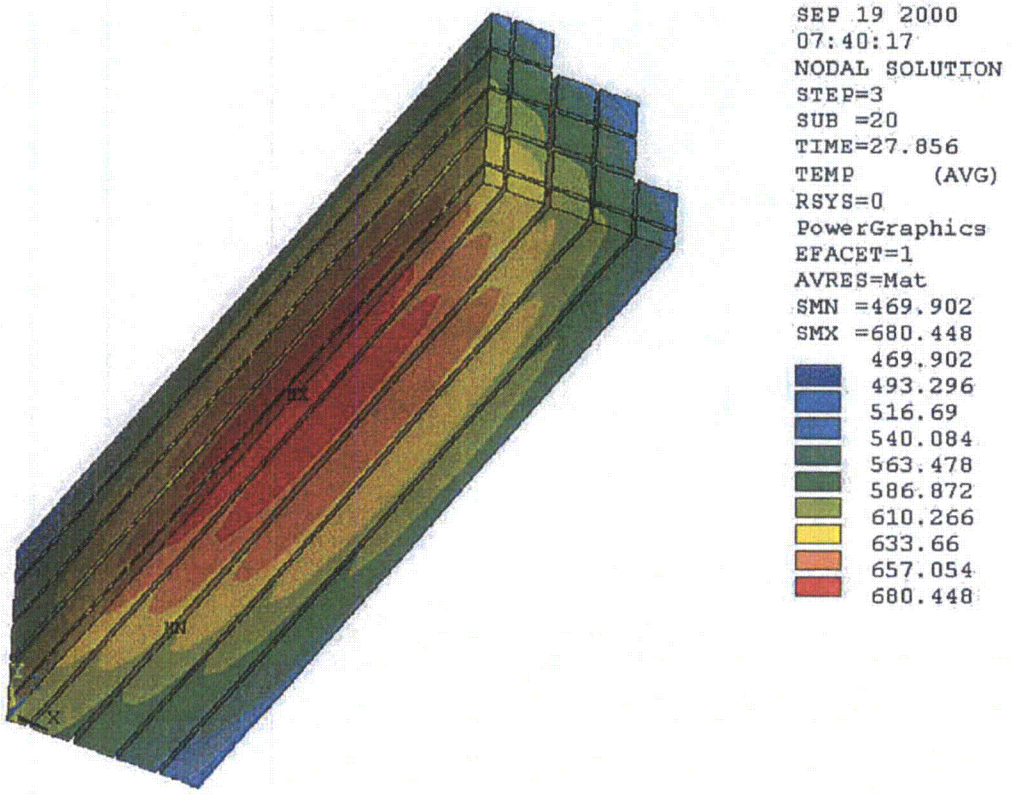

FIGURE 3-11

FINITE ELEMENT PLOT,
TRUNNION REGION MODEL

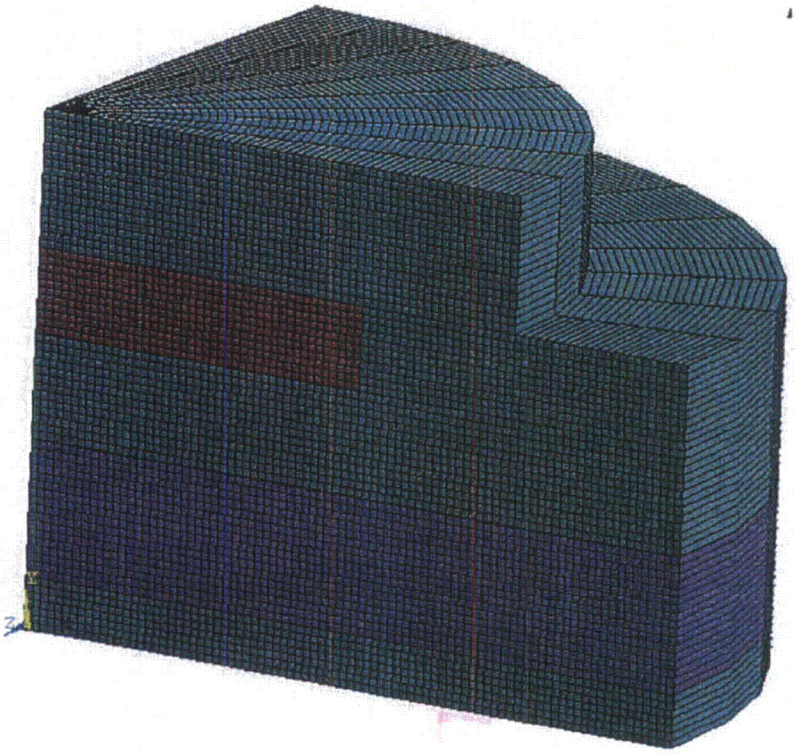

FIGURE 3-12

TEMPERATURE DISTRIBUTION,
TRUNNION REGION MODEL
(TIME = 4.7 HOURS)

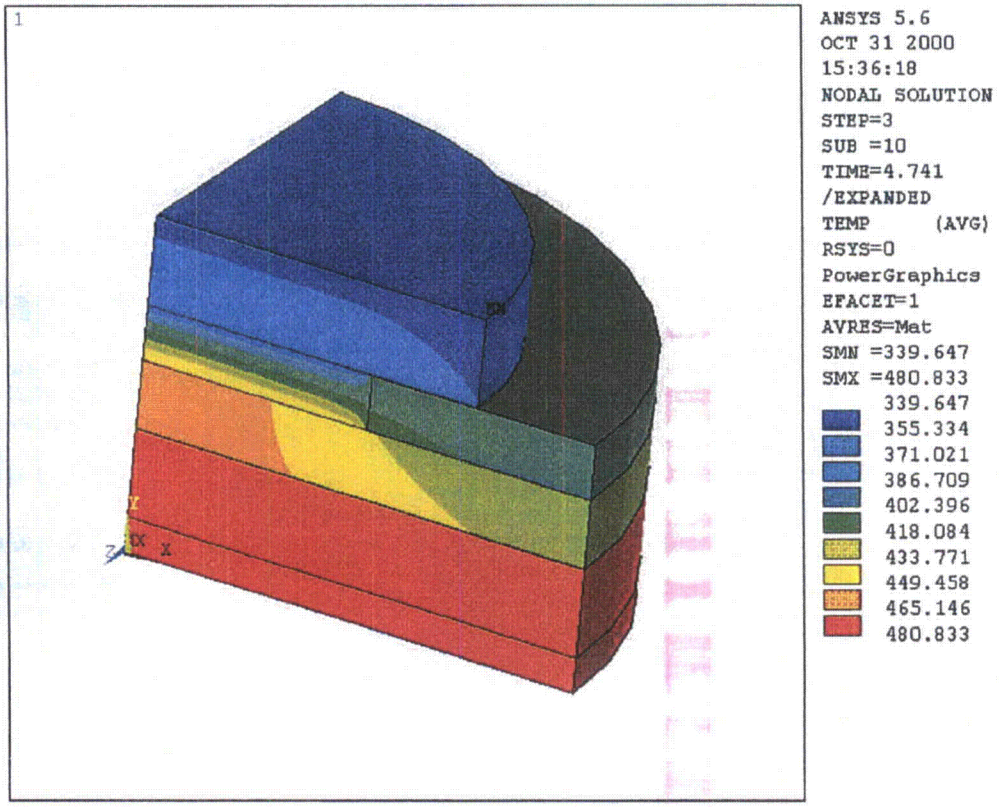

FIGURE 3-13

FINITE ELEMENT PLOT,
BEARING BLOCK REGION MODEL

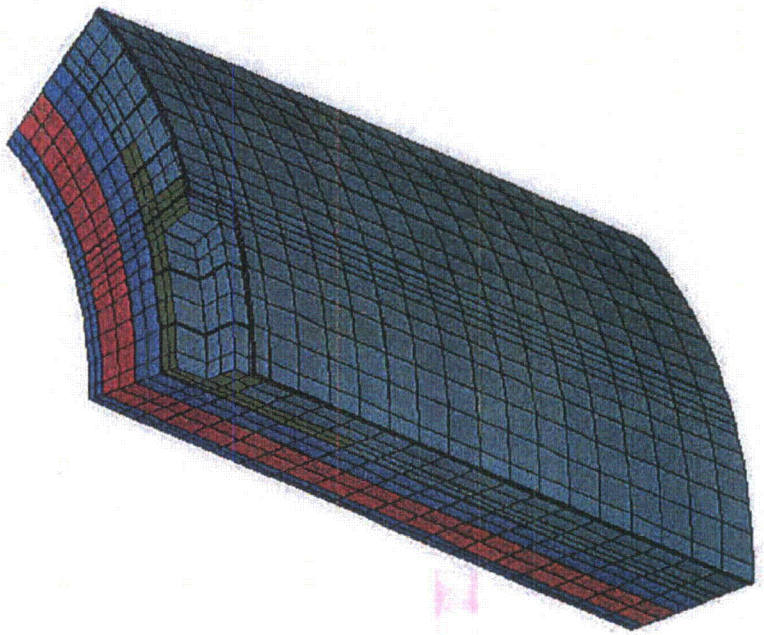

FIGURE 3-14

TEMPERATURE DISTRIBUTION,
BEARING BLOCK REGION MODEL
(TIME = 2.9 HOURS)

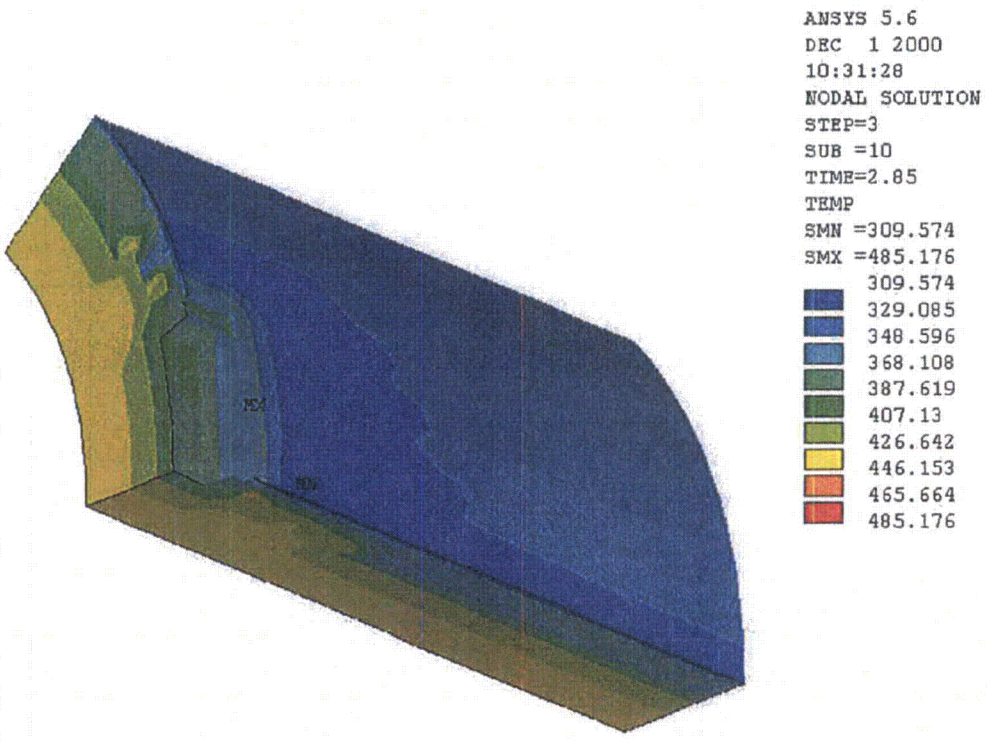

APPENDIX 3.7.1

TABLE OF CONTENTS

LIST OF TABLES

LIST OF FIGURES

APPENDIX 3.7.1

EFFECTIVE THERMAL CONDUCTIVITY FOR THE FUEL ASSEMBLY

3.7.1.1 Discussion

The transportable NUHOMS®-MP197 finite element models simulate the effective thermal properties of the fuel with a homogenized material occupying the volume within the basket where the active fuel lengths are stored. Effective values for density, specific heat, and conductivity are determined for this homogenized material for use in the finite element models.

The NUHOMS®-MP197 shall be capable of handling a wide variety of spent BWR fuel assemblies. In order to determine the appropriate effective thermal properties of the fuel assembly, a study was performed of the BWR fuel assemblies to be stored in the NUHOMS®-MP197 packaging. The lowest effective thermal conductivity, density, and specific heat of the studied fuel assemblies are selected to apply in the finite element model. Use of these properties would conservatively predict bounding maximum temperatures for the components of the NUHOMS®-MP197.
Parameters of the fuel assemblies to be stored in the NUHOMS®-MP197 are listed in Table 3.7.1-1.

3.7.1.2 Summary of Material Properties

a. UO_2 Fuel

Thermal Conductivity [2] (Btu/hr-in-°F)	Specific Heat [1] (Btu/lbm-°F)	Density [1] (lbm/in^3)
0.1926 (i)	0.0560 (ii)	0.396

(i) bounds values for temperatures below 750 K (890 °F)

(ii) bounds values found in reference

b. Zircaloy-2

Thermal Conductivity [2] (Btu/hr-in-°F)	Specific Heat [2] (Btu/lbm-°F)	Density [1] (lbm/in^3)	Emissivity [2] (---)
0.6019 (i)	0.0657 (i)	0.237	0.74 (i)

(i) bounds values found in reference

c. Helium

Temperature [3] (K)	Thermal Conductivity [3] (W/m-K)	Temperature (°F)	Thermal Conductivity (Btu/hr-in-°F)
200	0.1151	-100	0.0055
250	0.1338	-10	0.0064
300	0.150	80	0.0072
400	0.180	260	0.0087
500	0.211	440	0.0102
600	0.247	620	0.0119
800	0.307	980	0.0148
1000	0.363	1340	0.0175

d. Stainless Steel SA-240, Type 304

A stainless steel emissivity of 0.2, a measured value from Reference 5, is used in the analysis.

3.7.1.3 Effective Fuel Conductivity

3.7.1.3.1 Transverse Effective Conductivity

The purpose of the effective conductivity in the transverse direction of a fuel assembly is to relate the temperature drop of a homogeneous heat generating square to the temperature drop across an actual assembly cross section for a given heat load. This relationship is established by the following equation obtained from Reference 4:

$$k_e = \frac{Q}{4L_a(T_o - T_s)}(0.2947)$$

where:

k_e = Effective thermal conductivity (Btu/hr-in.-°F)
Q = Assembly head generation (Btu/hr)
L_a = Assembly active length (in.)
T_o = Maximum temperature (°F)
T_s = Surface temperature (°F)

Discrete finite element models of the fuel assemblies to be transported in the NUHOMS®-MP197 packaging are developed using the ANSYS computer code [6]. These two-dimensional models simulate heat transfer by radiation and convection and include the geometry of the fuel rods and fuel pellets. Helium is used as the fill gas in the fuel assembly. A fuel assembly decay heat load of 264 W is used for heat generation. An active length of 144 in. is assumed.

The finite element models are used to calculate the maximum radial temperature difference with isothermal boundary conditions. All components are modeled using 2-D PLANE55 thermal solid elements. LINK32 elements are placed on the exteriors of the fuel assembly components to set up the creation of the radiation super-element. The compartment wall is modeled using LINK32 elements and used only to set up the surrounding surface for the creation of the radiation matrix super-element using the /AUX12 processor in ANSYS. All LINK32 elements are unselected prior to solution of the thermal problem. The thermal properties used are as described in Section 3.7.1.2, and the fuel assembly geometries are as described in Section 3.7.1.1. The ANSYS finite element models of the assemblies are shown in Figures 3.7.1-1 through 3.7.1-7.

The effect of radial gaps between the fuel pellets and the fuel rods on the temperature distributions is negligible. These thermal gaps are not included in the finite element models.

Several computational runs were made for each model using isothermal boundary temperatures ranging from 100 to 600°F. In determining the temperature dependent effective conductivities of the fuel assemblies an average temperature, equal to $(T_o + T_s)/2$, is used for the fuel temperature.

3.7.1.3.2 Axial Effective Conductivity

The backfill gas, fuel pellets, and zircaloy behave like resistors in parallel. However, due to the small conductivity of the fill gas and the axial gaps between fuel pellets, credit is only taken for the zircalloy in the determination of the axial effective conductivities.

$K_{axl} = (K_{zirc})(A_{zirc}/A_{eff})$

$K_{zirc} = 0.6019$ Btu/hr-in-°F
$A_{eff} = (6.00") \times (6.00") = 36.00$ in^2

Assembly Type	GE2, GE3	GE11, GE13	GE 12
Fuel Array	7x7	9x9	10x10
Fuel Rod Outer Diameter, in.	0.563	0.440	0.404
Fuel Rod Clad Thickness, in.	0.032	0.028	0.026
A_{zirc}, in^2	2.616	2.683	2.842
K_{axl}, Btu/hr-in-°F	0.0437	0.0449	0.0475

Assembly Type	GE4	GE5, GE8-Type I	GE8-Type II	GE9, GE10
Fuel Array	8x8	8x8	8x8	8x8
Fuel Rod Outer Diameter, in.	0.493	0.483	0.483	0.483
Fuel Rod Clad Thickness, in.	0.034	0.032	0.032	0.032
A_{zirc}, in^2	3.089	2.812	2.722	2.722
K_{axl}, Btu/hr-in-°F	0.0516	0.0470	0.0455	0.0455

A bounding axial conductivity of 0.0437 Btu/hr-in-°F is used in the thermal analyses.

3.7.1.4 Effective Fuel Density

The mass of the zircalloy and fuel pellets within the 144 inch active length of the fuel assemblies is homogenized over the volume of the fuel elements:

$$\rho_{fuel} = (\rho_{UO_2} V_{UO_2} + \rho_{zirc} V_{zirc}) / V_{fuel}$$

$\rho_{UO_2} = 0.396$ lbm/in^3
$\rho_{zirc} = 0.237$ lbm/in^3
$V_{fuel} = (6.00 \text{ in})^2(144 \text{ in}) = 5{,}184$ in^3

Assembly Type	GE2, GE3	GE11, GE13	GE 12
Fuel Array	7x7	9x9	10x10
Fuel Rod Outer Diameter, in.	0.563	0.440	0.404
Fuel Rod Clad Thickness, in.	0.032	0.028	0.026
Fuel Pellet Outer Diameter, in.	0.487	0.376	0.345
V_{UO2}, in^3	1,314.34	1,183.20	1,238.45
V_{zirc}, in^3	376.66	386.37	409.22
ρ_{eff}, lbm/in^3	0.118	0.108	0.113

Assembly Type	GE4	GE5, GE8-Type I	GE8-Type II	GE9, GE10
Fuel Array	8x8	8x8	8x8	8x8
Fuel Rod Outer Diameter, in.	0.493	0.483	0.483	0.483
Fuel Rod Clad Thickness, in.	0.034	0.032	0.032	0.032
Fuel Pellet Outer Diameter, in.	0.416	0.410	0.410	0.411
V_{UO2}, in^3	1,233.05	1,178.72	1,140.70	1,146.27
V_{zirc}, in^3	444.83	404.90	391.93	391.90
ρ_{eff}, lbm/in^3	0.115	0.109	0.105	0.106

The bounding density of 0.105 lbm/in^3 is used in the thermal analyses.

3.7.1.5 Effective Fuel Specific Heat

A mass weighted average is used in determination of the fuel assemblies effective specific heats:

$$C_{p,fuel} = (C_{p,UO_2}M_{UO_2} + C_{p,zirc}M_{zirc}) / M_{tot}$$

$C_{p,UO_2} = 0.0560$ Btu/lbm-°F
$C_{p,zirc} = 0.0657$ Btu/lbm-°F

Assembly Type	GE2, GE3	GE11, GE13	GE 12
Fuel Array	7x7	9x9	10x10
M_{UO2}, lbm	520.5	468.5	490.4
M_{zirc}, lbm	89.3	91.6	97.0
M_{tot}, lbm	609.7	560.1	587.4
$C_{p,fuel}$, Btu/lbm-°F	0.0574	0.0576	0.0576

Assembly Type	GE4	GE5, GE8-Type I	GE8-Type II	GE9, GE10
Fuel Array	8x8	8x8	8x8	8x8
M_{UO2}, lbm	488.3	466.8	451.7	453.9
M_{zirc}, lbm	105.4	96.0	92.9	92.9
M_{tot}, lbm	593.7	562.8	544.6	546.8
$C_{p,fuel}$, Btu/lbm-°F	0.0577	0.0577	0.0577	0.0576

The bounding specific heat of 0.0574 is used in the thermal analyses.

3.7.1.6 Conclusion

The transverse effective conductivities for the fuel assemblies configurations are plotted below. For temperatures above 400°F, the 8×8 (GE4) fuel assembly has the lowest conductivity.

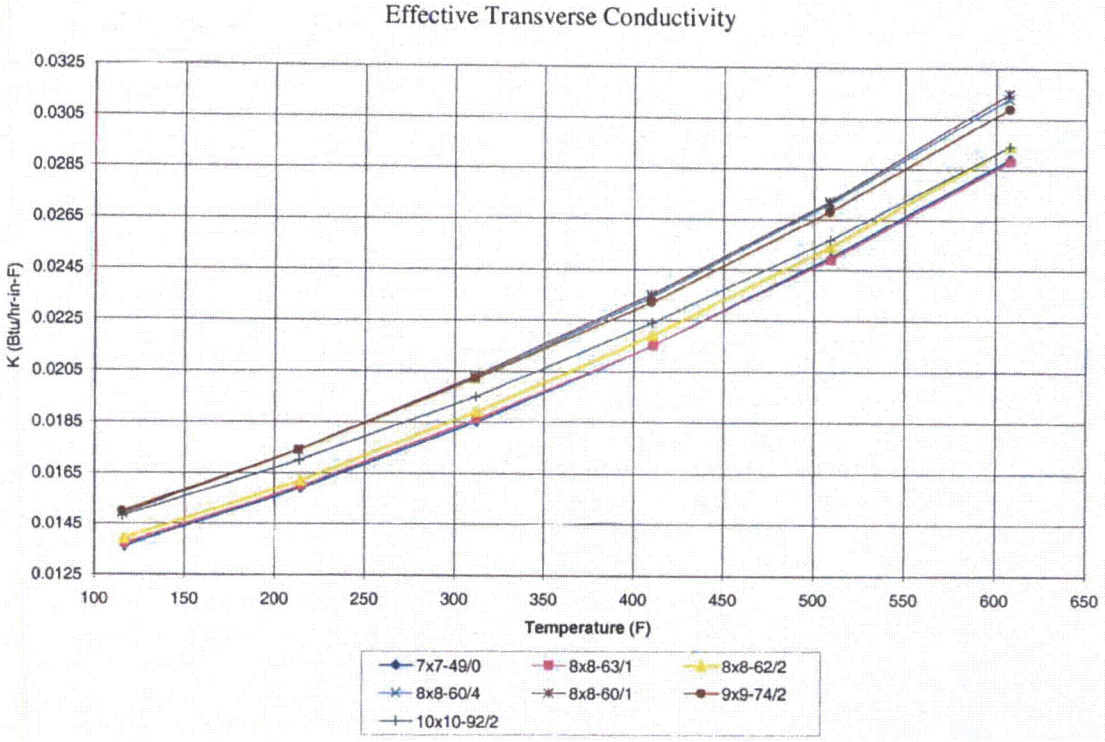

The transverse effective conductivity of the 8×8 (GE4) fuel assembly, and the bounding axial conductivity, density, and specific heat calculated in Sections 3.7.1.2 through 3.7.1.5 are used in the thermal analysis.

Average Fuel Temperature (°F)	Thermal Conductivity (Btu/hr-in-°F)		Density (lbm/in^3)	Specific Heat (Btu/lbm-°F)
	Transverse	Axial		
116.8	0.0137	0.0437	0.105	0.0574
214.4	0.0160	...	...	...
312.4	0.0186	...	...	...
410.7	0.0215	...	...	...
509.3	0.0249	...	...	...
608.0	0.0288	...	...	...
707.0	0.0329	...	...	...
806.1	0.0375	...	...	...
905.4	0.0425	...	...	...
1005.0	0.0461	0.0437	0.105	0.0574

3.7.1.7 References

1. NUREG/CR-0200, Vol. 3, Rev. 6, SCALE, A Modular Code System for Performing Standardized Computer Analyses for Licensing Evaluation.

2. NUREG/CR-0497, *A Handbook of Materials Properties for Use in the Analysis of Light Water Reactor Fuel Rod Behavior, MATPRO - Version 11* (Revision 2), EG&G Idaho, Inc., TREE-1280, August 1981.

3. *Handbook of Heat Transfer*, W. M. Rohsenow and J. P. Hartnett, McGraw-Hill Publishing, New York, 1973.

4. *Spent Nuclear Fuel Effective Thermal Conductivity Report,* TRW Environmental Safety Systems, Inc., Document Identifier BBA000000-01717-5705-00010 Rev 00.

5. COBRA-SFS: *A Thermal – Hydraulic Analysis Computer Code, Vol. III,* Validation Assessments, PNL-6049, 1986.

6. ANSYS, Inc., ANSYS Engineering Analysis System User's Manual for ANSYS Revision 5.7, Houston

TABLE 3.7.1-1

FUEL ASSEMBLY PARAMETERS

Assembly Type	GE2, GE3	GE11, GE13	GE 12
Fuel Array	7x7	9x9	10x10
Number of Fuel Rods	49	74	92
Fuel Rod Outside Diameter, in.	0.563	0.440	0.404
Fuel Rod Clad Thickness, in.	0.032	0.028	0.026
Fuel Pellet Outer Diameter, in.	0.487	0.376	0.345
Rod Pitch, in.	0.738	0.566	0.510
Number of Water Rods	0	2	2
Water Rod Outer Diameter, in.	N/A	0.980	0.980
Water Rod Inner Diameter, in.	N/A	0.920	0.920
Fuel Rod Material	Zr-2	Zr-2	Zr-2
Fuel Pellet Material	UO_2	UO_2	UO_2
Active Fuel Length, in.	144	146*	150*

Assembly Type	GE4	GE5, GE8-Type I	GE8-Type II	GE9, GE10
Fuel Array	8x8	8x8	8x8	8x8
Number of Fuel Rods	63	62	60	60
Fuel Rod Outside Diameter, in.	0.493	0.483	0.483	0.483
Fuel Rod Clad Thickness, in.	0.034	0.032	0.032	0.032
Fuel Pellet Outer Diameter, in.	0.416	0.410	0.410	0.411
Rod Pitch, in.	0.640	0.640	0.640	0.640
Number of Water Rods	1	2	4	1
Water Rod Outer Diameter, in.	0.493	0.591	2 @ 0.591 2 @ 0.483	1.340
Water Rod Inner Diameter, in.	0.425	0.531	2 @ 0.531 2 @ 0.419	1.260
Fuel Rod Material	Zr-2	Zr-2	Zr-2	Zr-2
Fuel Pellet Material	UO_2	UO_2	UO_2	UO_2
Active Fuel Length, in.	146*	150*	150*	150*

* Conservatively taken as 144 inches in the analyses.

FIGURE 3.7.1-1

FINITE ELEMENT MODEL OF 7x7 FUEL ASSEMBLY

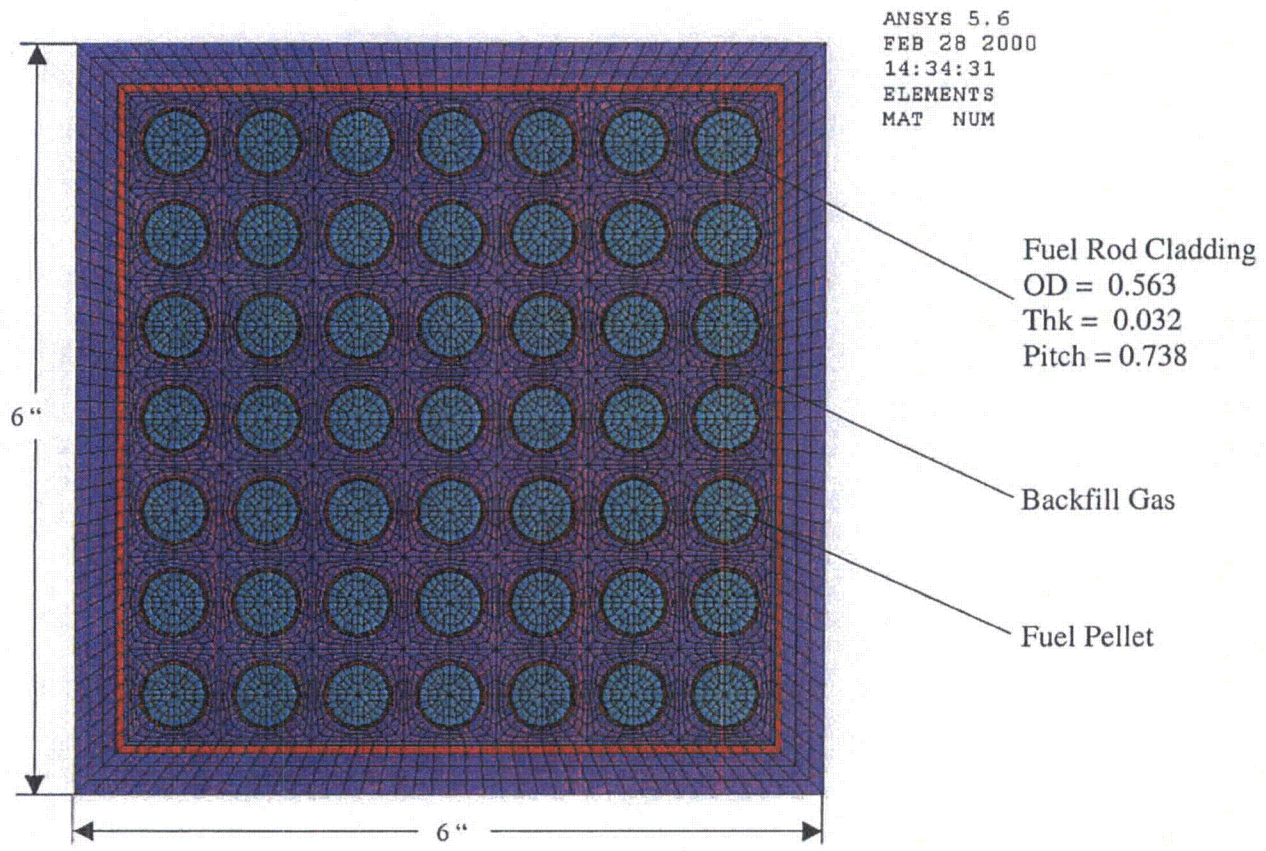

FIGURE 3.7.1-2

FINITE ELEMENT MODEL OF 9x9 FUEL ASSEMBLY

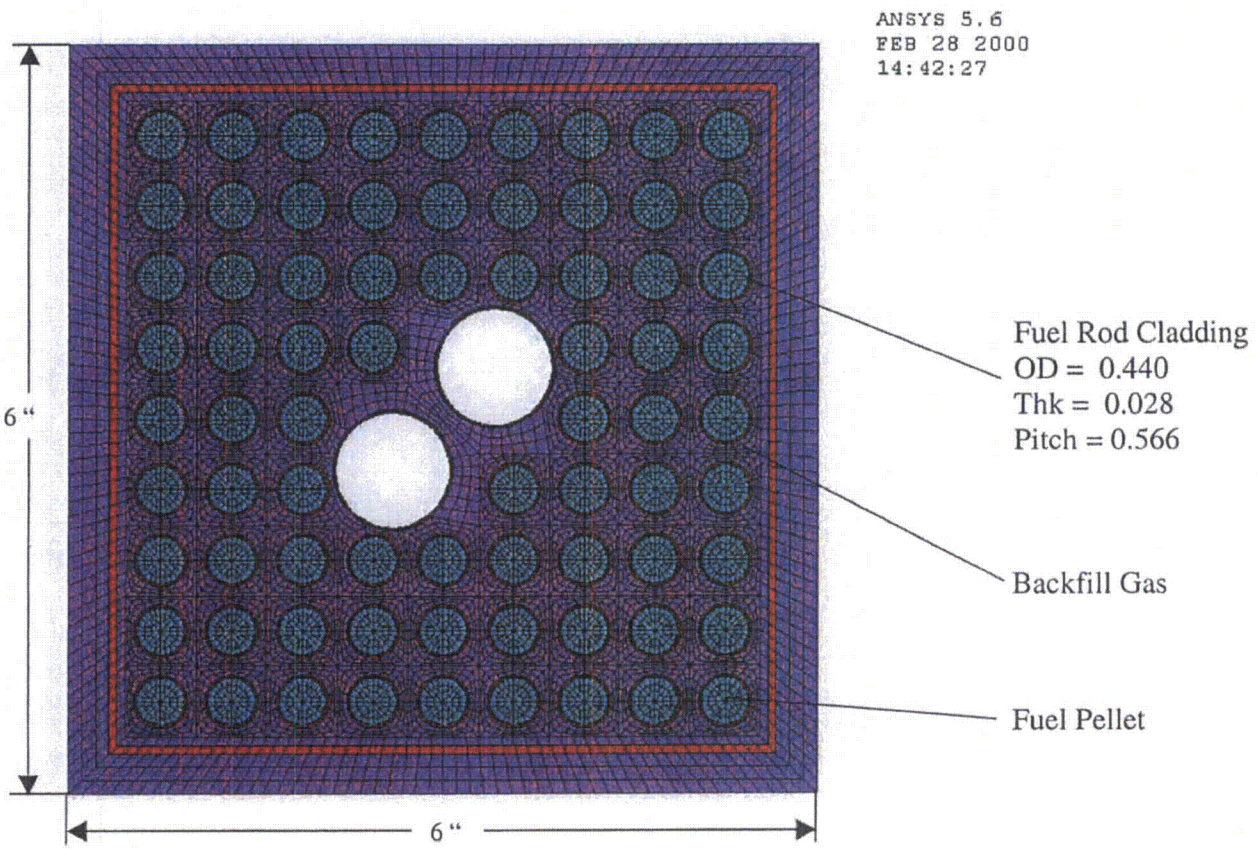

FIGURE 3.7.1-3

FINITE ELEMENT MODEL OF 10x10 FUEL ASSEMBLY

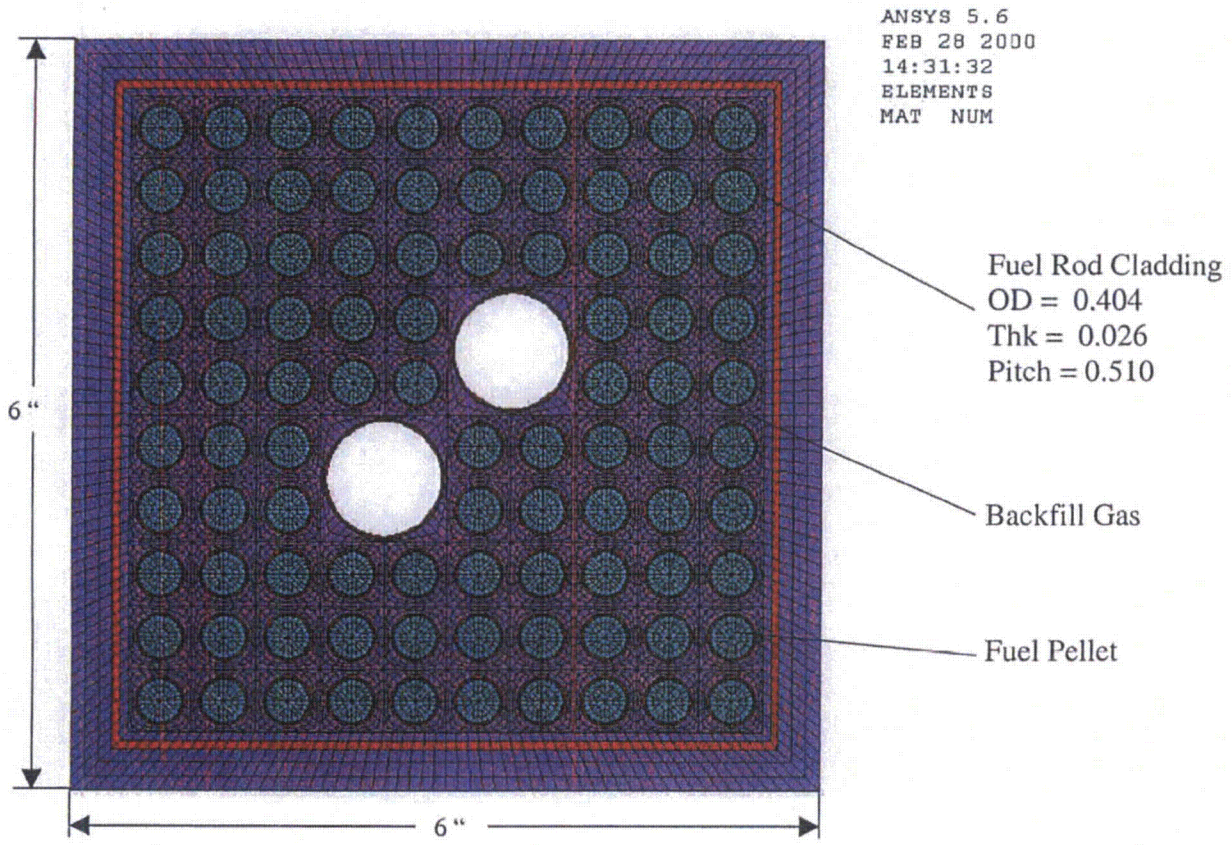

FIGURE 3.7.1-4

FINITE ELEMENT MODEL OF 8x8 (GE4) FUEL ASSEMBLY

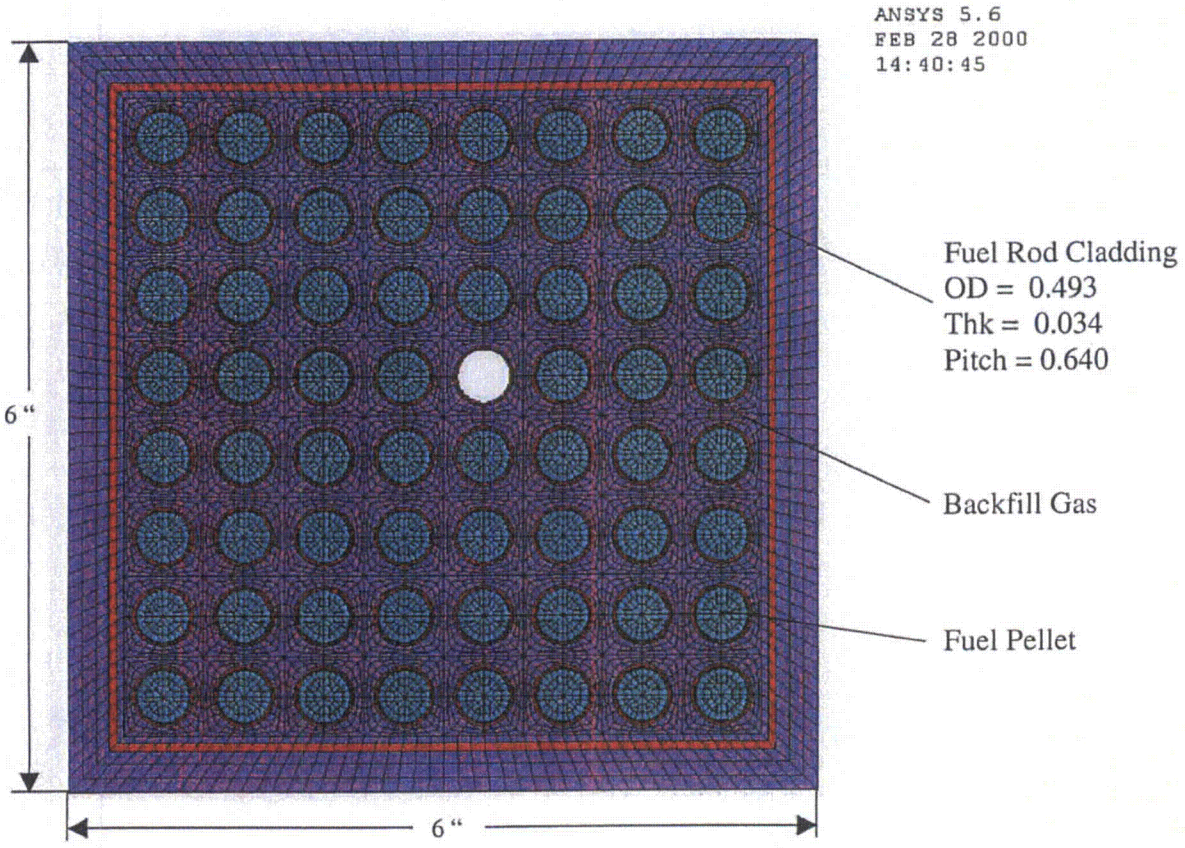

FIGURE 3.7.1-5

FINITE ELEMENT MODEL OF 8x8 (GE5, GE8-Type I) FUEL ASSEMBLY

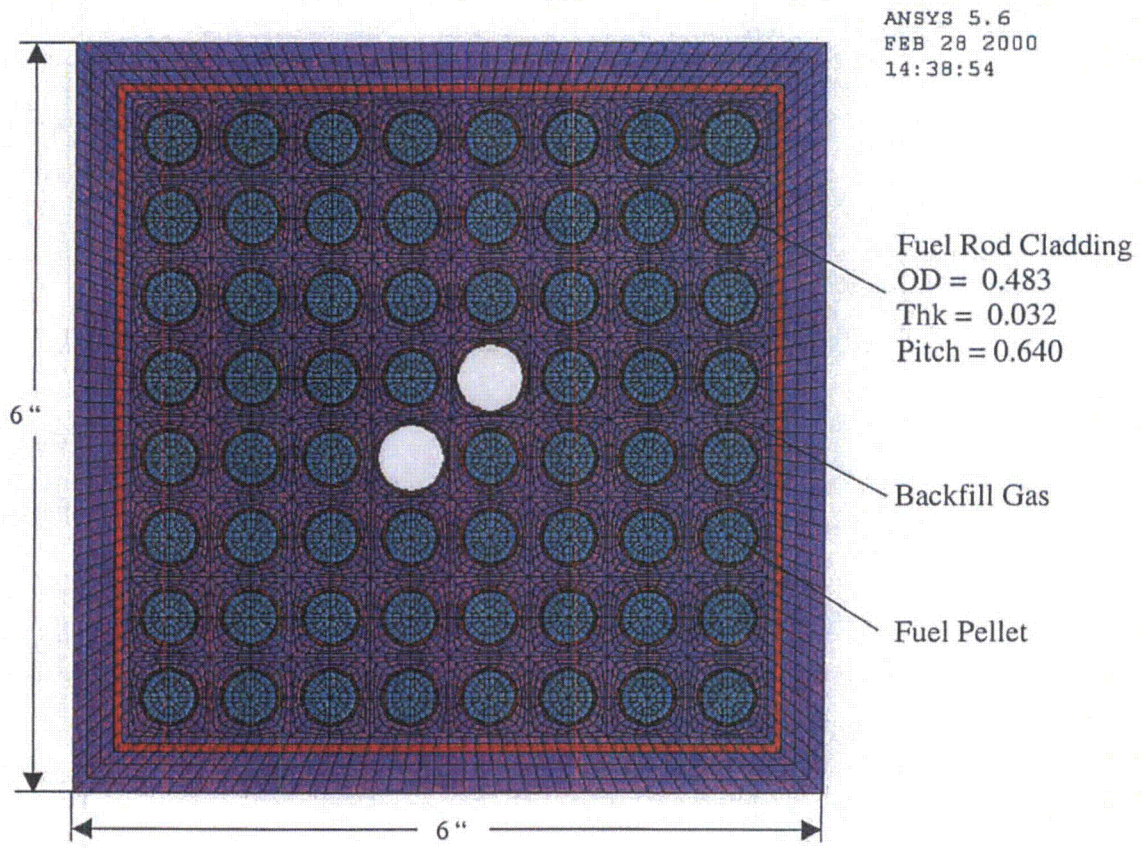

FIGURE 3.7.1-6

FINITE ELEMENT MODEL OF 8x8 (GE8-Type II) FUEL ASSEMBLY

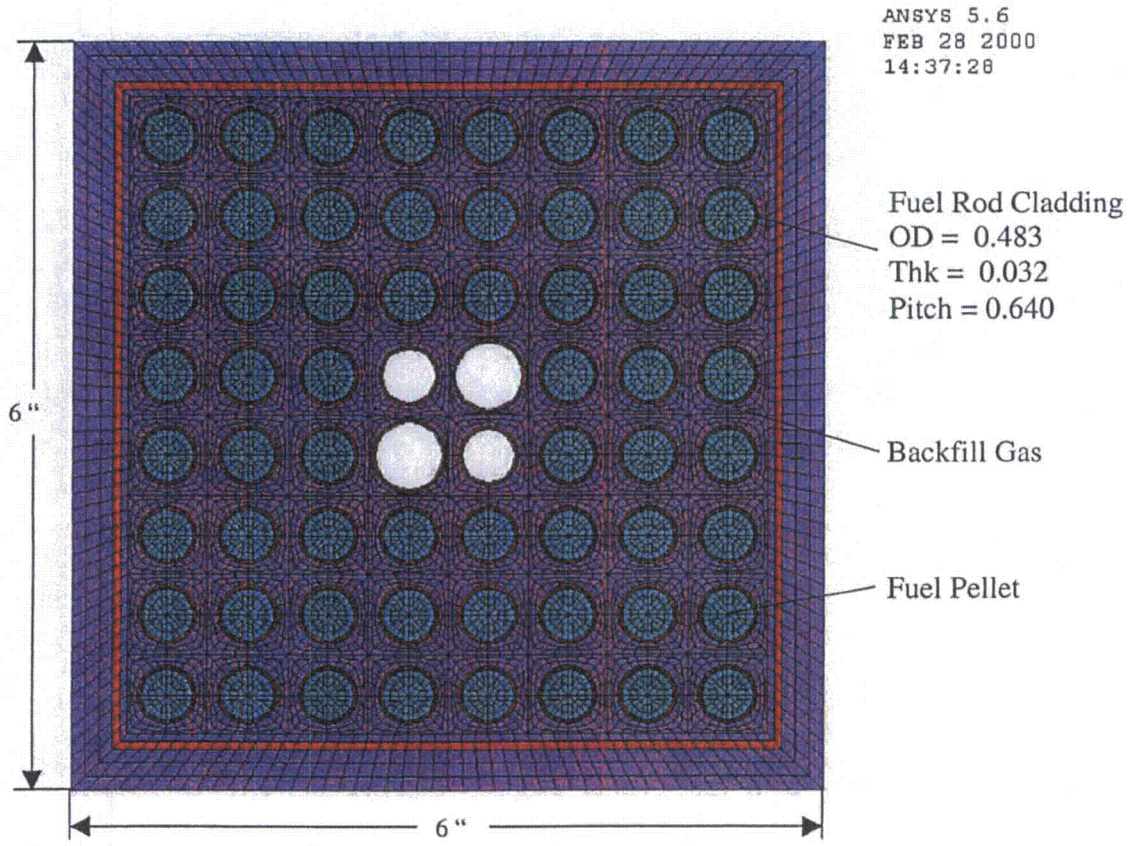

FIGURE 3.7.1-7

FINITE ELEMENT MODEL OF 8x8 (GE9, GE10) FUEL ASSEMBLY

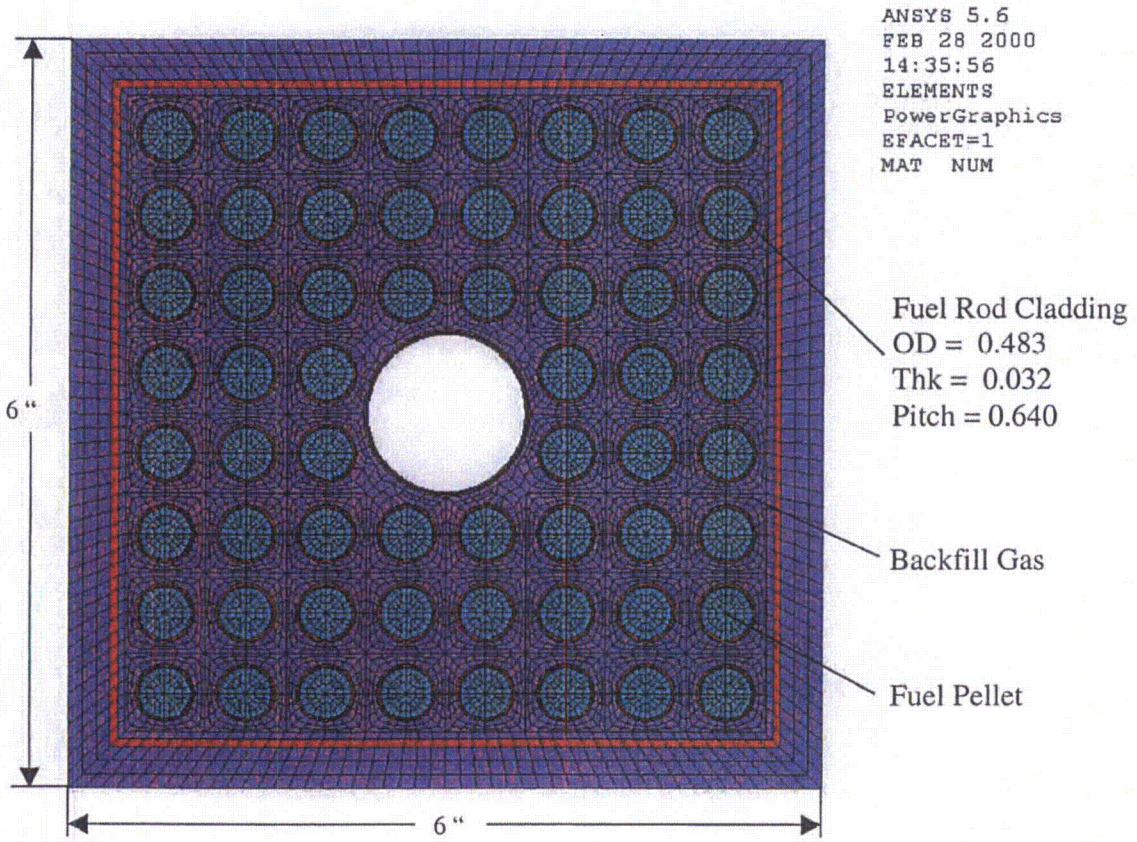

APPENDIX 3.7.2

TABLE OF CONTENTS

APPENDIX 3.7.2

AVERAGE CONVECTIVE HEAT TRANSFER COEFFICIENT FOR FIRE ACCIDENT CONDITIONS

3.7.2.1 Discussion

The NUHOMS®-MP197 finite element models for the fire accident conditions use an average convection heat transfer coefficient. This coefficient is determined assuming an average flame velocity of 15 m/s and an ambient fire temperature of 1475 °F.

3.7.2.2 Material Properties for Air

Temperature		ν [1]	μ [1]	Pr [1]	Conductivity		Kin. Visc.
(K)[1]	(°F)	(m^3/kg)	(Pa-s)	(---)	(W/m-K)[1]	(Btu/hr-ft-°F)	(ft^2/s)
200	-100	0.573	1.33E-5	0.740	0.0181	0.0105	8.203E-05
300	80	0.861	1.85E-5	0.708	0.0263	0.0152	1.715E-04
400	260	1.148	2.30E-5	0.694	0.0336	0.0194	2.842E-04
500	440	1.436	2.70E-5	0.688	0.0404	0.0233	4.173E-04
600	620	1.723	3.06E-5	0.690	0.0466	0.0269	5.675E-04
800	980	2.298	3.70E-5	0.705	0.0577	0.0333	9.152E-04
1000	1340	2.872	4.24E-5	0.707	0.0681	0.0393	1.311E-03

3.7.2.3 Average Convection Heat Transfer Coefficient

From Reference 1, the skin friction coefficient for a flat plate with constant fluid properties is:

$$\frac{C_f}{2} = \frac{0.185}{(\log_{10} Re)^{2.584}} \qquad (3.1)$$

For Pr near unity:

$$\frac{C_f}{2} = \frac{Nu}{(Re\ Pr)} \qquad (3.2)$$

From equations (3.1) and (3.2):

$$h = \frac{\left(\frac{k}{L}\right)(0.185)(Re\ Pr)}{(\log_{10} Re)^{2.584}}$$

Properties are evaluated at the average temperature between the ambient fire and ambient cool-down condition temperatures. The length of the cask is taken to be 13 ft.

T_{avg} = (1475 + 100)/2 = 788 °F
U = 15 m/s = 49.21 ft/s
L = 13 ft
Pr = 0.697 (via linear interpolation)
k = 0.0299 Btu/hr-ft-°F (via linear interpolation)
ν = 7.294E-04 ft^2/s (via linear interpolation)

Re = (UL/ν) = 877,010

h_{avg} = 2.601 Btu/hr-ft^2-°F

For additional consveratism, a value of 2.750 Btu/hr-ft^2-°F is used in the analysis.

3.7.2.4 References

1. *Handbook of Heat Transfer*, W. Rohsenhow and J. Harnett, McGraw-Hill Publishing, New York, 1973.

APPENDIX 3.7.3

TABLE OF CONTENTS

APPENDIX 3.7.3

MAXIMUM INTERNAL OPERATING PRESSURES

3.7.3.1 Discussion

The following approach is used in the determination of maximum pressures within the cask body and canister during normal and hypothetical accident conditions of transport:

- First, average cavity gas temperatures are derived from component temperatures.
- Next, the amount of helium present within the canister and cask body after the initial backfilling of each is determined via the ideal gas law.
- Then, the total amount of free gas within the fuel assemblies, including both fill and fission gases, is calculated.
- Using the prescribed percentage of fuel rods that develop cladding breaches from the Standard Review Plan, the total amount of gas within the canister is determined
- Finally, the maximum cavity pressures are determined via the ideal gas law.

3.7.3.1.1 Average Cavity Gas Temperatures

For simplicity, the average cavity gas temperatures within the canister is taken to be the average of the maximum steady state or peak transient fuel cladding and canister wall temperatures. Within the cask body the average cavity gas temperature is taken to be the average of the maximum steady state or peak transient cask body and canister wall temperatures.

Component	Max. Temperature (°F)	
	Normal Conditions	Accident Conditions
Fuel Cladding	598	680
Canister Wall	388	485
Cask Body	302	535
Average Cavity Gas, Canister	493	583
Average Cavity Gas, Cask Body	345	504

3.7.3.1.2 Amount of Initial Helium Backfill

The amounts of helium present within the DSC and the cask body are calculated using the ideal gas law and a maximum initial helium fill of 3.5 psig within the canister and cask body. The initial fill temperature is assumed to be 273 °F; the value used within the NUHOMS®-MP197 Storage Application [1].

From the backfill pressure and average gas temperatures the amounts of helium backfill gas can be calculated.

$n = (PV)/(RT)$

P = initial fill pressure = 3.5 psig = 1.24 atm
V = Free volume (ft^3)
T = initial fill temperature = 273 °F = 733 R
R = universal gas constant = 0.730 atm-ft^3/lbmoles-R

	Canister	Cask Body
Free Volume, V	214.86 ft^3	9.03 ft^3
Amount of backfill, n	0.498 lbmoles	0.021 lbmoles

3.7.3.1.3 Free Gas within Fuel Assemblies

The amount of fission and fill gases within each of the fuel assembly types is taken from Reference 2. The amounts of fission gases tabulated below were determined from SAS2H/ORIGEN-S computer runs. I, Kr, and Xe gases are considered following irradiation. These numbers include the 30 percent release fraction for fission gases due to cladding breaches specified in the Standard Review Plan for Transportation (Reference 3).

Fuel Design	Fill Gas [5]	Fission Gas [6]	Total	Total
(---)	(kg moles/rod)	(kg moles/rod)	(kg moles/rod)	(lb moles/assy)
7x7-49-0	5.489E-06	6.640E-05	7.189E-05	7.767E-03
8x8-63-1	3.842E-06	4.889E-05	5.273E-05	7.325E-03
8x8-62-2	8.176E-06	4.923E-05	5.741E-05	7.848E-03
8x8-60-4	8.177E-06	5.016E-05	5.834E-05	7.718E-03
8x8-60-1	8.247E-06	5.041E-05	5.866E-05	7.760E-03
9x9-74-2	1.800E-05	3.927E-05	5.727E-05	9.345E-03
10x10-92-2	1.492E-05	3.318E-05	4.810E-05	9.758E-03

The General Electric 10x10 fuel assembly is the bounding case and is used in the determination of the cavity pressures.

3.7.3.1.4 Total Amount of Gases within Canister

The total amount of gas within the canister is equal to the amount of initial helium fill plus any free gases within the assemblies that are released.

The Standard Review Plan for Transportation prescribes the percentage of fuel rods that develop cladding breaches during normal conditions of transport and hypothetical accident conditions. All free gases within fuel rods that develop breaches will be released into the canister.

n_{total} = 0.498 lbmoles + (f_B)(61 assemblies)(9.758E-03 lb moles/assy)

n_{total} = total amount of gases
f_B = fraction of fuel rods that develop cladding breaches
= 0.03 for Normal Conditions of Transport [3]
= 1.00 for Hypothetical Accident Conditions [3]

	Normal Conditions	Accident Conditions
f_B	0.03	1.00
n_{total}	0.516 lbmoles	1.093 lbmoles

3.7.3.2 Maximum Pressures

Maximum cavity pressures are determined via the ideal gas law:

$P = (nRT)/V$

P = pressure	(atm)
V = Free volume	(ft^3)
T = average cavity gas temperature	(R)
R = universal gas constant = 0.730	(atm-ft^3/lbmoles-R)
n_{total} = total amount of gases	(lbmoles)

	Canister		Cask Body	
	N.C.T.	H.A.C	N.C.T.	H.A.C.
n_{total} (lbmoles)	0.516	1.093	0.021	0.021
T (R)	953	1043	805	964
V (ft^3)	214.86	214.86	9.03	9.03
Cavity Pressure (atm)	1.67	3.87	1.37	1.65

3.7.3.3 Results and Conclusions

During normal operating conditions the maximum pressure within the canister is 1.67 atm (9.8 psig). Within the cask body the maximum normal operating pressure is 1.37 atm (5.4 psig).

During hypothetical accident conditions the maximum pressure within the canister is 3.87 atm (42.2 psig). Within the cask body the maximum accident operating pressure is 1.65 atm (9.6 psig).

3.7.3.4 References

1. NUHOMS COC 1004 Amendment No. 3, 2000
2. *TN-68 Dry Storage Cask Final Safety Analysis Report*, Transnuclear Inc., Revision 0, Hawthorne, NY, 2000.
3. *Standard Review Plan for Transportation Packages for Spent Nuclear Fuel*, NUREG-1617, 2000.
4. ANSYS Engineering Analysis System, *User's Manual for ANSYS Revision 6*, ANSYS, Inc., Houston, PA.

APPENDIX 3.7.4

TABLE OF CONTENTS

APPENDIX 3.7.4

THERMAL EVALUATION FOR VACUUM DRYING CONDITIONS

3.7.4.1 Discussion

All fuel transfer operations occur when the packaging is in the spent fuel pool. The fuel is always submerged in free-flowing pool water permitting heat dissipation. After fuel loading is complete, the packaging is removed from the pool, drained and dried.

The loading condition evaluated is the heatup of the cask before its cavity can be backfilled with helium. This typically occurs during the performance of the vacuum drying operation of the cask cavity. A transient thermal analysis is performed for the vacuum drying procedure. The analysis determines the component temperatures after 86 hours of vacuum drying with the maximum decay heat load of 15.86 kW.

3.7.4.2 Finite Element Model

The cask cross-section finite element model developed in Section 3.5.2 is modified for this transient analysis. The vacuum drying of the cask generally does not reduce the pressure sufficiently to reduce the thermal conductivity of the air in the cask cavity. All gaseous heat conduction within the cask cavity is through air instead of helium. Radiation heat transfer within the cask cavity is neglected. The fuel properties were recalculated using air properties instead of helium. All temperatures in the cask are initially assumed to be at 100°F. Radiation and natural convection heat transfer are from the cask outer surface to the building environment at a temperature of 100°F.

3.7.4.3 Material Properties

BWR Fuel w/ Air Backfill

Temperature (°F)	Thermal Conductivity (Btu/hr-in-°F)		Specific Heat (Btu/lbm-F)	Density (lbm/in^3)
	Transverse	Axial		
150.796	0.0045	0.0437	0.105	0.0574
239.954	0.0058	...	...	...
331.555	0.0073	...	...	...
425.095	0.0092	...	...	...
520.134	0.0114	...	...	...
616.315	0.0141	...	...	...
713.356	0.0173	...	...	...
811.049	0.0209	...	...	...
909.232	0.0250	0.0437	0.105	0.0574

3.7.4.4 Evaluation of the Transient Analysis

The modified cask-cross section model was run to determine maximum component temperatures after 86 hours of vacuum drying. Total decay heat load is 15.86 kW in this analysis. The component temperatures after 86 hours of vacuum drying conditions are listed below.

Component	Maximum Temperature (°F)
Fuel Cladding	831
Basket	796
Basket Peripheral Inserts	659
Canister Shell	486
Cask Body	201
Lead	199
Resin	168
Outer shell	156

The results show that at the end of 86 hours, the basket temperature do not exceed 800°F. The resulting fuel cladding temperature is 831°F, well below the short-term fuel cladding temperature limit of 1058°F.

3.7.4.5 References

1. ANSYS Engineering Analysis System, *User's Manual for ANSYS Revision 6.0*, ANSYS, Inc., Houston, PA.

APPENDIX 3.7.5

TABLE OF CONTENTS

LIST OF TABLES

APPENDIX 3.7.5

SENSITIVITY ANALYSIS REGARDING THE SURFACE EMISSIVITY OF STAINLESS STEEL FOR THE CASK RADIAL SURFACE

3.7.5.1 Discussion

In Chapter 3 an emissivity value of 0.8 was assumed for the weathered stainless steel. This emissivity value was used to calculate the total heat transfer coefficient from the radial surface of the cask to the ambient as described in detail in Section 3.4.1.1. A sensitivity analysis is performed to investigate the effect of a lower emisivity value for the cask surface on the component temperatures within the transport cask. This investigation is focused on the normal conditions of transport. The emissivity value of the weathered stainless steel is only used for cask surface to calculate the pre-fire conditions in the evaluation of the hypothetical fire accident case. Therefore, the impact of using a lower emisivity on the fire accident analysis is close to its impact on the normal condition case.

3.7.5.2 Thermal Models

The two thermal models described in Chapter 3 are the bases for this sensitivity analysis. Only the basket model is modified to add conduction paths at the top and bottom of the basket towards the shield plugs of the canister. The length of the fuel assembly is extended from the active length (144") to the full assembly length of 176" (Reference 3). All the elements representing the fuel assembly are given the effective fuel conductivity calculated in Appendix 3.7.1. The decay heat load profile is unchanged and it is applied over the active fuel length of 144".

The top surface of the fuel assembly is considered to be oxidized. An emissivity value of 0.9 is considered for this oxidized surface to maximize the axial heat transfer. The inner surface of the canister front plug is made of carbon steel. An emissivity value of 0.8 is considered for the carbon steel from References 1 and 2. To simplify the model, an effective radiation conductivity is calculated for the helium elements between the top of fuel assembly and the front shield plug based on the following equation.

$$k_r = \frac{\sigma L}{\left(\frac{1-\varepsilon_f}{\varepsilon_f} + \frac{1}{F_{12}} + \frac{1-\varepsilon_p}{\varepsilon_p}\right)} \frac{\left(T_f^4 - T_p^4\right)}{\left(T_f - T_p\right)}$$

Where,

k_r = effective radiation coductivity (Btu/hr-in-F)

σ = Stefan-Boltzmann coefficient = 0.119×10^{-10} (Btu/hr-in^2-R^4)

L = distance between the top of fuel assembly to the inner surface of the shield plug = 3.375 (in)

ε_f = emissivity of the fuel assembly top plate = 0.9

ε_p = emiisivity of the shield plug inner surface = 0.8
F_{12} = view factor from top plate fuel assembly to the inner surface shield plug =1.0
T_f = average temperature of the fuel assembly top plate (R)
T_p = average temperature of the shield plug inner surface (R)

The effective conductivity values ($k_{eff} = k_r + k_{cond}$) are listed below.

T_{fuel}	T_{plug}	T_{avg}	k_r	k_{cond}*	k_{eff}
°F	°F	°F	Btu/hr-in-°F	Btu/hr-in-°F	Btu/hr-in-°F
350	150	250	0.0381	0.0086	0.0467
375	160	268	0.0410	0.0087	0.0498
400	185	293	0.0454	0.0089	0.0543
425	200	313	0.0491	0.0091	0.0582
450	215	333	0.0531	0.0093	0.0623
475	240	358	0.0582	0.0095	0.0676
500	250	375	0.0621	0.0096	0.0717

After solving the thermal models, the average temperatures at the inner surface of the front shield and the upper surface of the fuel assemblies are checked to verify the values in the above table.

A solar absorptivity of 0.5 is considered for the cask surface for the practical purposes (Reference1). All other boundary conditions and material properties are the same as those described in Chapter 3.

3.7.5.3 Maximum Temperatures

The maximum component temperatures resulted from the steady state runs of the thermal models with the cask surface emissivity of 0.5 are summarized in Table 3.7.4-1. This table also shows the maximum temperatures calculated with an emissivity value of 0.8 for the weathered stainless steel.

3.7.5.4 Effect of the Lower Emisivity on the Maximum Temperatures

A comparison of the maximum temperatures in Table 3.7.5-1 shows a maximum increase of 14°F for the component of the transport cask. This increase is due to a decrease of the cask surface emisivity value from 0.8 to 0.5.

The mechanical properties of cask component are evaluated at higher temperatures than those resulted from this analysis. Therefore, a temperature increase of maximum 14°F does not have any adverse effect on the structural analysis. The average maximum temperatures resulted from this analysis are compared to the temperatures used for structural analysis in Table 3.7.5-2.

* Interpolated and converted from Helium conductivity values in Chapter 3.

Adding the axial conduction and radiation paths in the basket model causes a reduction in the maximum temperatures at the hottest cross section of basket. The temperatures of the shield plugs, seals and impact limiters are increased due to the higher axial heat transfer in the modified model. The maximum temperatures of these components remain below their corresponding thermal limits (see Table 3.5.7-1).

Since all the maximum temperatures are well below their limits, the temperature increase resulted from this analysis is not significant, and does not have any adverse effect on the component performances.

3.7.5.5 References

1. *Principles of Heat Transfer, Fourth Edition,* Kreith et. al., Harper & Row, Publishers, New York, 1986.

2. *Standard Handbook for Mechanical Engineers, Seventh Edition,* Baumeister & Marks, McGraw-Hill Book Co., New York, 1969

3. *Domestic Light water Reactor Fuel Design Evolution, Vol. III, J. M. Viebrock, 1981*

4. ANSYS Engineering Analysis System, *User's Manual for ANSYS Revision 6.0,* ANSYS, Inc., Houston, PA.

TABLE 3.7.5-1

Maximum Temperatures Normal Conditions of Transport
(Comparison of the modified and original models)

Component	Maximum Temperature Modified model with conduction and radiation in DSC, ε =0.5	Maximum Temperature Original model, ε =0.8	Temperature Difference (Modified – Original)	Thermal Limits
(---)	(°F)	(°F)	(°F)	(°F)
Shield Shell	241	227	+14	---
Resin	263	249	+14	300
Lead	312	299	+13	---
Cask Body	315	302	+13	---
Outer Surface of Outer Shell	272	258	+14	
Impact Limiters	198	195	+3	---
Cask Lid	201	199	+2	---
Thermal Shield	192	186	+6	---
Flourocarbon Seals, Lid	206	204	+2	400
Flourocarbon Seals, Ram Plate	231	217	+14	400
Canister	393	388	+5	---
Peripheral Inserts	477	482	-5	---
Basket	568	578	-10	---
Fuel Cladding	588	598	-10	1058

TABLE 3.7.5-2

Maximum Average Temperatures Compared to the Temperatures used in the Structural Analysis

Component	Maximum Temperature Modified model with conduction and radiation in DSC, ε =0.5	Maximum Temperature Original model, ε =0.8	Temperature used for Structural Analysis Limits
---	(°F)	(°F)	(°F)
Cask Body, $T_{avg,max}$*	294	280	300
Peripheral Insetrs, $T_{avg,max}$	435	435	500
Canister Shell, $T_{avg,max}$	379	372	500
Basket, $T_{avg,max}$	523	530	600
Front Shield Plug, T_{avg}**	227	204	400
Rear Shield Plug, T_{avg}	260	223	400

* $T_{avg,max}$ is the average temperature at the hottest cross section for the Cask body, Peripheral Inserts, Canister Shell, and Basket.

** For the shield plugs, T_{avg} is the volume average temperature of the corresponding elements.

CHAPTER 4

TABLE OF CONTENTS

LIST OF TABLES

LIST OF FIGURES

CHAPTER 4

CONTAINMENT

4.1 CONTAINMENT BOUNDARY

The containment boundary consists of a cylindrical inner shell, a bottom end (closure) plate with a ram access penetration with seal, a cask body flange, a top lid with seal, and vent and drain port closure bolts and seals. The containment boundary is shown in Figure 4-1. The construction of the containment boundary is shown on the drawings provided in Appendix 1.4. The containment vessel prevents leakage of radioactive material from the cask cavity. It also maintains an inert atmosphere (helium) in the cask cavity.

Additionally, the NUHOMS® -61BT DSC welded canister contains helium. Thus, the welded canister also provides a containment function. Helium assists in heat removal and provides a non-reactive environment to protect fuel assemblies against fuel cladding degradation which might otherwise lead to gross rupture.

4.1.1 Containment Vessel

The NUHOMS® -MP197 containment vessel consists of the inner shell, a 6.50 inch thick bottom plate with a 23.88 inch diameter, 2.5 inch thick RAM access closure, a top closure flange, a 4.50 inch thick top closure lid with closure bolts, vent and drain port closures and bolts, and double O-ring seals for each of the penetrations. A 68 inch diameter, 197 inch long cavity is provided.

The inner containment shell is SA-240, Type XM-19, and the bottom, and top flange materials are SA-182, Type FXM19. The top closure lid is constructed from SA-705, Type 630, H1100. The NUHOMS® -MP197 packaging containment vessel is designed, fabricated, examined and tested in accordance with the requirements of Subsection NB of the ASME Code [1] to the maximum practical extent. In addition, the design meets the requirements of Regulatory Guides 7.6 [2] and 7.8 [3]. Exceptions to the ASME Code are discussed in Section 2.11 of Chapter 2. The construction of the containment boundary is shown in drawings 1093-71-2, -3 and -4 provided in Appendix 1.4. The design of the containment boundary is discussed in Chapter 2.

The cask design, fabrication and testing are performed under Transnuclear's Quality Assurance Program which conforms to the criteria in Subpart H of 10CFR71.

The materials of construction meet the requirements of Section III, Subsection NB-2000 and Section II, Material specifications or the corresponding ASTM Specifications. The containment vessel is designed to the ASME Code, Section III, Subsection NB, Article 3200.

The containment vessel is fabricated and examined in accordance with NB-2500, NB-4000 and NB-5000. Also, weld materials conform to NB-2400 and the material specification requirements of Section II, Part C of ASME B&PV.

The containment vessel is hydrostatically tested in accordance with the requirements of the ASME B&PV Code, Section III, Article NB-6200.

Even though the code is not strictly applicable to transport casks, it is the intent to follow Section III, Subsection NB of the Code as closely as possible for design and construction of the containment vessel. The casks may, however, be fabricated by other than N-stamp holders and materials may be supplied by other than ASME Certificate Holders. Thus the requirements of NCA are not imposed. TN's quality assurance requirements, which are based on 10CFR71 Subpart H and NQA-1 are imposed in lieu of the requirements of NCA-3850. This SAR is prepared in place of the ASME design and stress reports. Surveillances are performed by TN and utility personnel rather than by an Authorized Nuclear Inspector (ANI).

Paragraph NB-4213 requires the rolling process used to form the inner vessel be qualified to determine that the required impact properties of NB-2300 are met after straining by taking test specimens from three different heats. If the plates are made from less than three heats, each heat will be tested to verify the impact properties.

The materials of the NUHOMS® -MP197 packaging will not result in any significant chemical, galvanic or other reaction as discussed in Chapter 2.

4.1.2 Containment Penetrations

The only penetrations into the containment boundary are the drain and vent ports, ram closure plate and the top closure plate (lid). Each penetration is designed to maintain a leak rate not to exceed 1×10^{-7} ref cc/sec, defined as "leak tight" per ANSI N14.5 [4]. To obtain these seal requirements, each penetration has an O-ring face seal type closure. Additionally, each penetration has a double O-ring configuration.

4.1.3 Seals and Welds

All containment boundary welds are full penetration bevel or groove welds to ensure structural and sealing integrity. These full penetration welds are designed per ASME III Subsection NB and are fully examined by radiography or ultrasonic methods in accordance with Subsection NB. Additionally, a liquid penetrant examination is performed on these welds.

Containment seals are located at the ram access port closure plate, the top closure (lid) plate, the drain plug and the vent plug. The inner seal in all cases is the primary containment seal. The outer, secondary seals, facilitate leak testing of the inner containment seal of the ram closure plate and the lid. There are also test ports provided for these two closures. The test ports are not part of the containment boundary.

All the seals use in the NUHOMS® -MP197 cask containment boundary are static face seals. The seal areas are designed for no significant plastic deformation under normal and accident loads as shown in Chapter 2. The bolts are torqued to maintain a seal load during all load conditions as shown in Appendix 2.10.2. The seals used for all of the penetrations are fluorocarbon elastomer O-rings. All seal contact surfaces are stainless steel and are machined to a 16 microinch (maximum) R_a surface finish. The dovetail grooves in the cask lid and the ram closure plate are intended to retain the seals during installation. The volume of the grooves is controlled to allow the mating metal surfaces to contact under bolt loads, thereby providing uniform seal deformation in the final installation condition.

Fluorocarbon has good sealing properties from -15°F up to 400°F for the seal configuration used in the cask, and it can withstand a maximum temperature of 700°F for the accident conditions [5]. At temperatures below -15°F, some fluorocarbon compounds (V0835-75) can maintain a sealing ability to approximately –40°F.

4.1.4 Closure

The containment vessel contains an integrally-welded bottom closure and a bolted and flanged top closure plate (lid). The lid plate is attached to the cask body with forty eight (48), SA-540, Grade B24, Class 1, 1 1/2" diameter bolts. Closure of the ram closure plate is accomplished by twelve (12), SA-540, Grade B24, Class 1, 1 inch diameter bolts. The bolt torque required for the lid and ram closure plate are provided in Drawing 1093-71-3 in Appendix 1.4 . The closure bolt analysis is presented in Appendix 2.10.2.

Closure of each of the vent and drain ports is accomplished by a single 3/4 inch SA-540, Grade B24, Class 1 bolt with seals under the head of the bolt tightened to the values shown in Drawing 1093-71-3.

4.2 REQUIREMENTS FOR NORMAL CONDITIONS OF TRANSPORT

4.2.1 Containment of Radioactive Material

As described earlier, the NUHOMS®-MP197 cask is designed and tested for a leak rate of 1×10^{-7} ref cc/s, defined as "leak tight" per ANSI N14.5. Additionally, The structural and thermal analyses presented in Chapters 2 and 3 , respectively, verify that there is no release of radioactive materials under any of the normal conditions of transport.

4.2.2 Pressurization of Containment Vessel

The NUHOMS®-MP197 cask contains a sealed (welded) canister which has been tested to a "leak tight" criteria. Therefore, the pressure in the MP197 cask is from helium that has been backfilled into an evacuated cask cavity to a pressure of 3.5 psig at the end of loading. If the MP197 cask contains design basis fuel at thermal equilibrium, the cask cavity helium temperature with 100°F ambient air and maximum solar load is 345°F. The maximum normal operating pressure is calculated in Appendix 3.7.3 to be 5.4 psig. The analyses in Chapter 2 and 3 demonstrate that the MP-197 cask effectively maintains containment integrity with a cavity pressure of 50 psig.

4.2.3 Containment Criterion

The NUHOMS®-MP197 cask is design to be "leak tight". The acceptance criterion for fabrication verification and periodic verification leak test of the MP197 containment boundary shall be 1.0×10^{-7} ref cm^3/s. The test must have a sensitivity of at least one half the acceptance criterion, or 5×10^{-8} ref cm^3/s.

4.3 CONTAINMENT REQUIREMENTS FOR HYPOTHETICAL ACCIDENT CONDITIONS

4.3.1 Fission Gas Products

The following equations from NUREG/CR-6487 [6] are used to determine the source term available for release.

$$C_{volatiles} = \{N_A f_B A_V f_v\} / V$$
$$C_{gases} = \{N_A f_B A_F f_F\} / V$$
$$C_{fines} = \{N_A f_B A_F f_F\} / V$$
$$C_{crud} = \{f_C S_C N_R N_A S_{AR}\}$$
$$C_{total} = C_{crud} + C_{volatiles} + C_{gases} + C_{fines}$$

Table 4-1 shows the free activity available for release from typical BWR spent fuel rods. Table 4-2 shows the activity concentration from each of the sources available for release. The release fractions for the radionuclides are taken from NUREG/CR-6487. Under hypothetical accident conditions, the cladding of 100% of the fuel rods is assumed to fail (f_B=1.0).

4.3.2 Containment of Radioactive Material

The NUHOMS®-MP197 cask is designed and tested to be "leak tight". The MP197 contains a sealed (welded) canister (DSC) which is also tested to a "leak tight" criteria. The results of the structural and thermal analyses presented in Chapters 2 and 3, respectively, verify the package will meet the leakage criteria of 10CFR71.51 for the hypothetical accident scenario.

4.3.3 Containment Criterion

This package has been designed and is verified by leak testing, to meet the "leak tight" criteria of ANSI N14.5. The results of the structural and thermal analyses presented in Chapters 2 and 3, respectively, verify the package will meet the leakage criteria of 10CFR71.51 for all the hypothetical accident conditions.

4.4 SPECIAL REQUIREMENTS

Solid plutonium in the form of reactor elements is exempt from the double containment requirements of 10 CFR 71.63.

4.5 REFERENCES

1. American Society of Mechanical Engineers, ASME Boiler and Pressure Vessel Code, Section III, Division 3, Subsection WB, 1998 including 1999 addenda.

2. USNRC Regulatory Guide 7.6, "Design Criteria for the Structural Analysis of Shipping Cask Containment Vessel", Rev. 1, March 1978.

3. USNRC Regulatory Guide 7.8, "Load Combinations for the Structural Analysis of Shipping Cask", Rev. 1, March 1989.

4. ANSI N14.5-1997, "American National Standard for Radioactive Material – Leakage Tests on Packages for Shipment," February 1998.

5. "Parker O-Ring Handbook", Publication No. ORD-5700, Parker Seals.

6. NUREG/CR-6487, "Containment Analysis for Type B Packages used to Transport Various Contents," Lawrence Livermore National Laboratory, 1996.

TABLE 4-1
RADIONUCLIDE INVENTORY

	Ci/assembly[1]
Volatiles	
Sr 90	1.36E+04
Cs134	1.30E+03
Cs137	2.02E+04
Total – Volatiles	3.51E+04
Gases	
H 3	6.40E+01
Kr 85	1.03E+03
I129	7.62E-03
Total - Gases	1.09E+03
Fines	
Pu238	8.19E+02
Pu239	6.32E+01
Pu240	1.09E+02
Pu241	1.81E+04
Am241	4.06E+02
Cm244	6.25E+02
Y 90	1.36E+04
Ru106	1.15E+02
Sb125	1.32E+02
Pm147	2.10E+03
Sm151	7.57E+01
Eu154	1.32E+03
Eu155	4.61E+02
Total – Fines	3.79E+04

1 Values are based on a 7x7 fuel assembly (40,000 MWD/MTU burnup, 3.3 wt% U-235 initial bundle average enrichment, and 10 year cooled).

2 Ba137m and Rh106 contribute 20.4% and 0.1%, respectively, to the total design basis activity. Ba137m and Rh106 are daughters of Cs137 and Ru106, respectively, with half lives of 2.6 min and 30 sec, respectively. In accordance with 10CFR71 Appendix A Note III, these radionuclides are evaluated with the parent nuclide.

TABLE 4-2

ACTIVITY CONCENTRATION BY SOURCE

Source	Fraction available for release from the fuel rod[1] (f_V / f_G / f_F / f_C)	Fraction of rods that develop cladding breach[1]
Normal Transport Conditions		
Volatiles	2E-04	0.03
Gases	0.3	0.03
Fines	3E-05	0.03
Crud[5]	0.15	not applicable
Hypothetical Accident Conditions		
Volatiles	2E-04	1.0
Gases	0.3	1.0
Gases - Kr-85 only	0.3	1.0
Fines	3E-05	1.0
Crud	1.0	not applicable

1 Values taken from NUREG/CR-6487 [6]

FIGURE 4-1

NUHOMS®-MP197 CONTAINMENT BOUNDARY COMPONENTS

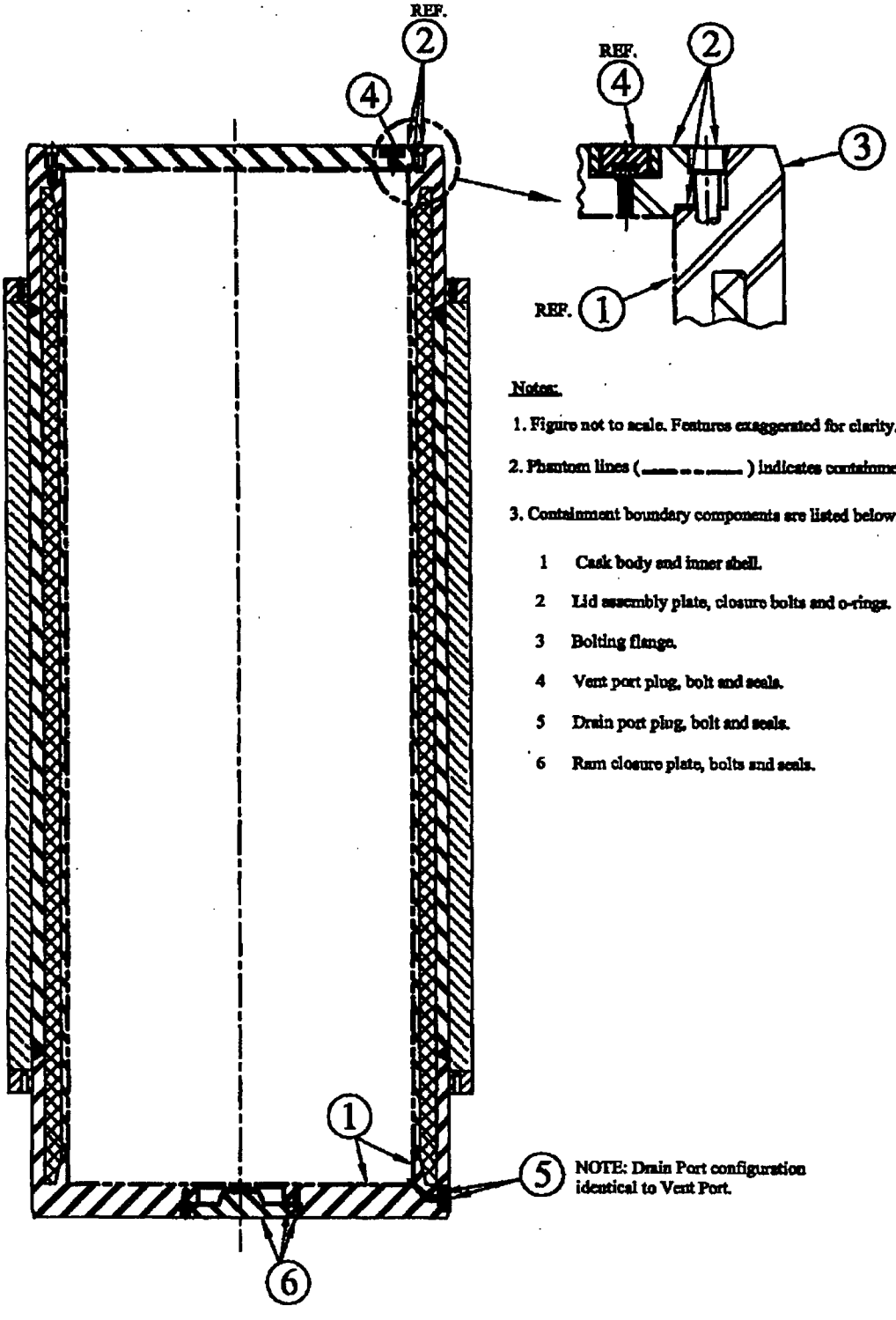

Notes:

1. Figure not to scale. Features exaggerated for clarity.
2. Phantom lines (_____ _ _ _____) indicates containment boundary.
3. Containment boundary components are listed below:

1	Cask body and inner shell.
2	Lid assembly plate, closure bolts and o-rings.
3	Bolting flange.
4	Vent port plug, bolt and seals.
5	Drain port plug, bolt and seals.
6	Ram closure plate, bolts and seals.

NOTE: Drain Port configuration identical to Vent Port.